Development of a damage detection framework for railway bridges using operational response

by

Md Riasat Azim

A thesis submitted in partial fulfillment of the requirements for the degree of

Doctor of Philosophy

in

Structural Engineering

Department of Civil and Environmental Engineering

University of Alberta

Abstract

Railway bridges are critical components of the railway infrastructure system. These bridges are subjected to various potential hazards resulting in different levels of damage. Therefore, developing operational response-based robust damage investigation strategies specifically tailored to railroad bridges is the goal of this doctoral research. In this research, non-parametric damage detection methods are proposed using operational acceleration and strain data. These methods only require basic information about the bridge (e.g. the type of the bridge, such as girder bridge or truss bridge, and its geometric configuration) during the setting up of the instrumentation/data collection plan. Once the system of operational response data acquisition is installed, the methods do not require further information from a numerical model or information about the design of the bridge. These methods then use the operational response to provide information about the structural condition of the bridge. The methods also incorporate operational variability in terms of train speed and loading.

The research contributions of this thesis are discussed in three parts. In the first part, a new damage detection method using acceleration data is proposed for railway bridges. This method applies a sensor cluster approach to the time-series analysis of operational acceleration data recorded during and after the passage of trains. The damage feature is investigated based on the difference of fit ratio of the time series models fit to the measured free acceleration response of the baseline bridge and unknown-state bridge. It is shown that the proposed framework provides useful

information on the existence, location, and relative severity of the potential damage in terms of nodal damage features.

In the second part, damage detection methods are developed for railway bridges that utilize statistical analysis techniques such as coefficient of variation and principal component analysis employing operational strain response that extracts damage features from structural elements. The damage features are investigated as the difference of coefficient of variations and the difference of geometric distances in the principal component space respectively. The numerical results demonstrate that the proposed methods are effective in identifying, locating, and relatively assessing the severity of damage in instrumented truss elements. The damage features extracted from elements using strain-based methods and those extracted from the nodes using acceleration-based methods could be utilized as independent damage assessment tools as well as complementary tools to each other.

In the third and final part, laboratory experiments are carried out on a steel deck type bridge and a timber truss bridge to validate the acceleration response-based damage detection method proposed in the first part of the thesis. The experimental results show that the presented method indeed has the potential for implementation in real-life bridges.

Finally, the thesis discusses the limitations of the present research and recommendations for future research.

Preface

This thesis is original research conducted by Md Riasat Azim. Four chapters of this thesis have been published/accepted and submitted for publication as follows:

A version of Chapter 2 has been published in the ***Journal of Structural Control and Health Monitoring*** as: **Azim MR, and Gül M. (2019). "Damage detection of steel girder railway bridges utilizing operational vibration response", 26(11), e2447**. Some of the contents of the published version have been modified, removed, and added for the consistency and coherence of this thesis and to avoid overlap of content across multiple chapters. Md Riasat Azim was responsible for concept formation, developing the finite element models, all analyses, and manuscript composition. Dr. Mustafa Gül was the supervisory author and was involved in concept formation, analyses, and manuscript composition.

A version of Chapter 3 has been published in the ***Journal of Structural Engineering, ASCE*** as: **Azim MR, and Gül M. (2020). "Damage detection of steel truss railway bridges using operational vibration data", 146(3), 04020008**. Some of the contents of the published version have been modified, removed, and added for the consistency and coherence of this thesis and to avoid overlap of content across multiple chapters. Md Riasat Azim was responsible for concept formation, developing the finite element models, all analyses, and manuscript composition. Dr. Mustafa Gül was the supervisory author and was involved in concept formation, analyses, and manuscript composition.

A part of Chapter 4 has been published in the ***Journal of Structural Control and Health Monitoring*** as: **Azim MR, and Gül M. (2020). "Damage detection framework for truss railway bridges utilizing statistical analysis of operational strain response", 27(8), e2573**. Some of the contents of the accepted version have been modified, removed, and added for the consistency and coherence of this thesis and to avoid overlap of content across multiple chapters. Md Riasat Azim was responsible for concept formation, developing the finite element models, all

analyses, and manuscript composition. Dr. Mustafa Gül was the supervisory author and was involved in concept formation, analyses, and manuscript composition.

Another part of Chapter 4 has been accepted for publication in the ***Journal of Structure and Infrastructure Engineering*** as: **Azim MR, and Gül M. (2020). "Data-driven damage identification technique for truss railroad bridges utilizing principal component analysis of strain response"**. Some of the contents of the accepted version have been modified, removed, and added for the consistency and coherence of this thesis and to avoid overlap of content across multiple chapters. Md Riasat Azim was responsible for concept formation, developing the finite element models, all analyses, and manuscript composition. Dr. Mustafa Gül was the supervisory author and was involved in concept formation, analyses, and manuscript composition.

A version of Chapter 5 has been published in the ***Journal of Structural Monitoring and Maintenance*** as: **Azim MR, Zhang H, and, Gül M. (2020). "Damage detection of railway bridges using operational vibration data: theory and experimental verifications", 7(2), 149-166**. Some of the contents of the submitted version have been modified, removed, and added for the consistency and coherence of this thesis and to avoid overlap of content across multiple chapters. Md Riasat Azim was responsible for concept formation, planning, designing, and building the experimental setups, all analyses, and manuscript composition. Haiyang Zhang, who is a Ph.D. Candidate of Civil and Environmental Engineering assisted Md Riasat Azim during the fabrication of experimental setup and contributed during the collection of experimental data. Dr. Mustafa Gül was the supervisory author and was involved in concept formation, analyses, and manuscript composition.

Dedication

To my parents: for their sacrifices, and for being the greatest source of inspiration and encouragement.

Acknowledgment

I wish to express my deepest gratitude to my dear parents and my brother for making many sacrifices to allow me to pursue my dreams. Words cannot describe my heartfelt feelings for their endless and unconditional love.

I am deeply grateful to my supervisory committee members, Dr. J.J. Roger Cheng, Dr. Vivek Bindiganavile, and Dr. Mustafa Gül, for their kind support, encouragement, and guidance. I am very pleased and honored to pursue my Ph.D. research project under the direct supervision of Dr. Mustafa Gül, who has inspired and motivated me throughout my Ph.D. program. He has been a wonderful teacher and mentor and had a great influence on my both personal and professional life.

I am greatly thankful to my colleagues: Qipei Mei, Haiyang Zhang, Ngoan Do, and Nima Shirzad of the Structural Health Monitoring Research Group at the University of Alberta for providing valuable feedback and assistance during various stages of my Ph.D. research. I would like to acknowledge IC-IMPACTS (India-Canada Centre for Innovative Multidisciplinary Partnerships to Accelerate Community Transformation and Sustainability, established through the Networks of Centres of Excellence of Canada) for facilitating and funding my Ph.D. project. I would like to thank the University of Alberta for awarding me with the Doctoral Recruitment Scholarship and the Government of Alberta for awarding me the Queen Elizabeth II Doctoral Scholarship.

I would like to thank Dr. Zengtao Chen from the University of Alberta, and Dr. Sriram Narasimhan from the University of Waterloo for serving as my committee members, and providing suggestions and recommendations.

TABLE OF CONTENTS

LIST OF TABLES

LIST OF FIGURES

1 INTRODUCTION

1.1 Motivation

The railway system is an integral part of the overall transportation network of many countries. Despite the significant development of other means of transportation like highways, waterways, and airways; the railway is still a major mode of transportation especially relied upon for carrying a large number of passengers, goods, and other products. Railway bridges are critical components of the railway infrastructure system and they contribute to the socio-economic development of the country. The majority of these bridges are approaching their estimated design life and, in addition, they are subjected to various potential risks, such as natural disasters, fatigue, corrosion, etc. These potential risks result in different levels of damage which may cause failure or even collapse of these bridges. In the previous few decades, the demands on the bridges have been burgeoning both in terms of increased axis loads and operational frequency. Therefore, it is paramount that railway bridges are maintained effectively.

The lack of proper maintenance was one of the major causes of failure and collapse of numerous highway and railway bridges in the past. Examples of such cases include the Mianus River Bridge in the United States [1], Somerton Bridge in Australia [2]. In 2001, a railway bridge BRIDGE-924 of the Indian railway network in Kerala, India failed when one of the girders collapsed as a train was passing over it, killing 59 people [3]. The bridge was over 120 years old and was severely distressed. But there were no proper maintenance practices in place to evaluate its operability. In 2009, a brick arch railway bridge (RDG148) near London in England failed while a train was passing [4]. Investigations revealed that one of the abutments was gradually undermined by scouring which was not assessed at an early stage due to lack of awareness.

A significant number of bridge failures could be averted by implementing a reliable and proactive maintenance strategy that would detect signs of deterioration at an early stage so that appropriate measures could be taken to prevent more severe

damage. This is where lies the importance of implementing a robust Structural Health Monitoring (SHM) system.

Structural Health Monitoring is a valuable tool to improve safety and reliability, in addition to formulating effective maintenance operations during the service life of the infrastructure systems, offering considerable savings in life-cycle cost. The last few decades witnessed rapid development in the field of SHM due to dramatic technological progress, which has allowed engineers to acquire desired data in a much easier way. Several SHM systems have been installed on different types of civil infrastructures in real-world scenarios [5-9].

Over the years, vibration-based indirect methods have been developed by researchers which rely on bridge responses to assist the on-site inspection strategies. However, these existing methods have also some drawbacks which limit their applicability to railway bridges. The most important challenge is that anomalies should be detected regardless of operational or loading conditions [10-13]. Therefore, developing a damage detection framework specifically tailored to railway bridges which are robust to operational condition changes is the goal of this Ph.D. research.

1.2 Condition of railway bridges around the world

Around 20000 bridges across Canada are vital components of the railway transportation systems as per the Canadian National Railway (CNR). Of these bridges, only 10% were built after 1990, 62% of the bridges were built between 1965 and 1989. Therefore, around 60% of these bridges are close to or older than 30 years. In the US, the railway network consists of over 100,000 bridges [14]. More than half of the railway bridges in the US were built before 1950 and show signs of distress [15]. The operation of these railway bridges is hampered by irregularities that cause accident or service interruptions. In Europe, there are over 300,000 railway bridges in the 212,000-km railway network with more than 35% of these built over 100 years ago [16]. These bridges are being pushed to their physical limit to improve railway capacity. These aging infrastructures pose a high

risk to the overall availability of railway network. India has one of the largest railway networks in the world with over 136,000 railway bridges. Out of 136,000 bridges over the Indian railway network, 27% are over 100 years old. Most of these bridges have passed or are close to reaching their design life and as of 2015, more than 4500 bridges were found to be requiring rehabilitation [17].

The railway bridges around the world have been subject to increases in the axle loads and are now running loads over the standards existing during the construction and design of these bridges. Also, modern bridges are also subjected to an ever-increasing demand for heavy axle loads and operational frequency. In the US, Federal Railway Association (FRA) forecasts about a 40% increase in passenger load by 2040 [14]. In the UK, the number of passengers has doubled in the last 20 years [18]. In India, over the last decade or so, the allowable axle loads were increased from 20.32 Tons axle load to 22.82 Tons. It is now proposed that this loading is increased to 25 Tons axle loads, signifying an increase in loads of almost 25% in the last decade. This increase in axle loads permitted is also accompanied by a significant increase in the number of trains resulting in a rapid increase in the total volume of traffic [19-20].

Lee et al. conducted a comprehensive study on U.S. bridge failure covering 1,062 bridge failures that occurred from 1980 to 2012 [21]. These studies do not specifically focus on railway bridges, rather give information on the failure of overall bridge infrastructure including railway bridges. According to this study, about 65% of the failed bridges were steel bridges, with concrete and timber bridges accounting for 22% and 12% respectively. It is a concern that even though there is more than twice the number of concrete bridges than steel bridges in the US, the failure rate of steel bridges is significantly high. Among the 615 incidences of steel bridge failure, the data showed that about 59% of the failed steel bridges are steel girder bridges and 37% are truss bridges. The study reported 19 instances of railway bridge failure and 11 of these are steel truss bridges. Transportation Research Board (TRB) published an article on the need for railway bridge health monitoring by investigating incidences of railway bridge interruptions in the U.S. [22]. Based on

177 railway bridge-related events that occurred between 1982 and 2010, the study reported that around 10% of the problem could be attributed to the structural member failure and foundation related issue.

In addition to aging, small-scale natural disasters, increase in operational demand, environmental effects and other internal causes (such as lack of maintenance) normally result in distressed bridges where some of the members/connections have been overstressed and/or lost stiffness/strength resulting in deterioration of bridge performance. A severe collision of railroad traffic or derailment of a train has the potential to damage structural members, connections, and support systems. Weathering and corrosion can result in a reduction of member thickness, change in support behavior, etc. If these distressed bridges are not maintained and repaired on time, it can result in collapse. While it may not be always possible to avert the sudden collapse of bridges due to major disasters like flooding and earthquakes, the goal of the SHM framework is to continuously monitor for distressed bridges so that serious failure can be prevented and maintenance operations can be done in a proactive manner reducing the life-cycle costs.

1.3 Review of damage detection methods

1.3.1 Background

Structural health monitoring (SHM) is a broad research area encompassing various disciplines and components, such as analytical, numerical and experimental investigations, data acquisition systems, data processing and analysis, damage detection methods, etc. Recent improvements in the area of computer science and electrical engineering, have made the process of collection of large amounts of data convenient and economical. However, despite the increased ability to possess a huge volume of data, it remains a challenge to utilize these data for damage detection especially for large civil infrastructures like bridges. The main objective of this thesis is to develop damage detection methods using commonly used parameters (i.e., acceleration and strain) which could be potentially useful for

railway bridges. In this section, a review of existing methods for damage detection is presented.

Damage detection is a vital component of any SHM system. Damage could be in the form of changes in the structural material and geometric properties, changes in the boundary restraints, etc. These damages could adversely affect the performance of the structure and its behavior. For any damage detection method to be useful, the following four objectives need to be addressed: 1) identifying the presence of damage; 2) localizing the damage; 3) quantifying the severity of damage; and 4) estimating the remaining useful life of the structure [23]. Addressing the first three objectives is the scope of the research conducted for this thesis. A thorough review of SHM applications and associated damage detection methods for structures can be found in the literature such as Brownjohn et al., Fan and Qiao, Das et al., Gomes et al. [24-27].

1.3.2 Vibration-based damage detection methods

Previous studies on bridge health monitoring have sought to evaluate changes in the modal properties of the given bridge (i.e., modal frequencies, shapes and curvature, modal energy) [28-35]. This method is known as the vibration-based method (also known as the modal-based method); it uses sensors (e.g., accelerometers) to measure the vibration response of the structure [36]. The philosophy underlying this method is that damage or change in the structure will result in a corresponding change in stiffness and/or mass of the structure, which in turn will affect the dynamic response. The identification approaches are mainly based on the change in the natural frequencies and mode shapes [37]. Scianna and Christenson, for instance, proposed a probabilistic damage detection method which analyzed the bridge's natural frequencies for healthy and damaged states to quantify and detect potential damage [38]. Ko et al. developed a multilayer neural network-based damage detection method for the cable-stayed bridge carrying both road and rail traffic [39]. The method relies on modal frequencies and shapes. Frequency and mode shape-based damage detection studies have also been conducted on truss

bridges as reported in the literature [40-41]. The study showed that modal frequency and curvature combined can be useful in detecting and locating damage.

In general, vibration-based methods are considered economically viable and suitable for assessing the overall condition of the structure. However, modal characteristics can be insensitive to localized damage. It also faces challenges in the case of time-varying systems and the uncertainty caused by environmental and operational variability in traffic loading and in the measurement itself. Besides, the location of damage cannot be identified by using only modal frequency. Incorporating mode shapes is could provide information on the location of damage, but mode shapes do not change significantly due to small damage and therefore, usually locate severe damage.

Therefore, different parametric and non-parametric SHM methods have been developed by various researchers. Parametric methods are very useful for damage detection of structures provided sufficient information on structural parameters are available allowing the possibility of building a detailed numerical model. Methods that rely on the changes in frequency, mode shapes as well as model updating techniques can be categorized as parametric methods. When a detailed numerical model is available, model updating techniques can be applied effectively to compare the existing bridge condition (experimental data) with its baseline (from the numerical model). However, building a detailed finite element model often is not possible due to limited data especially for large bridges [42]. This is also true for old bridges for which, construction details are not available.

Hence, non-parametric statistical-feature-based damage detection methods are becoming increasingly popular for the health monitoring of structures. These methods do not require knowledge of structural parameters as its parameters are not directly related to the physical characteristics of the system. In this method, damage-sensitive features are extracted from the measured vibration response (i.e., accelerations) of the undamaged structure, and the structure is monitored for any changes to these features [43-44]. The likelihood of damage could be estimated by comparing the damage feature of unknown condition to that of a reference

condition [45]. However, depending on the analysis type and method, the non-parametric analysis may not yield as much detailed information as parametric methods since the analysis is conducted only based on the measured data.

1.3.3 Application of time-series models for damage detection

Time-series-analysis-based damage detection of bridges has become popular in recent decades [46-56]. In this method, damage-sensitive features are extracted from the measured free vibration response (i.e., accelerations) of the baseline structure, and the structure is monitored for any changes to these features. Using autoregressive models with exogenous inputs (ARMAX) combined with outlier analysis, DFs can be obtained. This offers the potential to detect damage occurrence, location, and relative severity. In this thesis, time-series methods have been employed to develop an acceleration-based damage detection method. Therefore, some applications of time-series analysis for damage detection are briefly discussed in the following sections.

Sohn et al. [46-47] demonstrated a procedure for damage detection by applying time-series models to predict dynamic responses. Then, an outlier analysis was performed to compute the Mahalanobis distance which was utilized as the damage feature. This method was applied to the strain response of a patrol boat. It was shown that the method could detect the change in structural conditions. However, damage localization was a limitation of the presented method.

Monroig and Fujino [57] developed a damage detection method using time-series models and investigated, how the predicted responses compare with the measured acceleration responses of a structure. They investigated the suitability of the method by applying it to a frame structure similar to the ASCE benchmark problem in Bernal and Beck [11]. While the results showed potential for damage detection, there were instances of false-positive and false-negative results.

A new damage feature based on the time-series model coefficients was proposed by Nair et al. [48]. After applying the Auto-Regressive Moving Average (ARMA) model to predict the vibration response, the researchers conducted a hypothesis test to detect

damage. The results of applying the method to the ASCE benchmark structure showed the potential usefulness of the method. It was shown that the method could identify and localize small as well as severe damages. Its application to the real-life structure was not investigated.

Gül and Catbas [44] investigated a statistical pattern recognition technique utilizing time series analysis. The experimental results conducted on laboratory structures such as beams and frames demonstrated that this method was capable of detecting damage in most of the investigated damage scenarios. However, the complexity in determining the threshold damage feature for real-life structures under baseline condition was identified as a potential issue that needs to be addressed for the real-life application of the method.

Gül and Catbas [51] also proposed the concept of sensor clustering to the time series-based method for damage detection. Based on this concept, the vibration data collected from the instrumented accelerometers were analyzed through different clusters. Each cluster consisted of an output channel and input channels. ARX models were utilized to predict the outputs based on the input responses. By observing the changes in fit ratios for the ARX models, damages were identified, localized and relatively quantified. The method was validated through numerical and experimental investigations.

One of the limitations regarding the applications of the time-series methods described above is that the orders of time series models were estimated either by experience or by observing the fit ratio between the measured and the predicted data. Therefore, the models would change depending on the tested structure and the analyzed data. To overcome the complexity of determining the model orders, Mei and Gül [52-53] derived a procedure in which the model orders were determined directly from the equation of motion. They proposed two DFs that compare fit ratios and model coefficients. The presented methods were applied to 2-D frame type structures subjected to impact hammer excitation and it was shown that the method has potential for damage detection and localization. However, its application to the real-life structure under operational conditions was not explored. In this thesis, time-series analysis has been applied to predict the operational response due to the passage of trains over a

girder type and truss type railway bridges. In this thesis, time series analysis methods have been applied to predict vibration response when the bridge is excited by trains of variable speeds and axle loads in addition to the presence of measurement error. It is demonstrated that time-series models can be utilized to detect, locate, and relatively assess the severity of damage in a girder and truss type railway bridges which is a very useful new application of such technique.

1.3.4 Damage detection methods applied to bridges

Most of the bridges on rail networks are currently monitored by visual inspections and non-destructive testing, which could be time-consuming, prone to human error, and thereby unreliable and inconsistent in its findings [58]. Therefore, the SHM of railway bridges is increasingly becoming an area of interest, and implementation of various SHM techniques for railroad bridges management needs to be given high priority for research and development [59-61]. In recent decades, several researchers have reviewed SHM concepts for different types of bridge structures; these SHM concepts include vibration-based methods, model updating techniques, and application of neural networks [62-68]. The main focus of these studies has been on bridge monitoring to identify the existence of damage, in addition to assessing the condition, and serviceability of these bridges. Based on this approach, increasingly complex SHM concepts have been developed to expand their evaluation capacity for bridge conditions and decision-making on the use, repair, and strengthening of damaged and deteriorated structures.

In 2012, a wavelet transformation-based damage detection method was proposed by Beskhyroun et al. [69]. They used the dynamic response of a steel railway bridge to actuator-applied excitation as the data for wavelet transformation. In their study, the damage is detected by comparing the damage indicator under baseline and damaged conditions. While the method is successful in detecting and locating damage, it is not suitable for continuous maintenance under operational conditions.

Farahani and Penumado, meanwhile, proposed a damage feature based on the ratio of the standard deviation of the prediction error of the damaged bridge to the

healthy bridge [70]. This method used velocity response to impact loading on a steel girder bridge. While the method is encouraging, damage localization is still an issue, especially when data is contaminated by noise.

Kopsaftopoulos and Fassois conducted both parametric (i.e. modal parameter-based and residual-based) and nonparametric damage detection tests (Power Spectral Density and Frequency Response Function) on an experimental truss in which damage was simulated by removing bolts from joints [71]. The study concluded that while both methods have global damage detection capability, parametric methods offer increased accuracy. The method is yet to be tested under operational conditions.

Xu et al. proposed a strain energy-based damage detection method for long-span cable-stayed bridges [72]. In this study, an energy index based on the difference of mode shape curvature has been proposed to detect and locate damage. The proposed method was able to detect and locate damage under noisy data. However, in that study, severe earthquake excitations had been simulated to excite the bridge. Its applicability under daily operational conditions had not been discussed.

Wang et al. developed a multilayer genetic algorithm to obtain a correlation of Modal Strain Energy (MSE) of mode shapes of a steel truss bridge model [73]. They compare the MSE of the undamaged and damaged bridge to detect damage. In the presence of noise, the correlation method could not localize mild damage (25% stiffness loss) on a single member. The algorithm, however, can detect and locate severe damage where multiple members are affected.

Nuno experimentally verified a detection method for truss bridges by obtaining the Damage Index through the Frequency Response Function (FRF) curvature method [74]. However, the method was able to detect damage only at the center of the truss element and could not detect damage in cross-beams.

Siriwardane presented a parametric damage detection method through a case study by observing the changes in modal parameters of an undamaged bridge to a damaged truss bridge [75]. The method compares the variation of modal parameters

with respect to the position of the damage. While the method was validated using a numerical model, the performance of the modal based method under noisy condition was not discussed.

Prajapat et al. proposed a damage detection technique utilizing a Bayesian algorithm that analyzes a mode shape of a truss bridge and its derivative [76]. This method uses modal parameters and has limited performance under noisy measurement, even at high damage level (50% stiffness loss in a truss element).

Recently there has been increased interest in developing SHM techniques for bridge maintenance that rely on operational response. A train induced bridge acceleration response-based damage detection method has been developed by Zhan et al. [77]. The researchers demonstrated damage identification in terms of response sensitivity matrices which are updated using an iterative procedure to locate and quantify the damage in railway bridges. The method compares the existing bridge response to the damaged response and can detect and locate damage to the bridge. It is only effective when the same train at the same speed is used for measuring the response at the undamaged and damaged state.

Bowe et al. developed a damage detection method by analyzing vehicle accelerations induced by train-track-bridge interaction [78]. Using the wavelet transformation technique, this method showed the potential to detect and locate the damage in terms of changes in pseudo frequency. However, only a simple beam has been studied to represent a railway bridge, which may not be representative of an actual truss bridge. While the method is validated considering train loading, but it does not discuss the effect of operational variability.

George et al. developed an energy-based method to detect damage in the bridge under train traffic load by comparing the normalized signal energies of the vertical acceleration response of the healthy and damaged bridge [79]. At present, though, the method can detect the presence of damage only.

Kaloop et al. performed a railway bridge assessment utilizing acceleration and displacement response of the bridge to train passing over the bridge at high speed

[80]. These studies evaluate the performance of existing bridges without considering the effect of damage.

In another study, a damage detection strategy for railway bridges based on artificial neural networks (ANN) was developed by Gonzalez and Karoumi [81]. The study used bridge acceleration data as the primary input and proposed a damage indicator based on the prediction error of the ANN system. However, one limitation of their study is that a simply supported beam is represented as a railway bridge while a real-life railway bridge is a complex structure. The method is also limited in the sense that, to ensure accuracy, the train load's position and speed need to be known by the bridge weigh-in-motion system.

Another ANN-based damage detection method for railway bridges was developed and numerically verified by Neves et al. [82]. In their study, the difference between measured acceleration response and the predicted response was used as a damage indicator. The method showed potential for railway bridge monitoring but was limited by operational variability in terms of train loading. Also, limited damage locations were investigated in this study.

Quirke et al. developed a damage detection method for railway bridges by comparing the changes in the longitudinal profile of the bridge in response to a passing train [83]. The method relies on the difference in elevation along the length of the bridge. The method detects damage when the damage location is closer to the mid-span. When the damage is near the support, the performance of the proposed method is reduced.

In general, the modal-based and other acceleration-based methods usually provide global information of damage as shown by the researchers. Strain-based SHM can overcome some of these issues. Strain-based SHM is recently receiving increasing attention for damage assessment purposes as strain monitoring is usually less expensive compared to other measurements like acceleration [84-87]. Moreover, strain-based methods have high sensitivity to local damage [86] while acceleration-based methods are not so sensitive to damage [87]. Therefore, strain could be more reliable for health monitoring even under noisy conditions.

A strain-based bridge monitoring method was developed by Wipf et al. [88]. In this method, strain data were collected under vehicle loading. The damage was detected by observing the statistical relationship between target strain sensors and non-target strain sensors. This relationship includes regression models. While this method showed good performance for some damage cases but also a high degree of false indications for other cases. Santos et al. proposed a damage detection method in which strain gauges were used to identify strain mode shapes and concluded that change in strain modes are a good indicator of damage [87]. Posenato et al. showed that principal component analysis (PCA) can be used to detect and locate damage in a multi-span beam in which displacement data is used to compute the components [89]. More recently, Van Der Kooi and Hoult showed the application of distributed fiber optic sensors in detecting variations in strain and element forces of a steel truss bridge due to damage [90]. The cyclic load was applied to collect strain response in the laboratory on a scaled truss bridge. The method could be useful for monitoring a real-life railway truss bridge if it can identify damage using operational conditions. Catbas et al. developed a moving correlation analysis-based damage detection method utilizing highway bridges response to arbitrary vehicle loading [91]. The method was validated through laboratory and real-life bridge testing.

Railway bridges are integral components of the railway infrastructure system and the majority of these bridges are approaching their estimated design life. In addition to aging, these existing infrastructures are subjected to various potential risks, such as natural disasters, fatigue, corrosion, etc. These potential risks result in different levels of damage, which adversely affects their performance and may cause failure or even the collapse of these bridges. In the previous few decades, the demands on the railway bridges have been burgeoning both in terms of increased axis loads and operational frequency. Therefore, it is paramount that these systems are maintained effectively.

1.4 Statement of the problem

One of the challenges of today's structural engineering profession is to deal with the deterioration of the aging civil infrastructure system. Railway bridges are critical infrastructures of railway communication network and as discussed, these bridges around the world are aging. A significant portion of the railway bridges is made of steel and timber. Based on the analysis of railway bridges owned by Canadian National (CN), around 80% are steel and timber bridges. In Canada, about 67% and 56% of the steel and timber railway bridges owned by CN respectively were built before 1965 and hence more than 50 years old. Moreover, steel and timber bridges are vulnerable to degradation due to environmental effects and hence require frequent maintenance. Therefore, it is necessary to develop a damage assessment framework to monitor these railway bridges for signs of damage to avoid potential collapse and/or costly repair.

Traditionally, railway bridges are monitored by site inspections, the effectiveness of which is limited by the availability of personnel and their experience [58]. Monitoring railway bridges in this manner could be time-consuming, prone to human error, and thereby unreliable and inconsistent in its findings. In the last few decades, various damage detection methods have been developed for bridge type infrastructures and significant progress has indeed occurred in this regard. Based on the review of existing literature described in the previous section, it can be observed that only a small number of researches focused specifically on railway bridges. The studies which focus on railway bridges are still limited in their ability:

- Vibration-based methods that rely on data obtained from localized excitation through hammer testing, require on-site experimental investigations that are not convenient for the bridge owners and users and day-to-day continuous monitoring is not possible in this manner.
- Limited studies are available on the train-induced response-based damage detection. In recent years, some methods have been developed which are based on train loading. But most of these methods are not robust to operational condition changes and measurement noise.

- The modal frequency-and shape and based methods cannot always detect and locate small damage that occurs in a structural node or an element. Such damage does not change the mode shape and frequencies significantly and therefore these methods are most effective in detecting severe damages that affect the structures globally.

It is important to recognize that there is a need to develop an extensive damage detection framework tailored to common types of railway bridges relying on operational loading rather than on-site testing which can effectively identify and localize the damage, and quantify its relative severity. It is also important that the damage detection framework should be robust enough to operational condition changes and should be able to compensate for the measurement noise that affects the operational responses. The goal of this research is to develop a damage detection framework for common types of railway bridges that addresses some of the existing shortcomings discussed above through the application of new techniques.

1.5 Research objective

Around the world generally, girder or truss bridges are the most common types of railway bridges which are the focus of this research. Choosing effective damage sensitive parameters is critical for achieving satisfactory damage detection performance. While different types of bridge responses can be used to formulate the damage detection framework, this study will focus on using acceleration and strain response of the bridge. Displacement data can be useful for condition assessment of railway bridges [92-93]. However, it is also noted that in real-life bridges, it may be difficult to obtain displacements and velocity response accurately. Also, small damage is often not discernible using the variation of displacements [94]. At the same time, it is common practice to monitor bridge response using sensors that measure acceleration and strain-gauges [88]. The use of wireless accelerometers and strain gauges makes it convenient to collect the operational bridge responses that can be used to formulate condition assessment plans [95]. Therefore, the objective of this research is to develop damage detection

methods using operational acceleration and strain data from railway bridges, that are capable of extracting damage sensitive features and providing information on damage, its location, and relative severity for the damage cases investigated in this research.

In this thesis, the research objective is to develop two separate methods based on acceleration and strain data as acceleration and strain data are two of the most commonly measured operational parameters for bridge monitoring. Also, these two methods provide bridge owners with two independent tools for damage detection of railway bridges. Acceleration and strain data are used to obtain damage features from structural nodes and elements respectively and therefore provide two different damage features. The acceleration-based method developed in this research could assess global the condition of the bridge in terms of nodal damage features, while strain-based methods developed rely on data from the individual structural elements and could identify damage in instrumented elements.

Since these two methods are based on different types of data collected from different components of the bridge, there could be situations when one method individually might not provide adequate information on the location and severity of the damage. This research presents the bridge owners with the option to develop a plan for damage detection comprising both methods that have the potential to increase the efficiency of the damage detection framework over individual methods.

1.6 Research contribution

In the last few decades, various methods for damage assessment of bridges have been proposed by researchers around the world as described in the previous sections. However, a limited number of methods exclusively focus on railway bridges. Most of the damage detection methods which focus on railway bridges have limited ability. The main contribution of this research is that it presents a damage detection framework specifically for railway bridges utilizing commonly measured operational responses (such as acceleration and strain) which can be

efficient and simple to implement for continuous monitoring of these bridges on a day-to-day basis. This overcomes one of the limitations of the condition assessment methods that rely on visual inspections and on-site testing.

The proposed methods can be considered as hybrid methods. The information about the bridge (e.g. the type of the bridge, such as girder bridge or truss bridge, and its geometric configuration) are needed only during the development of instrumentation and data collection plan. However, once the data collection plan is implemented, the methods become mostly data-driven, which makes the application of the methods simpler compared to other parametric methods.

Another challenge that could be overcome using the proposed methods is that the condition of the bridge could be assessed even when the bridge response is obtained under variable train loads and speeds in addition to measurement errors. Therefore, the proposed methods are versatile compared to other methods that do not consider such issues. The developed methods will offer clear advantages to detecting and localizing structural changes and estimates relative severity. The proposed damage detection framework will allow the use of bridge responses monitored at critical locations with operating traffic on a bridge considering operational variability in terms of train speed and axle loads, which is usually the most economical and convenient measurement method for bridges without interrupting bridge operation.

1.7 Tasks towards accomplishing the research objective

The research scope consists of three steps.

Task 1: develop a damage detection method for railway bridge using operational acceleration response

- develop finite element models of a steel-girder and a steel truss railway bridge and;
- develop an instrumentation plan for collecting acceleration response of the bridge;

- calculate the acceleration response of the bridge in response to the passage of standard trains and extract free vibration response;
- propose a method for analyzing the acceleration response utilizing time-series analysis and equation of motion to define a Damage Feature (DF) which is sensitive to structural change;
- compare the DFs obtained from the baseline bridge to those from the damaged bridge which would provide information of damage in terms of nodal DFs;
- validate the proposed method for girder and truss bridges through numerical simulation under various damage scenarios.

Task 2: develop damage detection methods for railway bridge using operational strain response

- utilize the finite element model of the railway truss bridge developed during objective 1;
- develop a plan for collecting strain response of the bridge;
- calculate the operational strain response of the bridge in response to the passage of standard trains;
- analyze the strain responses utilizing statistical analysis tools such as coefficient of variation and principal component analysis and propose damage indicators for extracting element level information of structural change;
- compare the damage indicators obtained from the baseline bridge to those from the damaged bridge which would provide information of damage in terms of nodal DFs;
- validate the proposed method through numerical simulation under various damage scenarios;

The process of developing both methods is shown in Figure 1.1.

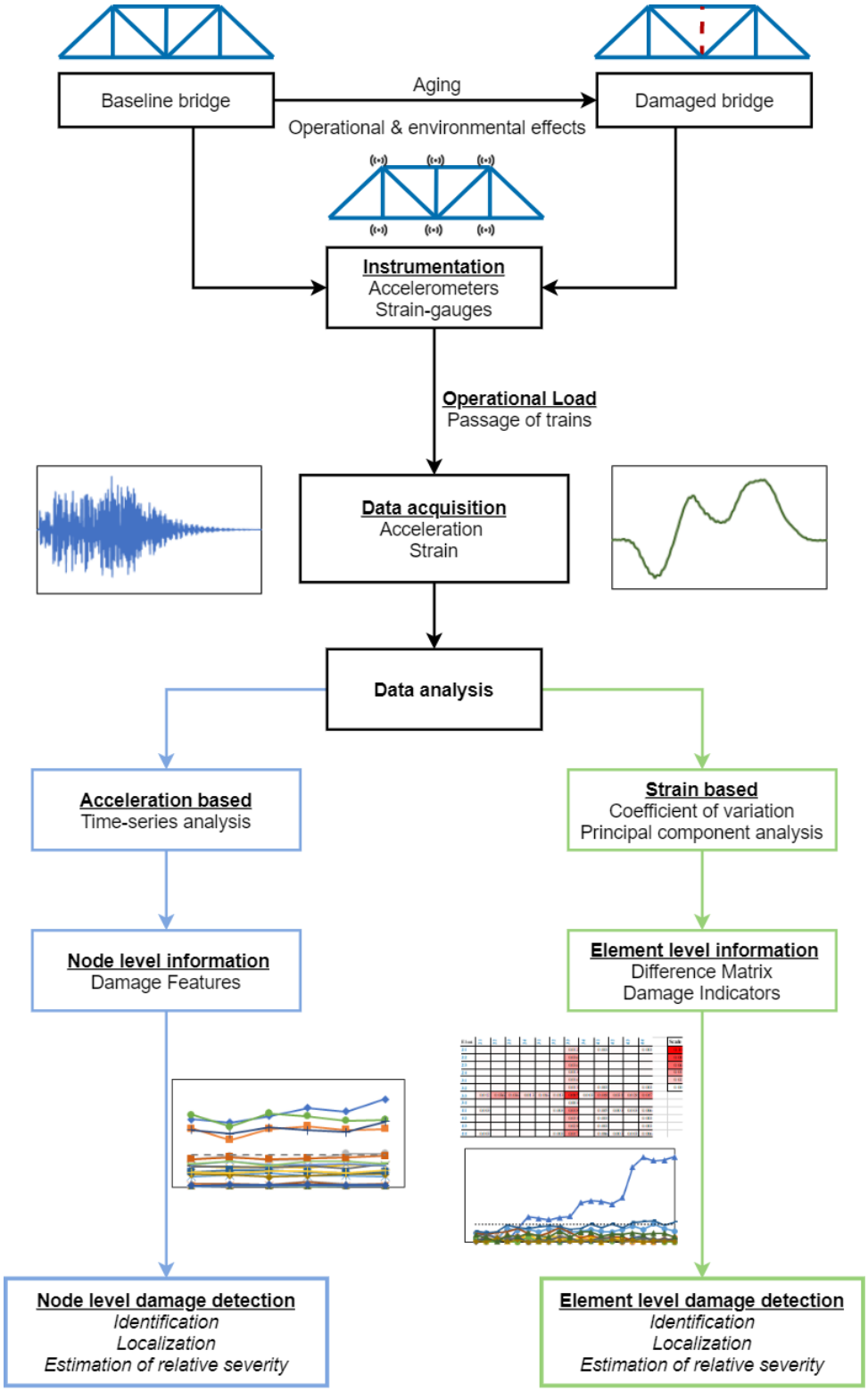

Figure 1.1 Flowchart depicting the development of damage detection methods

Task 3: validate the acceleration-based damage detection method through experimental investigation

- fabricate experimental prototypes of a simple steel deck bridge and a timber truss bridge;
- instrument these bridges with accelerometers to collect acceleration response to the passage of a vehicle;
- obtain acceleration response of the bridges to the passage of the vehicles
- analyze these responses through the proposed method developed for accomplishing Objective 1 and obtain DFs;
- validate the proposed acceleration-based method for different damaged bridge scenarios.

The research conducted in this thesis is summarized in Figure 1.2.

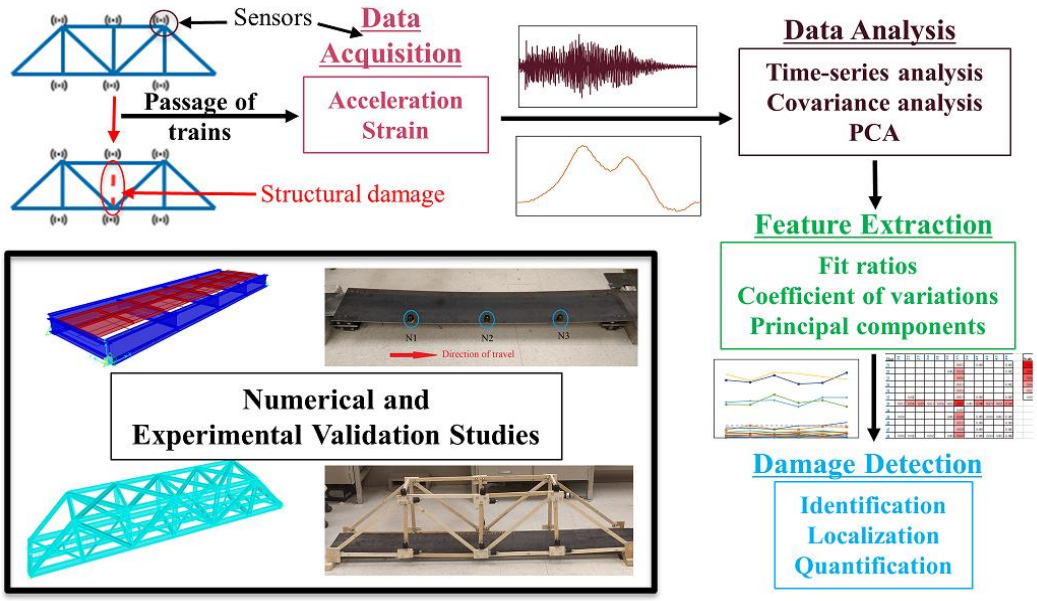

Figure 1.2 Summary of the research conducted in this thesis

1.8 Scope and applicability of the research

This research focuses on developing data analysis techniques for damage detection which have the potential to be useful for short to medium span railway bridges. While railway bridges like any other bridges can be damaged due to different environmental and operational effects, investigation of causes of damage is a separate research area that is not within the scope of this research.

The performance of the presented methods depends on the collection of useful bridge responses to the passage of a single operational vehicle at a time. In highway bridges, traffic movements are random; causing multiple vehicles passing over the bridge at a time. On the contrary, trains pass over railway bridges usually follows a fixed schedule and on a single-track bridge, only one train is present on the bridge at a time and there is a considerable gap between each passage of a train. Also, the live-load to dead-load ratio is considerably high for short-to-medium span railway bridges, which is essential for extracting useful free vibration response. Therefore, it is more practical to obtain useful free acceleration response in railway bridges after each passage of train compared to highway bridges.

The strain-based methods developed in this thesis utilize the total forced response. However, it is still based on the response of the bridge to the passage of a single-vehicle at a time which is more practical to railway bridges as discussed above.

In this research damaged bridge is represented as a bridge in which one or more structural members have distributed loss of stiffness along its entire length. Also, support problems are investigated as a change in boundary conditions (i.e., translational and rotational fixity). Highly localized damages (i.e., partial damage within a structural member, the formation of cracks) are not considered in this research.

In this research, the damage detection methods have been developed considering the linear behavior of the bridges dealing with low-levels of operational vibration and strain response. Damage detection of railway bridges when the bridge

responses are affected by non-linear behavior is not within the scope of this research.

While environmental factors like wind, humidity, temperature changes can certainly influence the structural response of the bridges and can make the process of actual damage detection complicated; formulation of methods to compensate for such environmental variabilities requires separate extensive research which is beyond the scope of this Ph.D. study.

1.9 Organization of the thesis

Chapter 1 provides an introduction to this research. It includes the problem statement and objective of this research along with the outline of steps towards accomplishing the research objectives. It also summarizes the various damage detection methods for bridges proposed by the researchers. This chapter includes a review of the most commonly used damage detection methods for bridges which include modal based methods and other parametric and non-parametric methods.

Chapter 2 presents the damage detection method for railway girder bridges using operational acceleration responses. The theoretical derivation of the method is presented in detail. Subsequently, the application of the proposed method for steel-girder bridges and the numerical validation studies are presented.

Chapter 3 presents the damage detection method for railway truss bridges using operational acceleration responses. The theoretical derivation and instrumentation plan for the application of the method are presented. Subsequently, the application of the proposed method for steel-truss bridges and the numerical validation studies are presented.

Chapter 4 presents two damage detection methods for railway truss bridges utilizing operational strain response. The theoretical derivations of the methods are presented in detail. Subsequently, the application of the proposed methods for steel-truss bridges and the numerical validation studies are presented.

Chapter 5 presents the details of the experimental investigations carried out to validate the acceleration-based method for railway bridges. The experimental setups for a steel deck type bridge and a timber truss bridge along with the instrumentation plans are described. Subsequently, the experimental results for the damage investigation results are presented.

Chapter 6 provides a summary of the findings of the studies presented in the other chapters along with conclusions and offers recommendations for future research.

2 DAMAGE DETECTION OF STEEL-GIRDER RAILWAY BRIDGES USING OPERATIONAL ACCELERATION RESPONSE[1]

2.1 Overview

According to *Task 1* presented in Chapter 1, in this chapter, a damage identification method is developed for continuous global monitoring of girder-type railway bridges using operational acceleration data. The proposed method utilizes a sensor-cluster-based time series analysis method. The potential usefulness of similar technique was shown by previous researchers [51-53] for frame-type 2D plane structures and demonstrated by analysis of vertical acceleration created by impact hammers. However, a girder bridge is a complicated system. Moreover, a train passing over a bridge is considered to be a case of global loading and it affects the bridge differently than does localized impact loading. In this chapter, a new damage detection method for girder railway bridges is proposed considering vertical acceleration data. One of the novel contributions of the proposed method over the existing literature on monitoring of railway girder bridges is that the method is capable of detecting and localizing the damage even under operational variability (i.e., when the vibration response is obtained in response to different train speeds and axle loading). The method applies an auto-regressive moving average model with exogenous inputs (ARMAX model) to analyze the free vibration response of railway girder bridges to extract damage features. It is shown that the proposed method can identify, locate, and estimate the relative severity of the structural damage, a development which constitutes a significant improvement over existing SHM methods for railway girder bridges since the efficiency of the method is demonstrated under variable operational conditions where different train loadings with different train speeds are used as initial conditions for obtaining free vibration responses. The following sections discuss the theory behind the proposed method,

[1] A modified version of this chapter has been published in the following journal as follows:
Azim, M.R., and Gül, M. (2019). Damage detection of steel girder railway bridges utilizing operational vibration response. *Structural Control & Health Monitoring*, 26(11), e2447.
It can be accessed using DOI: **https://doi.org/10.1002/stc.2447**

along with the results of the numerical case studies. Limitations of the method are also discussed.

2.2 Theoretical derivation

2.2.1 Equation of motion

The dynamic responses (accelerations, velocities, and displacements) of a structure are governed by the equation of motion (EOM). This equation, to which the linear dynamic response of a structure with N Degrees of Freedoms (DOFs) complies, can be expressed in simple form as Eq. (2.1). Here, m_{ij}, c_{ij}, and k_{ij} represent components of mass, damping, and stiffness matrices of the system, respectively. The vectors, $u, \dot{u}, \ddot{u}$ represent displacement, velocity, and acceleration, respectively. The external forcing function is denoted by P. If the external force is zero (as in the case of free vibration response), then the i^{th} row of Eq. (2.1) can be written as Eq. (2.2).

$$\begin{pmatrix} m_{11} & \cdots & m_{1N} \\ \vdots & \ddots & \vdots \\ m_{N1} & \cdots & m_{NN} \end{pmatrix} \begin{Bmatrix} \ddot{u}_1 \\ \vdots \\ \ddot{u}_N \end{Bmatrix} + \begin{pmatrix} c_{11} & \cdots & c_{1N} \\ \vdots & \ddots & \vdots \\ c_{N1} & \cdots & c_{NN} \end{pmatrix} \begin{Bmatrix} \dot{u}_1 \\ \vdots \\ \dot{u}_N \end{Bmatrix} + \begin{pmatrix} k_{11} & \cdots & k_{1N} \\ \vdots & \ddots & \vdots \\ k_{N1} & \cdots & k_{NN} \end{pmatrix} \begin{Bmatrix} u_1 \\ \vdots \\ u_N \end{Bmatrix} = \begin{Bmatrix} p_1 \\ \vdots \\ p_N \end{Bmatrix} \tag{2.1}$$

$$m_{i1}\ddot{u}_1(t) + \ldots + m_{iN}\ddot{u}_N(t) + c_{i1}\dot{u}_1(t) + \ldots + c_{iN}\dot{u}_N(t) + k_{i1}u_1(t) + \ldots + k_{iN}u_N(t) = 0 \tag{2.2}$$

Eq. (2.2) contains velocity and displacement terms. The time-series model used in the study only incorporates acceleration response since, in real-life bridges, obtaining velocity and displacement responses under a moving train can be very difficult. Therefore, a method has been developed to replace velocity and displacement terms with acceleration. To achieve this, first Eq. (2.2) is differentiated twice, resulting in Eq. (2.3). Then the central difference technique is used to replace the 3rd and 4th derivatives of u with Eq. (2.4) and Eq. (2.5), respectively.

$$(m_{i1}\ddot{\ddot{u}}_1(t) + \ldots + m_{iN}\ddot{\ddot{u}}_N(t)) + (c_{i1}\ddot{\ddot{u}}_1(t) + \ldots + c_{iN}\ddot{\ddot{u}}_N(t)) + (k_{i1}\ddot{u}_1(t) + \ldots + k_{iN}\ddot{u}_N(t)) = 0 \tag{2.3}$$

$$\ddot{\ddot{u}}_i(t) = \frac{\ddot{u}_i(t+\Delta t) - \ddot{u}_i(t-\Delta t)}{2\Delta t} \tag{2.4}$$

$$\ddot{\ddot{u}}_i(t) = \frac{\ddot{u}_i(t+\Delta t) - 2\ddot{u}_i(t) + \ddot{u}_i(t-\Delta t)}{(\Delta t)^2} \tag{2.5}$$

Making use of Eq. (2.4) and Eq. (2.5) in Eq. (2.3), Eqs. (2.6 to 2.8) are subsequently obtained.

$$\begin{aligned}&\left[m_{i1} \frac{\ddot{u}_1(t+\Delta t) - 2\ddot{u}_1(t) + \ddot{u}_1(t-\Delta t)}{(\Delta t)^2} + \ldots + m_{iN} \frac{\ddot{u}_N(t+\Delta t) - 2\ddot{u}_N(t) + \ddot{u}_N(t-\Delta t)}{(\Delta t)^2} \right] \\ &+ \left[c_{i1} \frac{\ddot{u}_1(t+\Delta t) - \ddot{u}_1(t-\Delta t)}{2\Delta t} + \ldots + c_{iN} \frac{\ddot{u}_N(t+\Delta t) - \ddot{u}_N(t-\Delta t)}{2\Delta t} \right] \\ &+ \left[k_{i1}\ddot{u}_1(t) + \ldots + k_{iN}\ddot{u}_N(t) \right] = 0\end{aligned} \tag{2.6}$$

Eq. (2.6) can be expressed as Eq. (2.7).

$$\begin{aligned}&\left[\sum_{j=1}^{N} m_{ij} \frac{\ddot{u}_j(t+\Delta t) - 2\ddot{u}_j(t) + \ddot{u}_j(t-\Delta t)}{(\Delta t)^2} \right] + \left[\sum_{j=1}^{N} c_{ij} \frac{\ddot{u}_j(t+\Delta t) - \ddot{u}_{ij}(t-\Delta t)}{2\Delta t} \right] + \\ &\left[\sum_{j=1}^{N} k_{ij}\ddot{u}_j(t) \right] = 0\end{aligned} \tag{2.7}$$

From Eq. (2.7), taking out $\ddot{u}_i(t+\Delta t)$ and rearranging the terms, the following expression is obtained.

$$\left(\frac{m_{ii}}{(\Delta t)^2} + \frac{c_{ii}}{2\Delta t} \right) \ddot{u}_i(t+\Delta t) = \left\{ \begin{aligned} &- \sum_{j=1, j\neq i}^{N} \left(\frac{m_{jj}}{(\Delta t)^2} + \frac{c_{jj}}{2\Delta t} \right) \ddot{u}_j(t+\Delta t) \\ &+ \sum_{j=1}^{N} \left(\frac{2m_{ij}}{(\Delta t)^2} - k_{ij} \right) \ddot{u}_j(t) + \sum_{j=1}^{N} \left(- \frac{m_{ij}}{(\Delta t)^2} + \frac{c_{ij}}{2\Delta t} \right) \ddot{u}_j(t-\Delta t) \end{aligned} \right\} \tag{2.8}$$

It can be seen that, for the i^{th} DOF, the sum of the j^{th} DOFs is the contribution from adjacent DOFs. Rewriting Eq. (2.8) for $\ddot{u}_i(t)$ by subtracting Δt from the acceleration components on both sides of Eq. (2.8), Eq. (2.9) is finally obtained. It can be seen that, for the i^{th} DOF, the sum of j^{th} DOFs is the contribution from the other DOFs which includes the i^{th} DOF itself for the $(t-\Delta t)$ and the $(t-2\Delta t)$ time-steps.

$$\ddot{u}_i(t) = \frac{1}{\left(\frac{m_{ii}}{(\Delta t)^2} + \frac{c_{ii}}{2\Delta t}\right)} \left\{ \begin{array}{l} -\sum_{j=1:N, j\neq i} \left(\frac{m_{jj}}{(\Delta t)^2} + \frac{c_{jj}}{2\Delta t}\right) \ddot{u}_j(t) \\ +\sum_{j=1:N} \left(\frac{2m_{ij}}{(\Delta t)^2} - k_{ij}\right) \ddot{u}_j(t-\Delta t) + \sum_{j=1:N} \left(-\frac{m_{ij}}{(\Delta t)^2} + \frac{c_{ij}}{2\Delta t}\right) \ddot{u}_j(t-2\Delta t) \end{array} \right\} \quad (2.9)$$

2.2.2 Formulation of time-series models

In this research, time series models are used to predict the above dynamic response of a structure. A brief description of time-series modeling is provided here. Further details about time-series models can be found in the literature [96-97].

The general form of the time-series model is known as the ARMAX model (Auto-Regressive Moving Average model with eXogenous inputs). This time series model to represent the relationship of input, output, and error terms of a system can be written as Eq. (2.10),

$$\begin{aligned} &y(t) + a_1 y(t-\Delta t) + \cdots + a_{n_a} y(t-n_a\Delta t) \\ &= b_1 u\left(t-\Delta t\right) + \cdots + b_{n_b} u(t-n_b\Delta t) + e(t) + d_1 e\left(t-\Delta t\right) + \cdots + d_{n_d} e(t-n_d\Delta t) \end{aligned} \quad (2.10)$$

where y(t), $u(t)$, and $e(t)$ are the output, input, and error terms, respectively, of the model, and $a_1, \ldots, a_{n_a}, b_1 \ldots, b_{n_b}, \ldots, d_1 \ldots, d_{n_d}$ are model parameters. It can be used in a more concise form as in Eq. (2.11),

$$A(q)y(t) = B(q)u(t) + D(q)e(t) \quad (2.11)$$

here, $A(q)$, $B(q)$, and $D(q)$ are the polynomials in the delay or backshift operator q^j including coefficients of the model as shown below in Eq. (2.12). A variable $U(t)$ at time t multiplied by q^j is equal to $U\left(t-j\Delta t\right)$.

$$\begin{aligned} A(q) &= 1 + a_1 q^{-1} + \cdots + a_{n_a} q^{-n_a} \\ B(q) &= b_1 q^{-1} + b_2 q^{-2} + \cdots + b_{n_b} q^{-n_b} \\ D(q) &= 1 + d_1 q^{-1} + \cdots + d_{n_d} q^{-n_d} \end{aligned} \quad (2.12)$$

The model orders are n_a, n_b, and n_d. The ARMAX process is shown using a block diagram in Figure 2.1.

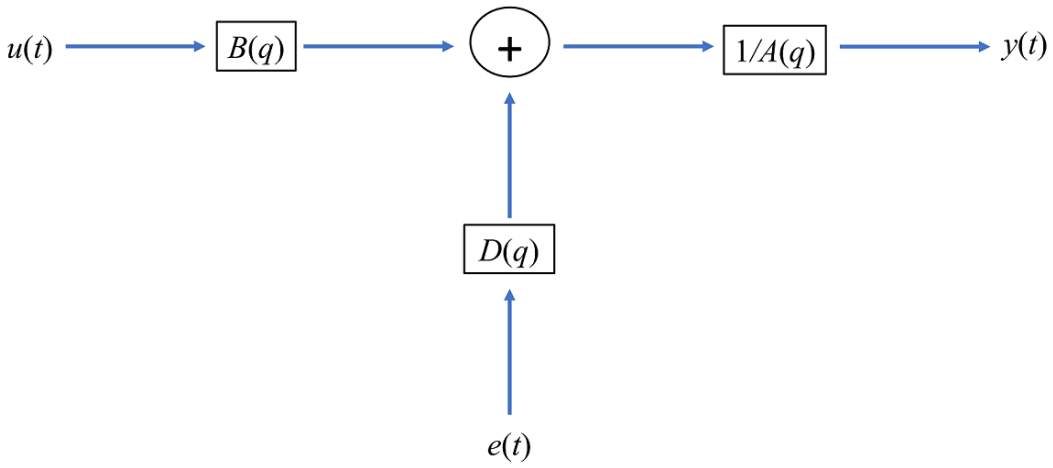

Figure 2.1 Block diagram of the ARMAX process (adapted from Ljung [96])

By changing the model orders, several other time series models can be formulated which are derived from the general ARMAX model. For instance, the AR model is formulated by setting the orders of n_b and n_d both to zero which is the simplest form of a time-series model. AR models can be used when there are no measured responses available to be used as exogenous input for the model, and therefore, the output at a previous time step is used to predict the output at the current time. The model is called a moving average model (MA model) if n_a and n_b are both set as zero. If only n_d is set to zero, an auto-regressive model with exogenous input (ARX) is obtained as shown in Eq. (2.13) and can be written more concisely in the form of Eq. (2.14)

$$y(t)+a_1 y(t-\Delta t)+\cdots+a_{n_a} y(t-n_a\Delta t)=b_1 u\left(t-\Delta t\right)+\cdots+b_{n_b} u(t-n_b\Delta t)+e(t) \quad (2.13)$$

$$A(q)y(t)=B(q)u(t)+e(t) \quad (2.14)$$

The ARX process is shown using a block diagram in Figure 2.2.

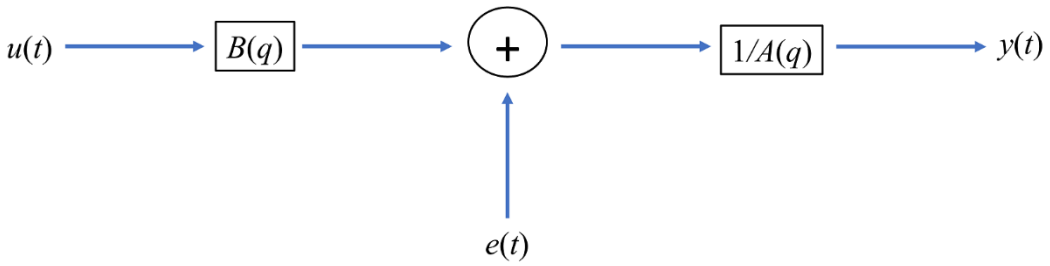

Figure 2.2 Block diagram of the ARX process (adapted from Ljung [96])

To apply the ARX model, the first step is to estimate the model parameters. Among various techniques, the least square criteria (LSC) is often used to estimate those parameters. The response of *y* at time *t* can be represented using data from previous time steps in the manner shown in Eq. 2.15.

$$y(t) = -a_1 y(t-\Delta t) - \cdots + a_{n_a} y(t-n_a\Delta t) + b_1 u\left(t-\Delta t\right) + \cdots + b_{n_b} u(t-n_b\Delta t) + e(t) \tag{2.15}$$

The predicted response of the *y(t)* can be calculated using Eq. 2.16.

$$y_p(t) = -a_1 y(t-\Delta t) - \cdots + a_{n_a} y(t-n_a\Delta t) + b_1 u\left(t-\Delta t\right) + \cdots + b_{n_b} u(t-n_b\Delta t) \tag{2.16}$$

Eq. (2.16) can be written in the form of Eq. (2.17),

$$y_p(t) = \delta^T(t)\alpha \tag{2.17}$$

where,

$$\delta(t) = [-y(t-\Delta t)\ldots - y(t-n_a\Delta t) \quad u(t-\Delta t)\ldots u(t-n_b\Delta t)] \tag{2.18}$$

$$\alpha = [a_1 \ldots a_{n_a} \quad b_1 \ldots b_{n_b}]^T \tag{2.19}$$

$\delta(t)$ consists of the time series vectors, and α includes the model parameters that are to be estimated. The error in predicted values of $y(t)$ can be estimated as:

$$e(t) = y(t) - y_p(t) = y(t) - \delta^T(t)\alpha \tag{2.20}$$

here, $e(t)$ is the error term in the ARX model and its value is related to the estimated model parameters. So, the least square criteria can be expressed as Eq. (2.21), where

S is the number of data points. This solution minimizes the error term. Derivation of other search methods can be found in the literature [96].

$$\alpha^{LS} = \left[\frac{1}{S}\sum_{t=1}^{S}\delta(t)\delta^{T}(t)\right]^{-1}\left[\frac{1}{S}\sum_{t=1}^{S}\delta(t)y(t)\right] \tag{2.21}$$

2.2.3 Development of sensor clusters

From Eq. (2.9), a model can be created to predict the output of the i^{th} DOF by using the response of other DOFs of the structure as inputs. Any change at a given location in this model can provide information about the change in properties of that region of the system. Similar equations can be written for each row and different models can be created for each DOF of the structure. In a real-life structure, there can be an infinite number of DOFs. However, its mass and stiffness matrices are both sparse matrices with the majority of the elements being zero. Therefore, the response generated from a particular DOF is related mostly to its adjacent DOFs. So, Eq. (2.9) can be considered as a sensor cluster with a reference DOF and its adjacent DOFs.

The method discussed above can be utilized to develop different sensor clusters. These models can then be used to extract damage-related features to identify, locate, and quantify the damage. To explain the method schematically, a simple 3-DOF system as shown in Figure 2.3 is considered. Here, *ü* represents acceleration responses of different channels of the system. Therefore, for the 3 DOF system, the sensor cluster consists of three reference channels. For each reference channel, the adjacent channels that are directly connected to it are included in the sensor cluster for the given reference channel. For the first sensor cluster, the reference channel is the 1st DOF whose output is predicted using the response of the DOFs of the same cluster that includes responses from DOFs 1 and 2. Similarly, the second sensor cluster is developed with 2nd DOF as the reference channel and includes DOFs 1, 2, and 3 in the cluster. To estimate the dynamic response of reference channels, data fitting tools such as time-series models can be utilized.

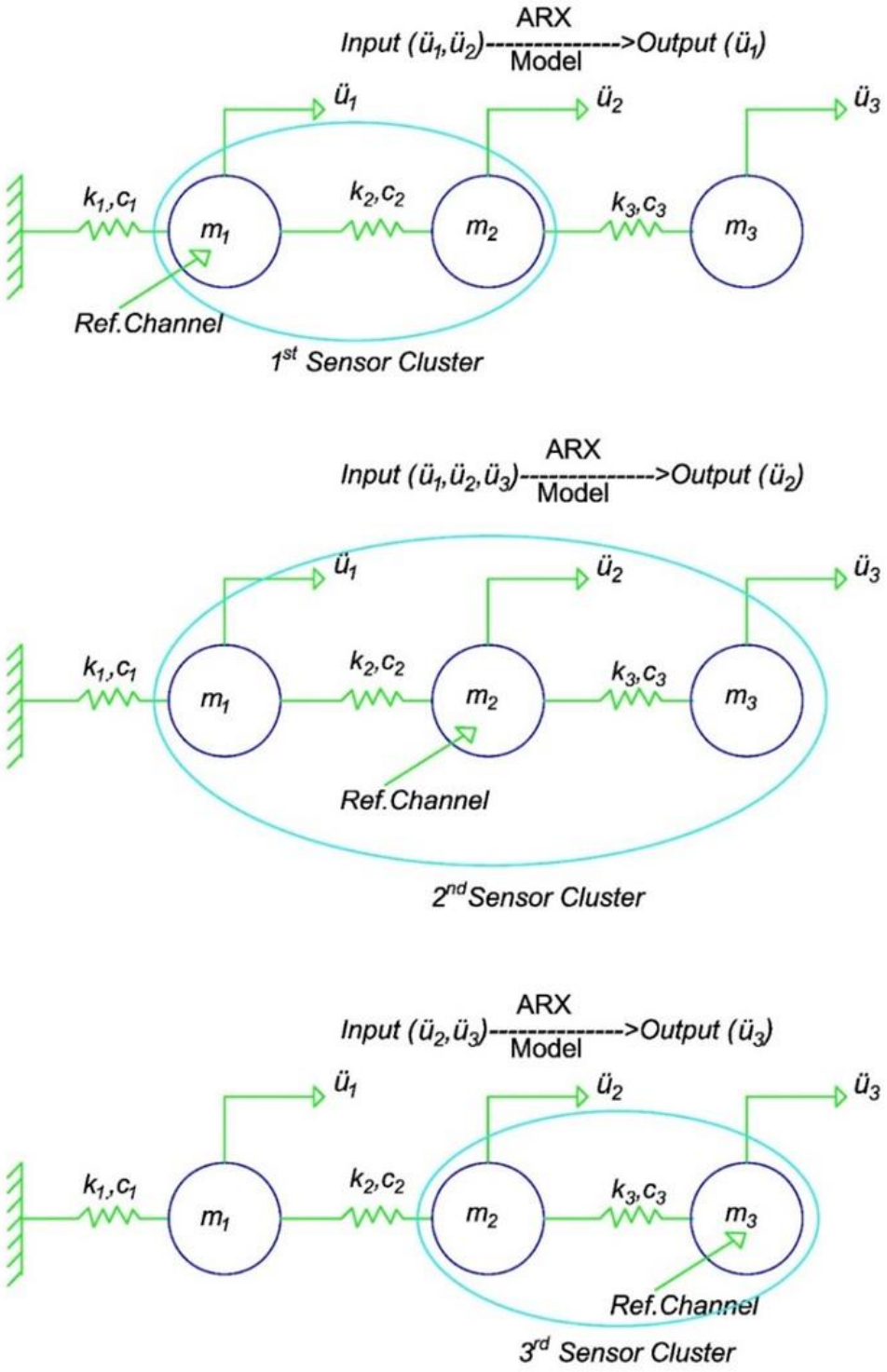

Figure 2.3 Different ARX models for each sensor clusters:(top) 1st sensor cluster, (middle) 2nd sensor cluster, (bottom) 3rd sensor cluster

In this research, the ARMAX model is used, since the measured responses from the adjacent channels are utilized as exogenous inputs to predict the response of the reference channels at the current time. Model orders are obtained directly from the EOM, by comparing the orders of Δt terms of Eq. (2.9) with those of Eq. (2.13). There are no Δt terms on the left side. Therefore, the order n_a for coefficients of output a_i fixed as 0. From Eq. (2.9) it is also seen that the input $\ddot{u}_j(t)$ consists of the term $2\Delta t$. Therefore, the order of n_b for the coefficients of input b_i is set as 2. The final form of the ARMAX equation is shown in Eq. (2.22). As can be seen, Eq. (2.22) looks similar in form as the Eq. (2.9), which indicates that the selected model could be used to predict the dynamic response of the reference channel. Similar ARMAX equations can be formulated for all the other DOFs in this manner.

$$\ddot{u}_i(t) = \sum_{j=1, j\neq i}^{N} b_{i,j}^1 \ddot{u}_j(t) + \sum_{j=1}^{N} b_{i,j}^2 \ddot{u}_j(t-\Delta t) + \sum_{j=1}^{N} b_{i,j}^3 \ddot{u}_j(t-2\Delta t) + e(t) + \ldots + d_{n_d} e(t-n_d\Delta t) \quad (2.22)$$

2.2.4 Fit ratios and damage features

The responses from the channels of each sensor cluster are analyzed using the ARX model to predict the output response of the particular reference channel of that cluster. After creating the ARX models for both the baseline and damaged conditions using the sensor cluster framework, damage features (DFs) are extracted from the ARX models to detect the damage. Therefore, different linear time series models can be created to establish models for each sensor cluster, and changes in these models can indicate the presence of damage, along with its location and severity.

For this study, DF is defined as the difference between fit ratios (FR). FR, in turn, is expressed in percentage as the normalized root mean squared error, as shown in Eq. (2.23), where y_m, y_p, and $\bar{y}_m$ are the measured output, predicted output, and mean of measured output data, respectively.

$$FR = \left(1 - \frac{\|y_m - y_p\|}{\|y_m - \bar{y}_m\|}\right) \quad (2.23)$$

The DF is calculated using Eq. (2.24). Here FR_1 is the fit ratio of the baseline bridge data to the baseline ARMAX model. FR_2 is the fit ratio obtained by fitting the damaged bridge response to the baseline ARMAX model. When the structure is damaged, the ARMAX model based on the baseline data cannot fit the damaged bridge data adequately enough (compared to the ARMAX models based on damaged data due to the changes in structural properties). Therefore, by comparing the differences in values of DFs between different DOFs, the presence, location, and relative severity of damage can be assessed.

$$DF = \frac{\left|FR_2 - FR_1\right|}{FR_2} \times 100 \tag{2.24}$$

2.3 Finite element model of the bridge

The railway bridge model developed for this study is a 22 m long single-span deck type steel plate girder bridge, as shown in Figure 2.4. The bridge consists of 2 main girders. The width of the bridge is 6.2 m center-to-center between the main girders. The bridge also features a concrete deck 150 mm thick and 5.4 m wide. The deck rests on 5 cross girders at equal distance to each other, with two of them at the abutments. The supports of the bridge are modeled as hinges that are fixed against translation but are free to rotate. The bridge modeling and analysis has been performed using software CSiBridge [98].

The depth of the main girders is 1,350 mm each. The top and bottom flange widths are 500 mm, while the flange and web thicknesses are 50 mm and 16 mm, respectively. The cross girders are 900 mm deep and have the same properties as the main girders. The material for both the main girder and diaphragm is ASTM A709 Gr50 steel. The deck material is 27.6 MPa normal weight concrete.

The bridge consists of a single track for the train. It has a typical Canadian Track gauge of 1.435 m. To represent train load, the COOPER E80 train, which is a standard train load for designing railway bridges in North America as per the

American Railway Engineering and Maintenance-of-Way Association (AREMA), is chosen.

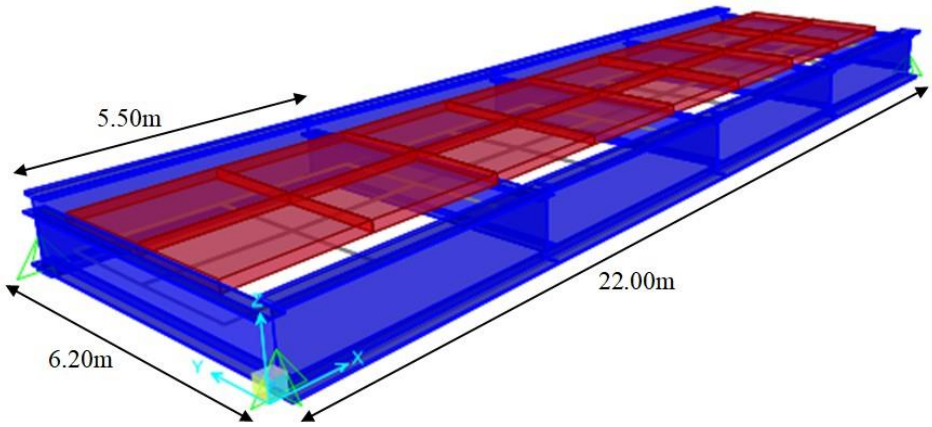

Figure 2.4 Finite element model of the railway girder bridge

As described above, a sensor cluster technique is used for damage detection of the bridge. For the bridge modeled in this study, all the joints/nodes between the main girder and diaphragms are considered locations of interests at which accelerometers are placed to obtain bridge response. (The accelerations of the support nodes are excluded from the model since these are very close to zero and cause instability in the ARX model.) To capture the presence of damage in the deck, accelerometers are also placed at the centers of each of the four-deck segments between the cross-girders. In total, 10 accelerometers are placed on the bridge (excluding supports). The positions of the accelerometers on the bridge are shown in Figure 2.5. The nodes, which are part of the main girder, are N1, N2, N3, N4, N5, and N6. The nodes that are placed on the deck are N7, N8, N9, and N10. Each node acts as a reference channel, the output of which is predicted using inputs from its adjacent channels. In total, ten different sensor clusters are created for each reference channel as described in Table 2.1.

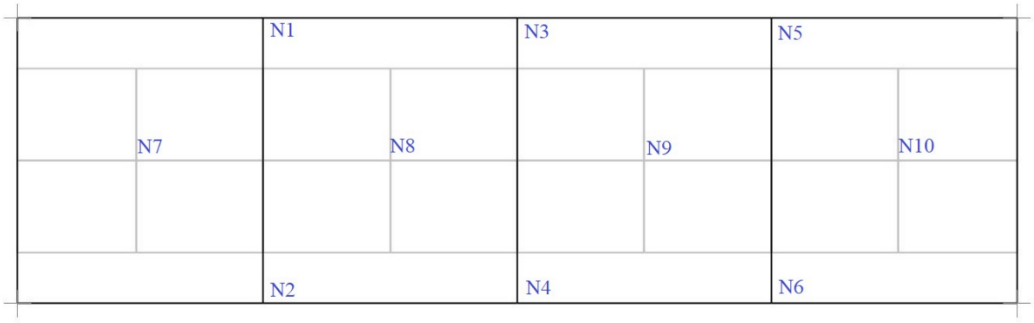

Figure 2.5 Node numbers of the bridge

Table 2.1 Sensor cluster design for the bridge

Sensor Cluster	**Output of the ARX Model** (Reference channel)	**Inputs to the ARX model** (Reference channel+ Adjacent channels)
1	N1	N1, N2, N3, N7, N8
2	N2	N1, N2, N4, N7, N8
3	N3	N1, N3, N4, N5, N8, N9
4	N4	N2, N3, N4, N6, N8, N9
5	N5	N3, N5, N6, N9, N10
6	N6	N4, N5, N6, N9, N10
7	N7	N1, N2, N7, N8
8	N8	N1, N2, N3, N4, N7, N8, N9
9	N9	N3, N4, N5, N6, N8, N9, N10
10	N10	N5, N6, N9, N10

In the proposed method, the bridge acceleration response from different sensors to train load is used as the input to the ARMAX model. The response is obtained in the form of vertical acceleration for the entire duration of the train passing over the bridge, plus additional free response after the train has fully crossed the bridge. The proposed method, it should be noted, is based on the free response of the bridge. As such, for this study, only the initial portion of the free-response is considered.

The train load is simulated as a series of axle loads moving at a specific speed while on the bridge. The responses are obtained at a frequency of 200 Hz (time step of 0.005 seconds), which is deemed adequate upon conducting a modal analysis of the bridge. The responses are obtained by performing linear time-history analysis with

a time step of 0.005 seconds. The moving train axle loads are positioned at the beginning of the bridge (support) at time zero and the response of the bridge is collected. Then the position of the train on the bridge at 0.005 seconds is calculated based on the speed of the train and again the responses of the sensors are calculated. In this manner, the response of the bridge is calculated at the specified frequency for the entire duration of the passage and then free vibration is calculated using the initial condition of the last position of the train on the bridge before the train is off the bridge. To collect the responses, the modal superposition technique is applied which combines the free vibration mode shapes to characterize displacement patterns. It is to be noted that, in this research, each train is modeled as a series of axle loads moving at a specific speed. The mass of the train is not considered during the dynamic time-history analysis. To consider the effect of the mass of train on the dynamic response of the bridge, detailed train-bridge interaction analysis is needed which is not within the scope of the present research. Further details regarding the process of the analysis are provided in the CSI analysis reference manual [98].

The performance of the presented method depends on the collection of useful bridge responses to the passage of a single operational vehicle at a time. In highway bridges, traffic movements are random; causing multiple vehicles passing over the bridge at a time. On the contrary, trains pass over railway bridges usually follows a fixed schedule and on a single-track bridge, only one train is present on the bridge at a time and there is a considerable gap between each passage of a train. Therefore, it is more practical to obtain useful free acceleration response in railway bridges after each passage of train compared to highway bridges, and as such the presented method is considered for railway bridges.

For the undamaged baseline case, the original train passes over the bridge at a speed of 20 km/h. The AREMA COOPER E80 loading consists of 2 cars. However, to account for the speed and train variability, it is assumed that, for each damage case, the train passes at a speed of 50 km/h and with one additional car added to the original configuration. The damping ratio of the bridge is kept constant at 1% for the dynamic time-history analysis. In the modeled bridge, the load from the train is

transferred to the main girders through the thick deck. Therefore, the vertical acceleration responses are high in amplitude for the sensors in the decks compared to the main girders. The typical total acceleration responses from the deck and the girder with the initial few seconds of free responses are shown in Figure 2.6.

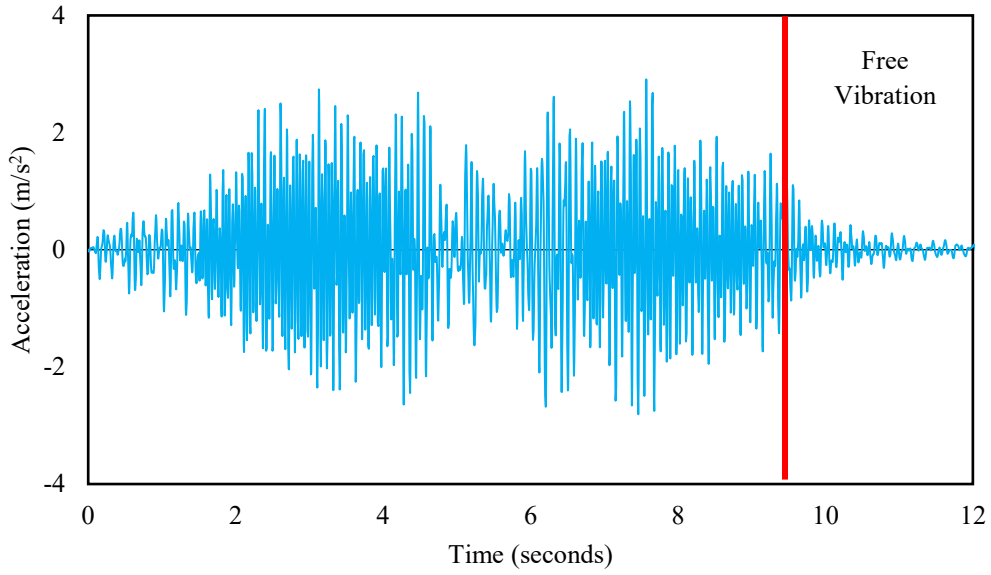

(a)

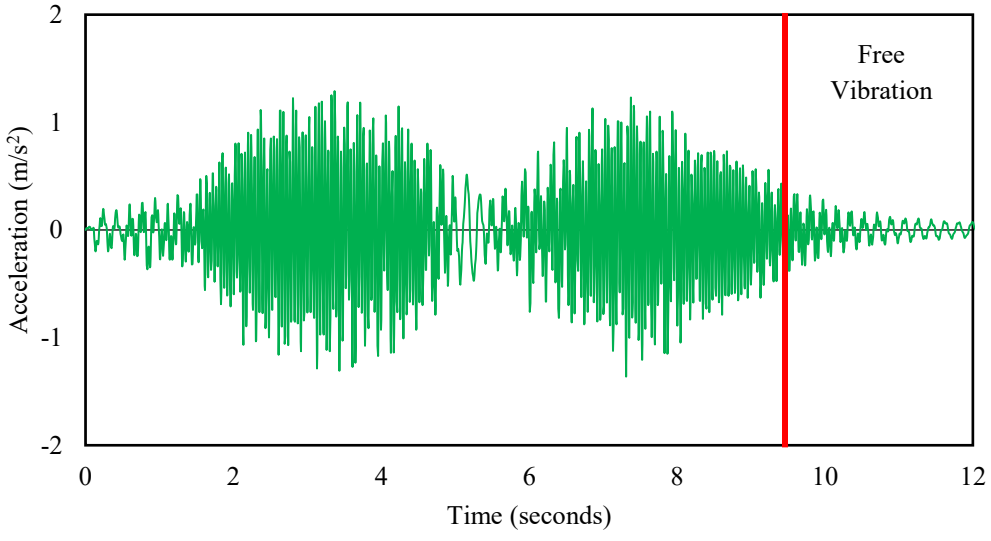

(b)

Figure 2.6 Vertical acceleration response of the baseline bridge to COOPER E80 train at 20 km/h: (a) from the deck (N8), (b) from the girder (N4)

In real-life applications, the structural responses are inevitably contaminated by the noise introduced by varying environmental, operational, and mechanical conditions. These noisy results can mask the effect of structural damage or can lead to false-positive alarms. To address the issue of data noise, 5% random noise is added to all the obtained responses artificially for the time-series analysis.

2.4 Analysis and results

2.4.1 Analysis of residual errors

A critical decision in time-series modeling is choosing the model order. Autocorrelation functions are often used to help choose model order [99,100]. Initially, the residual errors are computed from the baseline bridge. Residual errors are the differences between actual and predicted responses. Then autocorrelation is performed on the residual errors for different orders of moving average terms (n_d). Figure 2.7Figure 2.10 and Figure 2.8 show the autocorrelation results with 95% confidence limits for model orders of 0,1 and 2 for two nodes of the bridge (N1, and N3). It can be seen from that as the order of n_d increased from 0 to 1 and 2, the correlations function behave similarly to white noise. In theory, these values should decay, but it is clear from the figures they do not tend to zero. A possible cause of this effect due to the series not being infinite and can be ignored [100]. For both the nodes, the correlation functions are generally very small (within 95% confidence limit of +/- 0.075) even at n_d=0. These levels of residuals can be considered appropriate based on studies in the literature [100,101].

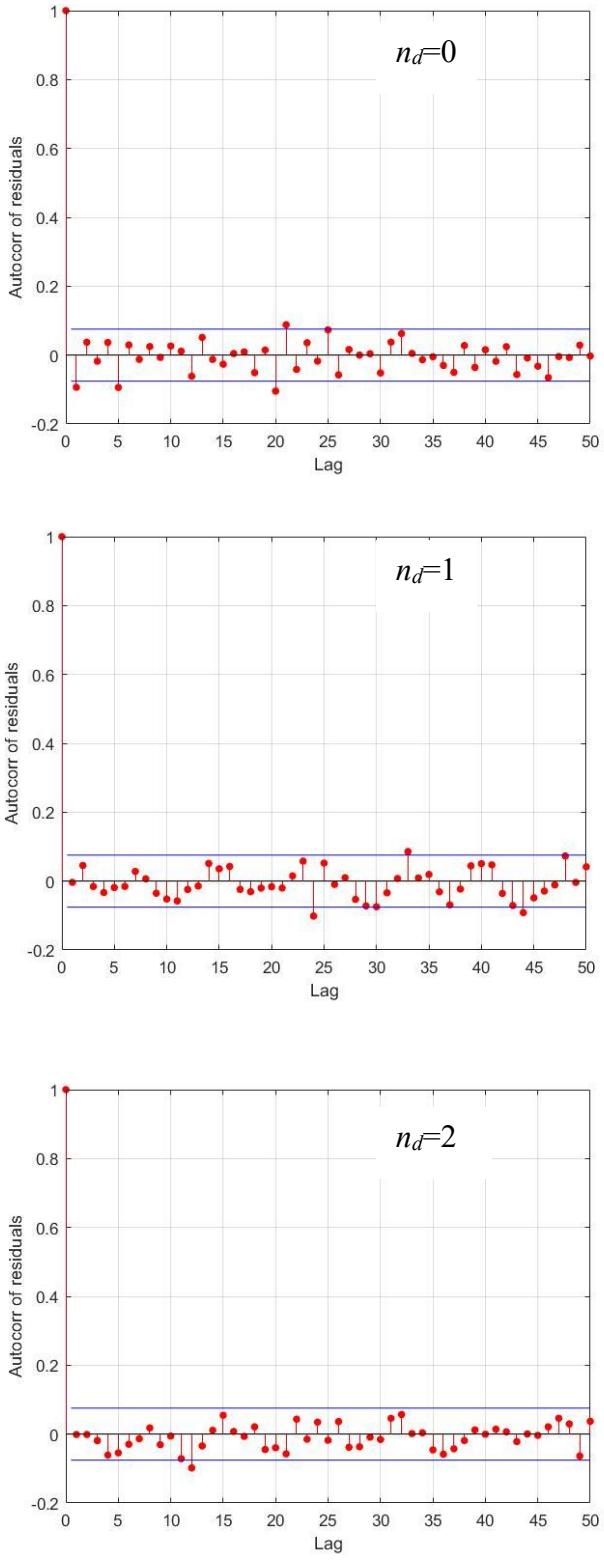

Figure 2.7 Correlation function of residuals by fitting time-series models at baseline bridge node N1

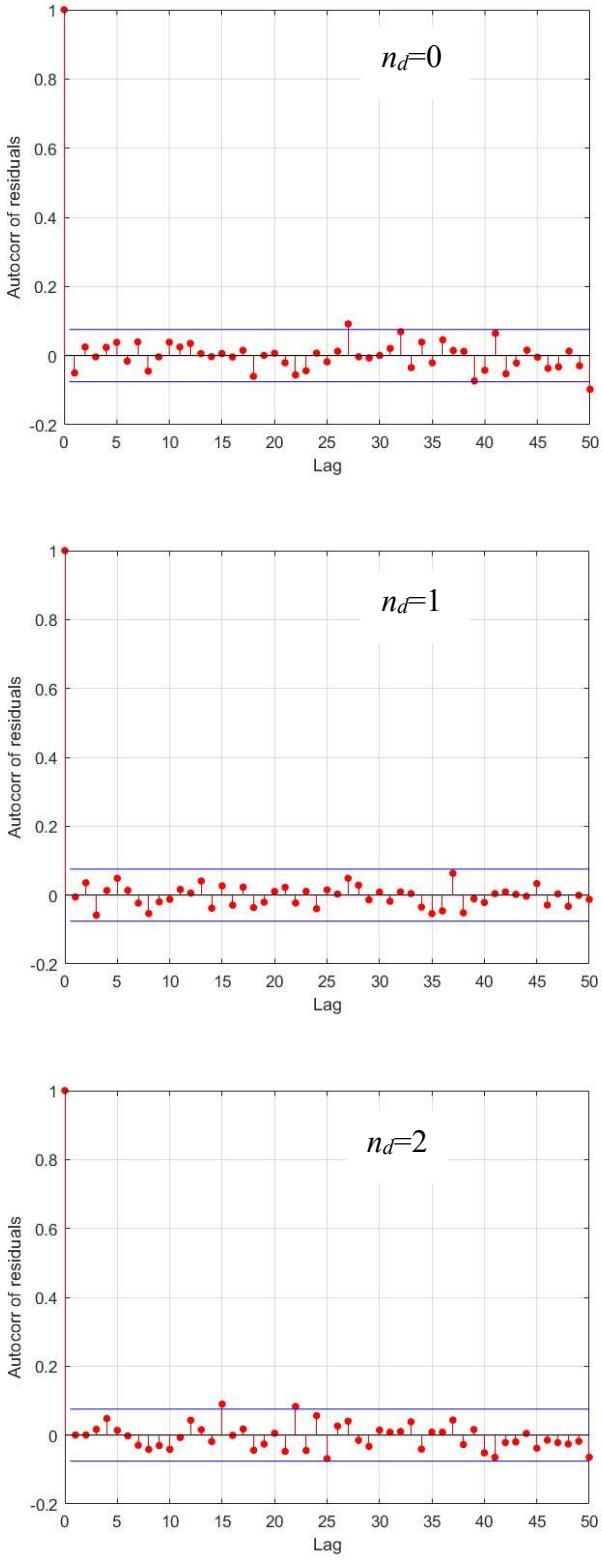

Figure 2.8 Correlation function of residuals by fitting time-series models at baseline bridge node N3

2.4.2 Estimation of threshold damage feature

Before damage identification, the threshold for DFs under noisy conditions should be established to ascertain the change in DF due to damage from the change resulting from noise. In this study, the threshold is determined by comparing the acceleration response obtained from the baseline bridge before any damage has been introduced. Two different acceleration responses for the baseline bridge are obtained from two trains (the original train and the modified train as mentioned in the model description) at speeds of 20 km/h and 50 km/h, respectively, contaminated by 5% random noise. These are then analyzed using the time-series method to obtain damage features (DF).

To create a statistically meaningful model, the whole process is repeated 300 times, and the 299th-highest DF among 300 DFs is selected as the threshold of damage based on the baseline bridge response to operational train loading to achieve a 99.7% confidence level. The threshold represents the highest DF caused by operational variability and measurement noise without the effect of any structural change. Therefore, any DF above this value is expected to indicate potential structural change. Such an approach minimizes false positives/false negatives in a real application, as shown by researchers [50-51]. In the present study, the value of this threshold is obtained at 0.43. So, for damage detection, any DF values above 0.43 are expected to indicate the presence of damage.

In a real-world application, if the proposed method is implemented on a newly constructed bridge, it will be able to identify all the future changes. If the proposed method is applied to an existing bridge, the method can still be applied considering the existing condition as a baseline for threshold estimation, and any subsequent damage could be identified. This method can also be applied to detect existing damage by applying model updating techniques, provided the original structural design details are available.

2.4.3 Damage identification, localization, and quantification

In the present study, different damage case scenarios on the railway bridge are considered. Based on numerous railway bridge events occurring during the period 1982–2010, a study by Otter et al. reported some of the major causes of damage as being derailed trains, foundation problems, fire, collision, and structural failure [22]. The rest of the accidents were due to natural hazards and environmental degradation. The study also found that failed and defective structural members pose a great risk to the performance of railway bridges. Indeed, damage cases involving failed and defective structural members and foundation problems cause a normalized annual risk exposure of around 8 million USD according to their study. All these types of reported issues can cause damage to the structural members through cracking, buckling, thickness loss, etc., resulting in strength and/or stiffness loss. Furthermore, with time, the deck can lose its thickness due to abrasion and weathering, and cracks can form in the concrete. This problem is simulated on the railway bridge model by reducing the modulus of elasticity of the affected girder and the deck; this approach is a common way to simulate damage as reported in various literature. Meanwhile, sometimes connections can lose their moment carrying capacity due to accidental removal of bolts, decaying of welds, etc. This is represented by forming a hinge at a connection. Foundation problems involve a change in boundary conditions caused by the corroded or blocked bridge supports that develop unintended fixity at the abutments. This problem is simulated by fixing the support. Also, sometimes supports settle due to scouring of the river floor, resulting in inactive support. The damage cases investigated in this study are described in Table 2.2 and illustrated in Figure 2.9. Each damage case has been analyzed 10 times and the corresponding DFs are plotted against the datasets.

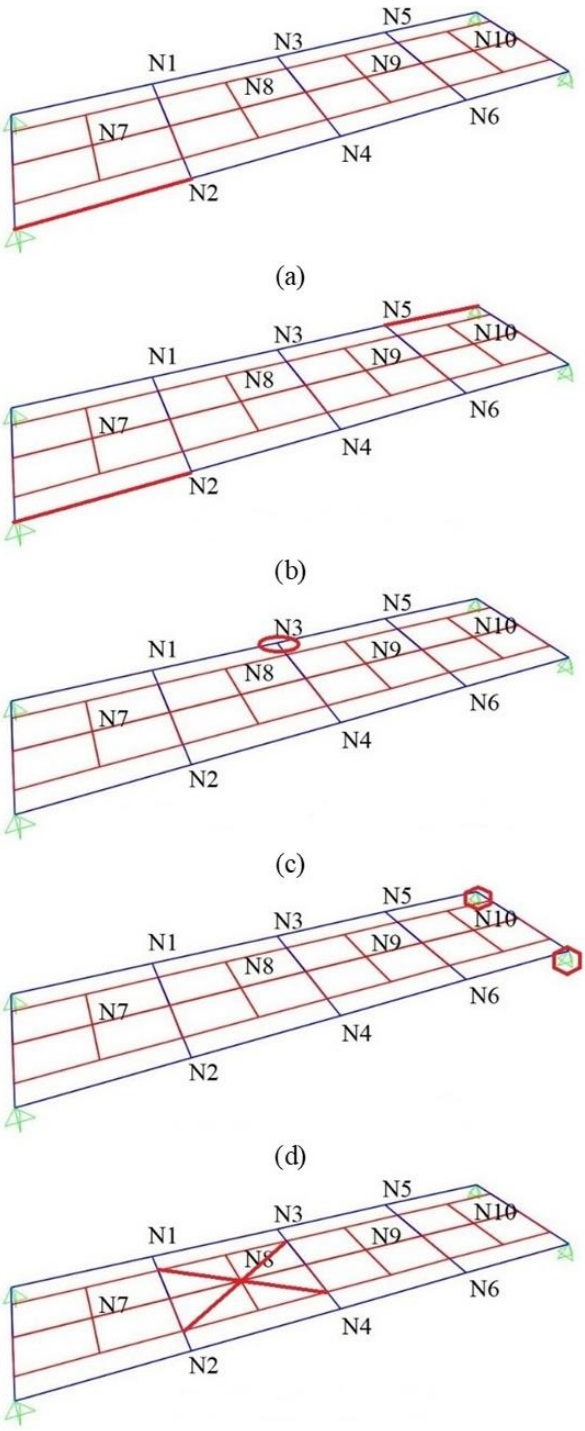

Figure 2.9 Damage cases investigated: (a) DC-1(a-d), (b) DC-1(e) (c) DC-2 (d) DC-3, (e) DC-4

Table 2.2 Description of the damage cases simulated in this study

Damage Case	Description of the damage
DC-1	Stiffness loss in the main girder portion between left abutment and N2 a) 10% b) 20% c) 30% d) 40% e) 30% loss applied to the same girder portion and also girder between N5 and right abutment
DC-2	Moment capacity loss (hinge formation) at N3
DC-3	Unintended fixity at the right supports
DC-4	20% stiffness loss in the deck portion marked by N8

2.4.3.1 Damage case (DC)-1: stiffness reduction in main girders

In this damage case, shown in Figure 2.9(a), for cases 1(a) to 1(d) the main girder section between the left support and N2 is assumed to have lost its stiffness by 10%, 20%, 30 %, and 40%, respectively. The damage features (DFs) for cases (a) to (d) are shown in Figure 2.10. For DC-1(a) the DFs for N2 are very close to the threshold value while all other DFs are below the threshold. For DC-1(b), the average of the DFs for N2 is around 1.5 (the same as for N4). The DFs for the other nodes on the girders are all above the threshold. Thus, this is a good indicator that damage has occurred, but, since there is no clear separation between N2 and N4, the likely location of the damage is identified as the entire girder rather than being close to N2 specifically.

Damage identification performance is much improved at damage levels of 30% and 40%. For cases 1(c) and 1(d), it can be observed that the highest DFs (maximum 3.5 for case 1(c) and 4.6 for 1(d)) are obtained for N2 since N2 is closest to the location of the damage. The DFs for N1 and N4 are smaller than those for N2 by at least 28% for case 1(c) and around 35% for 1(d) but are higher than those of all the other nodes. This is because N1 is connected to N2 by a cross girder, while N4 is a direct neighbor to N2 and is part of the same girder, which is damaged. For case 1(d), the DFs of N6 are also close to those of N1 and N4, owing to the increase in the damage severity resulting in the entire girder being affected. The DFs for all the other nodes are much lower compared to these three. For case 1(c) and 1(d), DFs on the decks are below the threshold indicating no damage to the deck. The plots

for cases 1(c) and 1(d) indicate that damage has occurred in the girder and that its location is likely near N2.

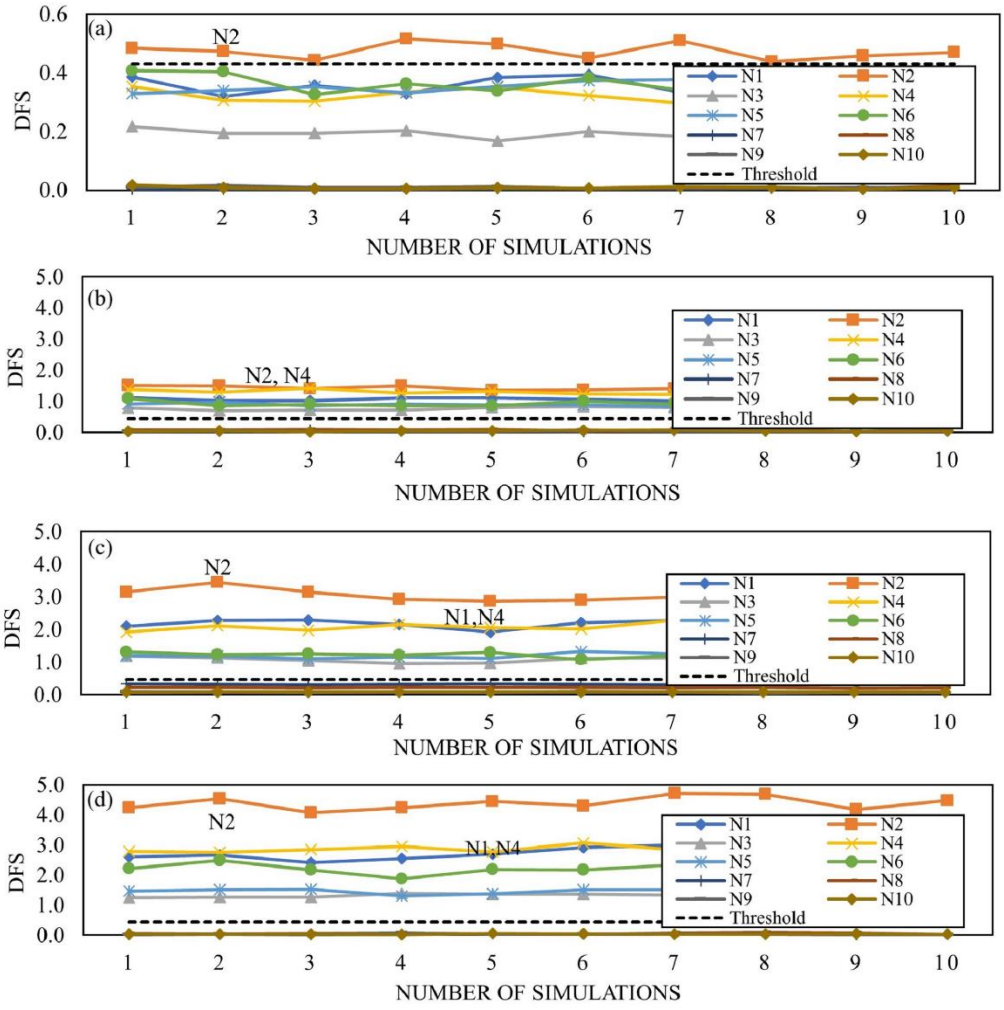

Figure 2.10 Damage features (DFs) for damage case DC-1: (a) 10% damage, (b) 20% damage, (c) 30% damage, and (d) 40% damage

In damage case 1(e), shown in Figure 2.9(b), 30% stiffness loss is applied to the previous section, and, also, 30% loss is applied to the girder portion between N5 and the right support. The DFs from different sensors for this case are shown in Figure 2.11. In this case, N2 and N5 exhibit the highest DFs (maximum around 3.5). This is expected since these two nodes are closest to the location of the damage. Other nodes of the main girder show lower DFs than do N2 and N5. The DFs for the sensors on the deck, meanwhile, are below the threshold. It is observable that the method is still able to detect and locate the presence of damage.

Since the severity of damage is 30%, which is the same as DC-1(c), the maximum DFs for N2 and N5 are similar to that of N2 in DC-1(c). Overall, it can be seen that, at a damage severity level 10% or more, the method performs effectively in detecting the presence of damage and as the damage severity increases, the location of the damage is identified with increased accuracy.

In a real-world application, it is not practical to monitor the vibration response from all the nodes. In such a situation, however, this method could still be useful and provide important diagnostic information regarding the presence of damage and its likely location, especially at moderate-to-severe damage cases in terms of the DFs of the closest monitored nodes.

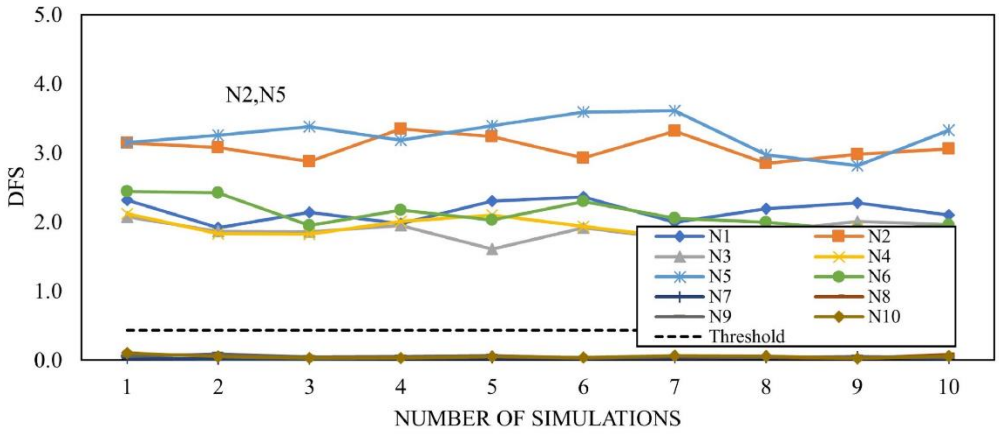

Figure 2.11 Damage features (DFs) for damage case DC-1(e)

2.4.3.2 Damage case (DC)-2: moment capacity loss at N3

The damage case, DC-2, is shown in Figure 2.9(c). In this damage case, the node, N3, in the left main girder is assumed to have lost its moment carrying capacity. The results obtained, illustrated in Figure 2.12, show that N3 has the highest DFs with a maximum of around 12.5, which is well above the threshold. For this damage case, N1 and N5 also show high DFs, but still approximately 35% smaller than those of N3. This can be considered a good result since N3 is the location of damage and N1, N3, and N5 are part of the same damaged girder. (If a hinge forms at any location of a girder, it is going to affect the moment distribution capacity of the

entire girder.) N4 is connected to N3 through a cross girder, and, as a result, it shows a relatively high DF compared to N2, N6, and the nodes on the deck. The nodes on the deck show DFs close to or below the threshold, indicating that there is likely no damage in the deck. Therefore, the method is successful in detecting the location of damage, which is close to N3.

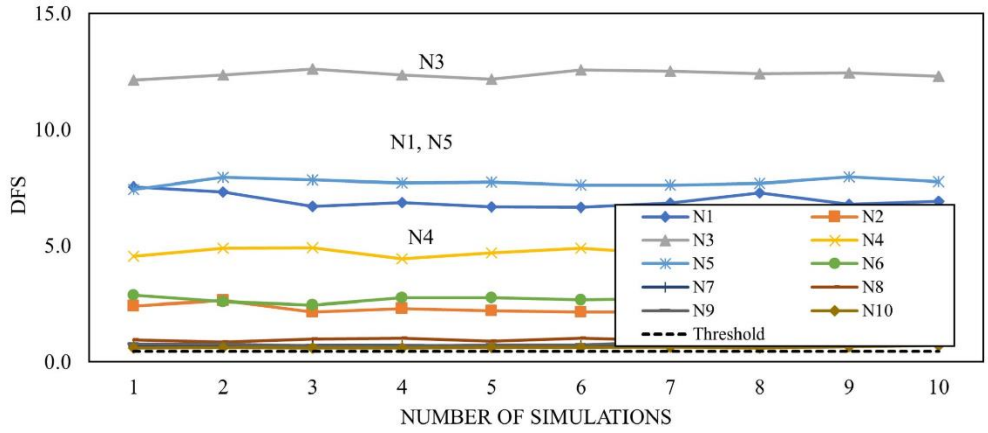

Figure 2.12 Damage features (DFs) for damage case DC-2

2.4.3.3 Damage case (DC)-3: unintended fixity at the right supports

The damage case, DC-3, is shown in Figure 2.9(d). In this damage case, the right abutment of the bridge is assumed to have become fixed support, while the original bridge supports have no rotational fixity to prevent shrinkage. The results (shown in Figure 2.13) demonstrate that the highest DFs are obtained at N5 and N6 and that these DFs are significantly higher (by an average of approximately 23) than previous damage cases. The results also show that the DFs at N3 and N4 are much higher than the threshold, but on average 40% lower than those of N5 and N6. N5 and N6 are the closest nodes to the restrained supports and hence have the highest DFs, while N3 and N4 are the closest neighbors to N5 and N6. The other DFs on the girders (N1 and N2) exhibit an average DF of around 6, which is still high in comparison to the threshold. Any change in the support restraint, it should be noted, affects the behavior of the entire bridge globally. The DFs of the nodes on the deck show there is no damage to the deck. Moreover, comparing the DFs with previous damage cases (DC-1 and DC-2), it can be observed that this is the most severe

damage case. Overall, the proposed method can identify, locate, and assess the severity of this global damage case.

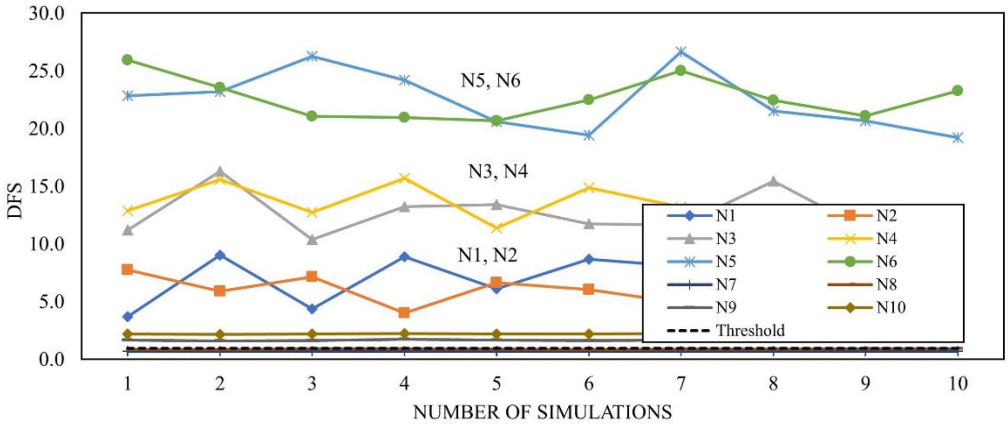

Figure 2.13 Damage features (DFs) for damage case DC-3

2.4.3.4 Damage case (DC)-4: damage to the deck

The damage case, DC-4, is shown in Figure 2.9(e). In this damage case, the portion of the deck indicated by N8 is assumed to have lost 20% of its stiffness. The results shown in Figure 2.14 demonstrate that the highest DFs (around 2.5) are obtained at N8, which is at the location of the damage. The results also show that all the other DFs are significantly lower than the DF at N8 and are close to the threshold. Therefore, the method predicts that there is damage and that it is likely in the deck portion with center node N8. It is to be noted that the DFs in this damage case are lower compared to the previous damage cases as 20% stiffness loss in a portion of the deck is not as critical as any kind of damage to the girder or support.

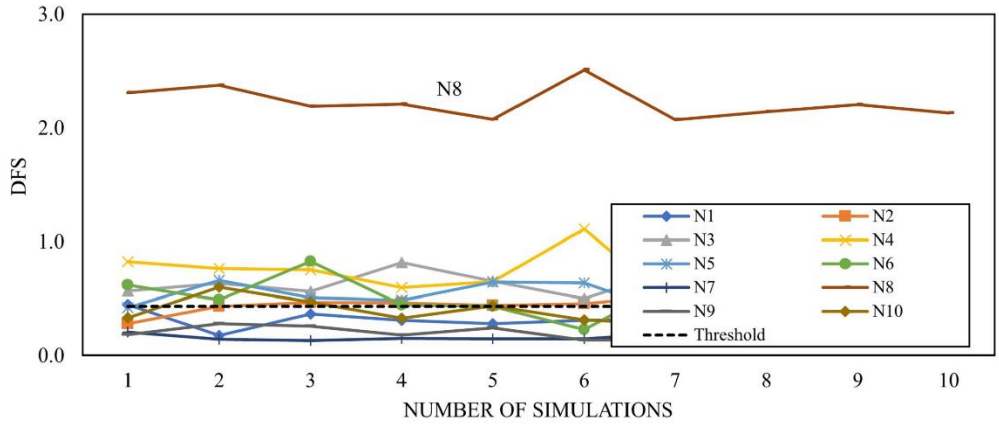

Figure 2.14 Damage features (DFs) for damage case DC-4

2.5 Conclusions

In this chapter, a damage detection method for girder type railway bridges is presented that analyzes operational acceleration response. The acceleration response is analyzed using time-series models and structural change is detected by comparing the measured acceleration response to the predicted response from the time-series model. The results demonstrate the potential of the proposed method for continuous condition assessment of steel girder railway bridges under operational loads. The major advantage of this method is that damage is detected, localized, and estimated using bridge response under operational train loading while considering the variability of train configuration, speed, and measurement uncertainty due to data noise. This method could be especially useful for detecting damage in inaccessible bridge locations where on-site testing could be difficult. Moreover, once the system is installed, continuous real-time monitoring is possible.

One of the limitations of the proposed method is that small localized damage, while identifiable, is difficult to locate accurately. The method assumes linear behavior of structure considering low levels of operational vibration. Furthermore, the effect of the train–track–bridge interaction is not considered in this study since the study is based on free response (i.e., when the train is off the bridge), and, therefore, the effects of such phenomena would be minimal on the proposed damage detection method. Finally, the effect of environmental condition changes on the measurement

error, which could affect the performance of the method as it affects all damage detection methods in the literature, is also not considered in this study. Despite such limitations, the method has great promise for practical implementation, and further research to address these limitations would improve its efficiency and robustness. Overall, the presented sensor-cluster-based damage detection method for health monitoring of railway bridges utilizing time series analysis of operational acceleration response is shown to be effective. The verification of this method using experimental results has been conducted and discussed in Chapter 5. The real-life application of this method is beyond the scope of this research.

3 DAMAGE DETECTION OF STEEL-TRUSS RAILWAY BRIDGES USING OPERATIONAL ACCELERATION DATA[2]

3.1 Overview

In Chapter 2, a damage detection method has been developed for railway steel-girder bridges which using only operational acceleration response in the vertical direction. This makes the potential implementation of the method simple for girder type railway bridges. However, railway bridges that utilize truss type structures that are more complex than a simple girder bridge system and it is observed that analysis of only vertical acceleration response is not adequate to identify damage in major truss elements. Therefore, in this chapter, an improved damage identification method is presented for steel-truss railroad bridges which utilize the same sensor-cluster principal presented in Chapter 2 but is based on analysis of bi-axial operational acceleration responses. The results are presented in terms of Damage Features from each sensor, which are obtained by comparing the actual acceleration response from the sensor to the predicted response from the time-series model. The damage in the bridge is detected by observing the change in damage features of the bridge as structural changes occur in the bridge. The relative severity of the damage can also be quantitatively assessed by observing the magnitude of the changes in the damage features. A finite element model of a steel truss railroad bridge is utilized to verify the method.

3.2 Theoretical derivation

The detailed derivation of the method has been provided in Chapter 2, Section 2.2.

3.3 Sensor-cluster network for time-series analysis

The procedure for employing the method for truss railway bridges will be explained using a detailed example by using a finite element model of a truss bridge which

[2] A modified version of this chapter has been published in the following journal as follows:
Azim, M.R., and Gül, M. (2020). Damage detection of steel truss railway bridges using operational vibration data. *Journal of Structural Engineering, ASCE,* 146(3), 04020008.
It can be accessed using DOI: **https://doi.org/10.1061/(ASCE)ST.1943-541X.0002547**

was built in CSiBridge [99]. The analyzed truss bridge is inspired by a bridge analyzed by Banerji and Chikermane [19]; however, it is not the same bridge. The actual bridge situated in India consists of 5 spans of 31.92 m center to center distance and 5.32 m width as well as height. Each span is divided into six commensurate parts each having a length of 5.32 m. These parts are longitudinally aligned to the track. In this study, only the 1st span is considered. In the finite element model, the abutment end of the bridge is supported by hinges while the pier end is supported by rollers. For simplicity of the model, it is assumed the supports are smooth with no frictional resistance to provide translational restraint only without inducing rotational restraint. All parts of the bridge consist of steel with a modulus of elasticity of 200 GPa, yield stress of 345 MPa, ultimate tensile stress of 448 MPa and a Poisson ratio of 0.3. According to Salcher et al. [102], the damping of steel truss bridges of 20m or more in length varied from 0.5% to 4.5% with mean damping for steel bridges being around 1.2%. Since the bridge investigated has a span length of 32m, the damping ratio of the bridge is assumed to be constant at 1.1 % for the dynamic time-history analysis. Different existing cross-sections of the structure are listed in Table 3.1. The bridge model is shown in Figure 3.1.

Table 3.1 Different steel sections of the truss bridge

Steel Profile	**Section Type**	**Bridge component**	**Section properties**	**Dimension (mm)**
HSS-200	Hollow Structural	Top and bottom chord bracing	Outside depth and width	200.0
			Flange and web	16.0
HSS-400	Hollow Structural	Diagonals	Outside depth and width	400.0
			Flange and web	20.0
I-500	Wide Flange Beam	Verticals & top chords	Outside height	500.0
			Flange width	300.0
			Flange thickness	28.0
			Web thickness	14.5
I-800	Wide Flange Beam	Bottom Chords	Outside height	800.0
			Flange width	300.0
			Flange thickness	33.0
			Web thickness	17.5

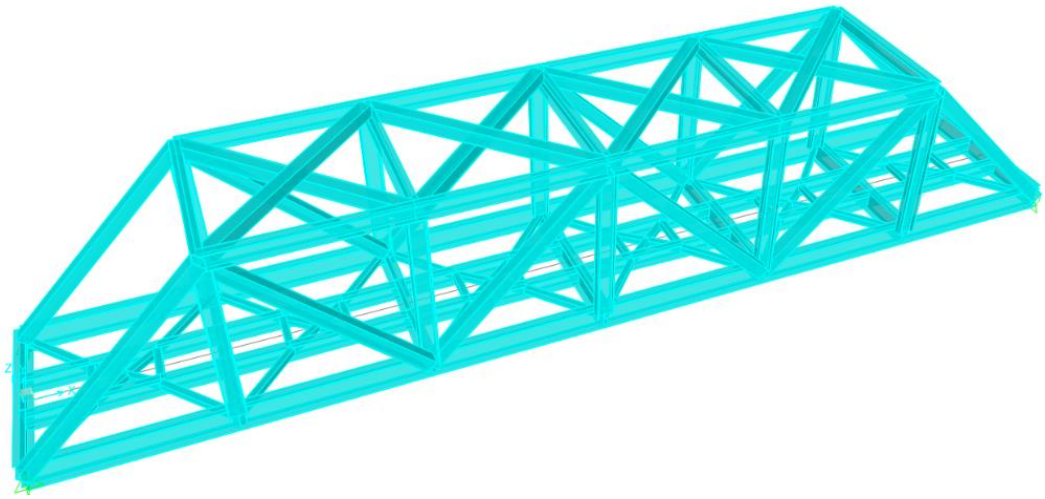

Figure 3.1 Finite element model of the bridge

From the derivation of the method presented in Section 2.2, it is observable that the response of a particular DOF can be predicted from the response of its adjacent DOFs. Therefore, develop different sensor clusters can be developed for different DOFs. These models can then be used to extract damage related features to identify, locate, and quantify the damage. For this bridge, 20 joints between top chords, bottom chords, verticals, and diagonals are considered locations of interests obtain bridge response.

The accelerations of the support nodes are excluded from the model since these are practically zero and cause instability in the ARMAX model. The position of assumed accelerometers in the bridge is shown in Figure 3.2. A bi-axial accelerometer is assumed to collect data at each join in vertical and longitudinal directions. A total of 40 sensor clusters are created for 40 channels. While each channel acts as a reference channel (output of ARMAX model) for a sensor cluster, the adjacent channels for each sensor cluster are determined based on their connectivity, which is explained in detail in the following paragraphs.

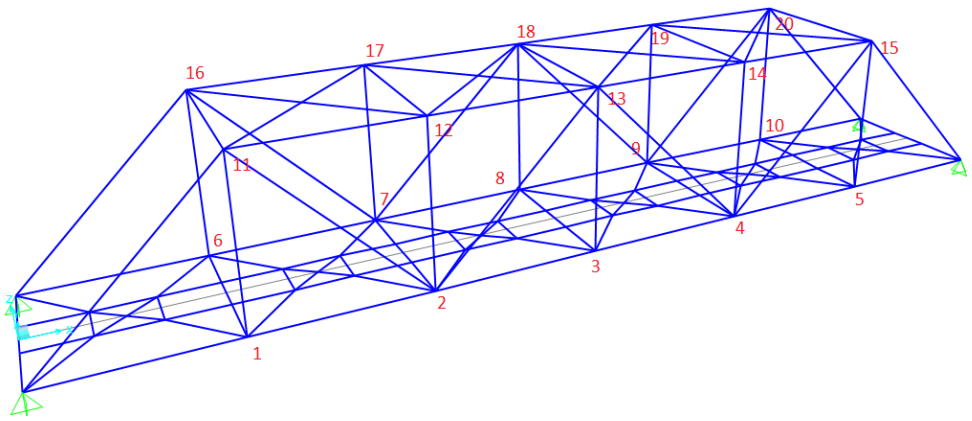

Figure 3.2 Node numbers for the bridge for developing sensor cluster

Two separate sensor cluster systems are implemented: One cluster is based on vertical DOFs and the other cluster is based on longitudinal DOFs. For the former system, vertical acceleration responses and for the latter longitudinal acceleration responses are utilized for the time series analysis. The philosophy is that trusses carry the load mainly through the axial force transfer mechanism. Therefore, any structural change in the members aligned in vertical and longitudinal directions will result in high DFs in the corresponding cluster systems. So, any damage in a vertical member should show high DFs in the vertical cluster analysis and no damage in the longitudinal cluster system. Similarly, damage in the top and bottom chords will show high DFs in the longitudinal cluster only. The diagonal members have both vertical and longitudinal directional components and hence should indicate the presence of damage in both the clusters. The transverse bracings, which do not have vertical and longitudinal components are usually not effective during operational train loading and therefore not considered in this study. A separate cluster using transverse acceleration (caused by transverse loading, e.g. wind) could be developed to detect damage in those members.

For the vertical cluster system, each assumed vertical sensor (denoted with initial ‘V’) act as a reference channel. The response of each reference channel is predicted using ARMAX analysis of the output of the adjacent channels. Here, all nodes (including the reference channel itself) which are connected to the reference channel through a vertical and/or a diagonal member is included in the ARMAX

model as inputs. For example, when V1 is the reference channel, the input channels to the model channel are V1 and V11, while for V2, the input channels are V2, and V11, V12, and V13. For the longitudinal cluster system, similarly, each assumed longitudinal sensor (denoted with initial 'L') acts as reference channel the response of which is predicted using ARMAX analysis of the output of the adjacent channels. Here, all sensors (including the reference channel itself) which are connected to the reference channel through a longitudinal and/or diagonal as well as a longitudinal bracing member is included in the ARMAX cluster. For example, when L1 is the reference channel, the input channels to the ARMAX model are L2 and L7, while for L2, the input channels are L1, L2, L3, L6, L8, L11, and L13. These clusters are shown in Table 3.2.

Vertical and longitudinal acceleration responses are obtained from each node of the bridge as the train crosses the bridge. The response is obtained for the entire duration the train is over the bridge plus the initial few seconds of the free response after the train fully crossed the bridge.

In this study, for the baseline case, the original train crosses the bridge at 40 km/h speed. The AREMA COOPER E80 loading consists of 2 cars. To account for the speed and train variability, different train load and speed are used for the damage cases. It is assumed that for each damage case, the train passes at 50 km/h speed and with the 2nd car carrying 25% more load than the original configuration. The damping ratio of the bridge is kept constant at 1.1 % for the dynamic time-history analysis.

Table 3.2 Sensor cluster network for the truss bridge

Vertical Sensor Clusters		**Longitudinal Sensor Clusters**	
The output of the ARMAX model (Reference channel)	**Inputs to the ARMAX model** (Reference channel+ Adjacent channels)	**The output of the ARMAX model** (Reference channel)	**Inputs to the ARMAX model** (Reference channel+ Adjacent channels)
V1	V1, V11	L1	L1, L2, L7
V2	V2, V11, V12, V13	L2	L1, L2, L3, L6, L8, L11, L13
V3	V3, V13	L3	L2, L3, L4, L7, L9
V4	V4, V13, V14, V15	L4	L3, L4, L5, L8, L10, L13, L15
V5	V5, V15	L5	L4, L5, L9
V6	V6, V16	L6	L2, L6, L7
V7	V7, V16, V17, V18	L7	L1, L3, L6, L7, L8, L16, L18
V8	V8, V18	L8	L2, L4, L7, L8, L9
V9	V9, V18, V19, V20	L9	L3, L5, L8, L9, L10, L18, L20
V10	V10, V20	L10	L4, L9, L10
V11	V1, V2, V11	L11	L2, L11, L12, L17
V12	V2, V12	L12	L11, L12, L13, L16, L18
V13	V2, V3, V4, V13	L13	L2, L4, L12, L13, L14, L17, L19
V14	V4, V14	L14	L13, L14, L15, L18, L20
V15	V4, V5, V15	L15	L4, L14, L15, L19
V16	V6, V7, V16	L16	L7, L12, L16, L17
V17	V7, V17	L17	L11, L13, L16, L17, L18
V18	V7, V8, V9, V18	L18	L7, L9, L12, L14, L17, L18, L19
V19	V9, V19	L19	L13, L15, L18, L19, L20
V20	V9, V10, V20	L20	L9, L14, L19, L20

3.4 Analysis and results

The analysis results are discussed in the subsequent sections. The results are displayed in terms of DFs vs Simulations, where each data set corresponds to DF obtained at a particular simulation. Each damage case is simulated 6 times with an added artificial noise applied as 5% of maximum normalized root mean square (RMS) of the acceleration response.

3.4.1 Damage cases analyzed

An article on the need for railway bridge health monitoring by investigating incidences of railway bridge interruptions in the U.S. was published by Otter et al. [22]. Based on 177 railway bridge-related events that occurred between 1982 and 2010, the study reported that more than 22% of the accidents were caused by damage due to derailed train while scouring and other foundation problems accounted for 13.5% accidents. 6.8% of accidents were caused by fire damage, 5.1% were due to collision by railroad traffic and 4.5% were due to structural member failure. The rest of the accidents were due to other hazards including environmental degradation. The study also found that failed and defective structural members pose a great risk towards the performance of railway bridges.

All these types of issues reported can cause damage to the structural members through cracking, buckling, thickness loss, etc. which results in strength and/or stiffness loss. In this study, the damage associated with stiffness reduction of truss members will be presented. This damage is simulated on the railway bridge model by reducing the modulus of elasticity of the affected member. All these damage cases are described in Table 3.3. These damage cases and the damaged members are visually shown in Figure 3.3 and Figure 3.4.

Table 3.3 Damage cases investigated in this study

Damage Case	Damage location and severity
DC-1	Vertical members between nodes 1-11 and 6-16: i) 20% and ii) 30% stiffness loss
DC-2	Longitudinal members between nodes 1-2 and 6-7: i) 20% and ii) 30% stiffness loss
DC-3	Diagonal members between nodes 2-13 and 7-18: 30% stiffness loss
DC-4	Longitudinal member between nodes 6-7 and vertical member between nodes 2-12: 30% stiffness loss
DC-5	Vertical member between nodes 2-12 and diagonal member between nodes 7-18: 30% stiffness loss
DC-6	Longitudinal member between nodes 14-15 and bracing member between nodes 12-18: 30% stiffness loss in both members

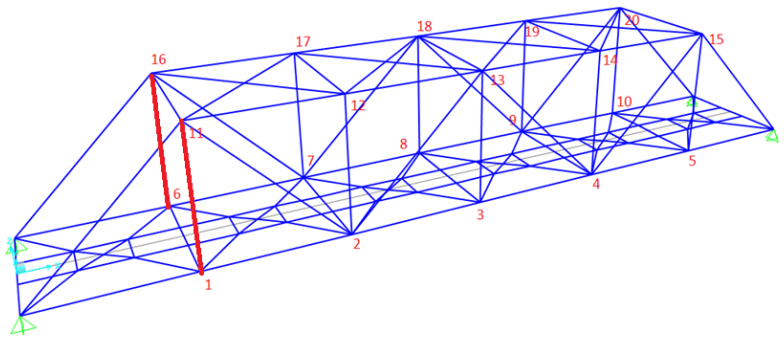

(a)

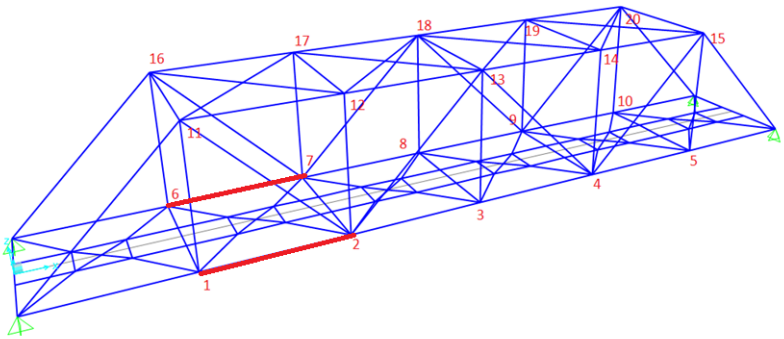

(b)

Figure 3.3 Damage Cases analyzed: (a) DC-1, (b) DC-2

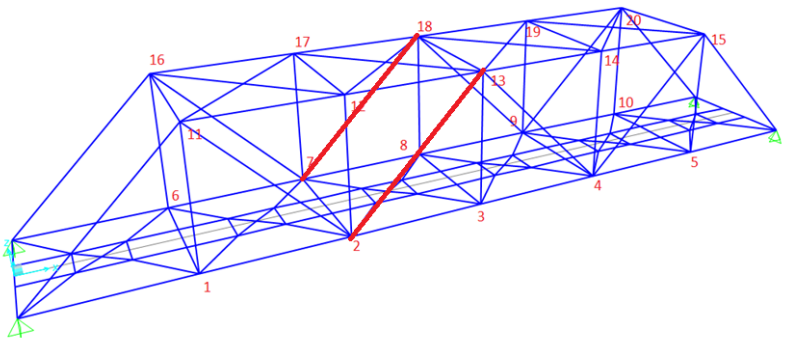

(a)

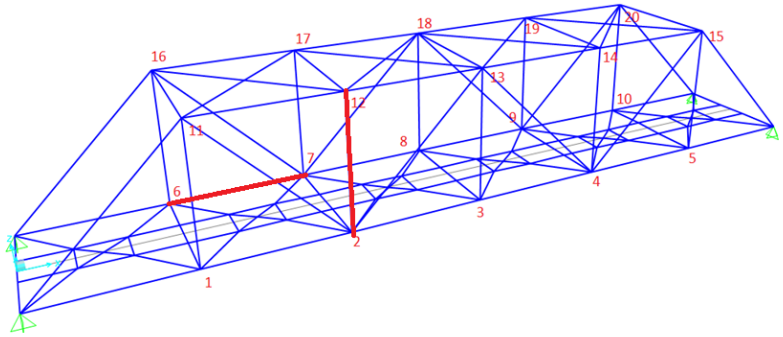

(b)

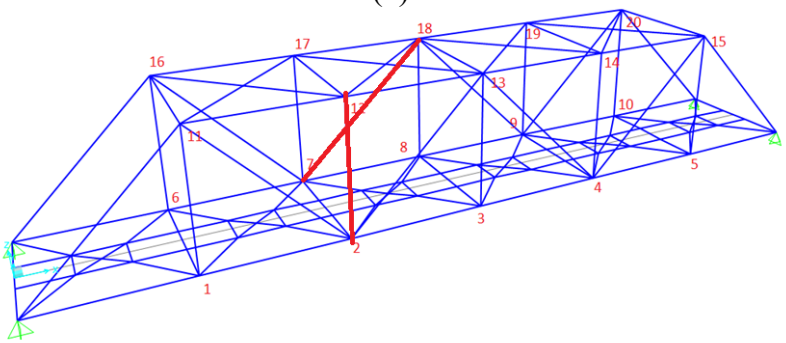

(c)

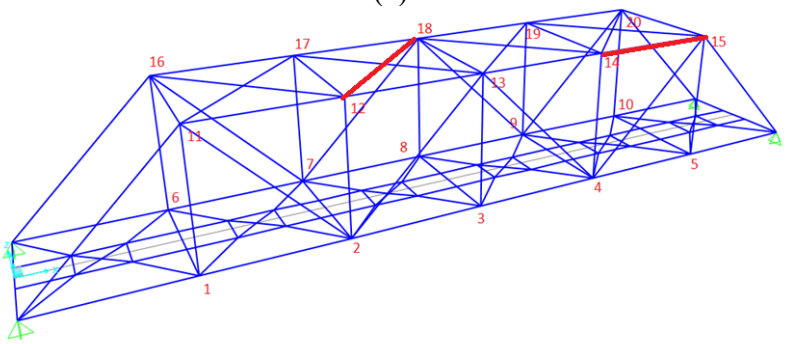

(d)

Figure 3.4 Damage Cases analyzed: (a) DC-3, (b) DC-4, (c): DC-5, (d) DC-6

3.4.2 Estimation of threshold damage feature

In this study, it is assumed that the obtained responses contain artificial noise. Therefore, before any damage identification, a threshold for DFs needs to be established to separate the change in DFs due to actual damage to those caused by noise.

To establish the threshold, two sets of acceleration responses from the baseline bridge are obtained. The first set is with an original train at 40 km/h speed while the second set is with a modified train at 50 km/h speed. These data are then simulated 200 times and damage features are obtained for each simulation. In this case, the damage features obtained based on the difference of fit ratios are the effect of measurement noise without the presence of damage. Based on 200 simulations on the baseline bridge, values of 0.31 and 1.43 are obtained as thresholds with a 99.0% confidence level for vertical cluster and longitudinal cluster respectively meaning that the likelihood of DF exceeding the threshold without damage in the bridge is only 1%. So, any DF above these values will be considered as indicative of damage in the corresponding clusters.

In a real-world application, if the proposed method is implemented on a newly constructed bridge, it will be able to determine all the future changes. If it is applied to an already existing bridge, the method can still be applied considering the existing condition as a baseline for threshold estimation and any damage onwards could be identified.

3.4.3 Sensor cluster analysis for various damage cases

The vertical and longitudinal cluster system in combination is utilized to detect damage in various members which are discussed in the subsequent articles.

3.4.3.1 Damage case DC-1: vertical members between nodes 1-11 and 6-16: (i) 20% stiffness loss (ii) 30% stiffness loss

In this damage case, the vertical member between nodes 1-11 and 6-16 are assumed to have lost (i) 20% and (ii) 30% of its stiffness. The Damage Feature (DFs) for the

case are shown in Figure 3.5 and Figure 3.6 for case 1(i) and case 1(ii) where (a) and (b) represent results from the vertical and longitudinal cluster, respectively.

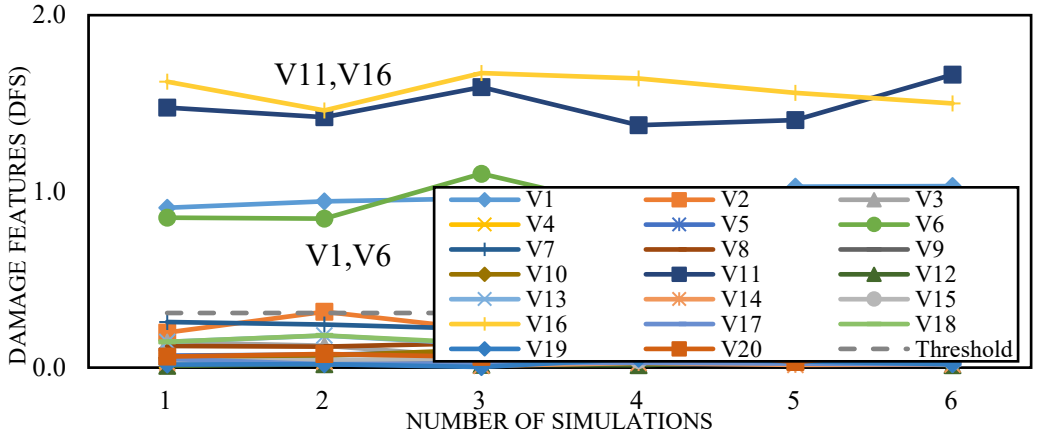

(a)

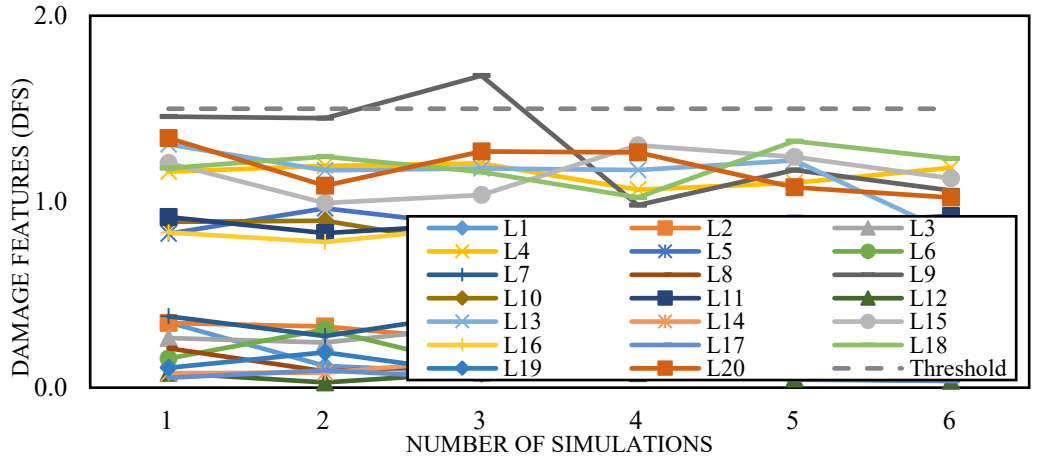

(b)

Figure 3.5 Damage Features (DFs) for DC-1(i): (a) Vertical Cluster, (b) Longitudinal Cluster

It can be observed that the highest DFs are obtained for V11 and V16, followed by V1 and V6 for both 20% and 30% damage levels. From vertical cluster analysis, for 20% damage shown in Figure 3.5(a), the average of DFs for V11 and V16 is around 1.53, while an average of 0.92 is obtained for V1 and V6. For 30% damage shown in Figure 3.6(a), the DFs increase to average values of 3.50 for V11 and V16 and 1.99 for V1 and V6 respectively. These four nodes exhibit significantly higher DFs compared to the DFs of the rest of the nodes which are close to or below the threshold. The longitudinal clusters show that all the DFs are very close to or below

the threshold indicating that no damage likely in the longitudinal direction. Overall, by observing the DFs of both vertical and longitudinal clusters, it can be inferred that damage is present and its likely location is in the vertical members between nodes 1-11 and 6-16. The results also show that the presented method can relatively quantify the severity of damage levels.

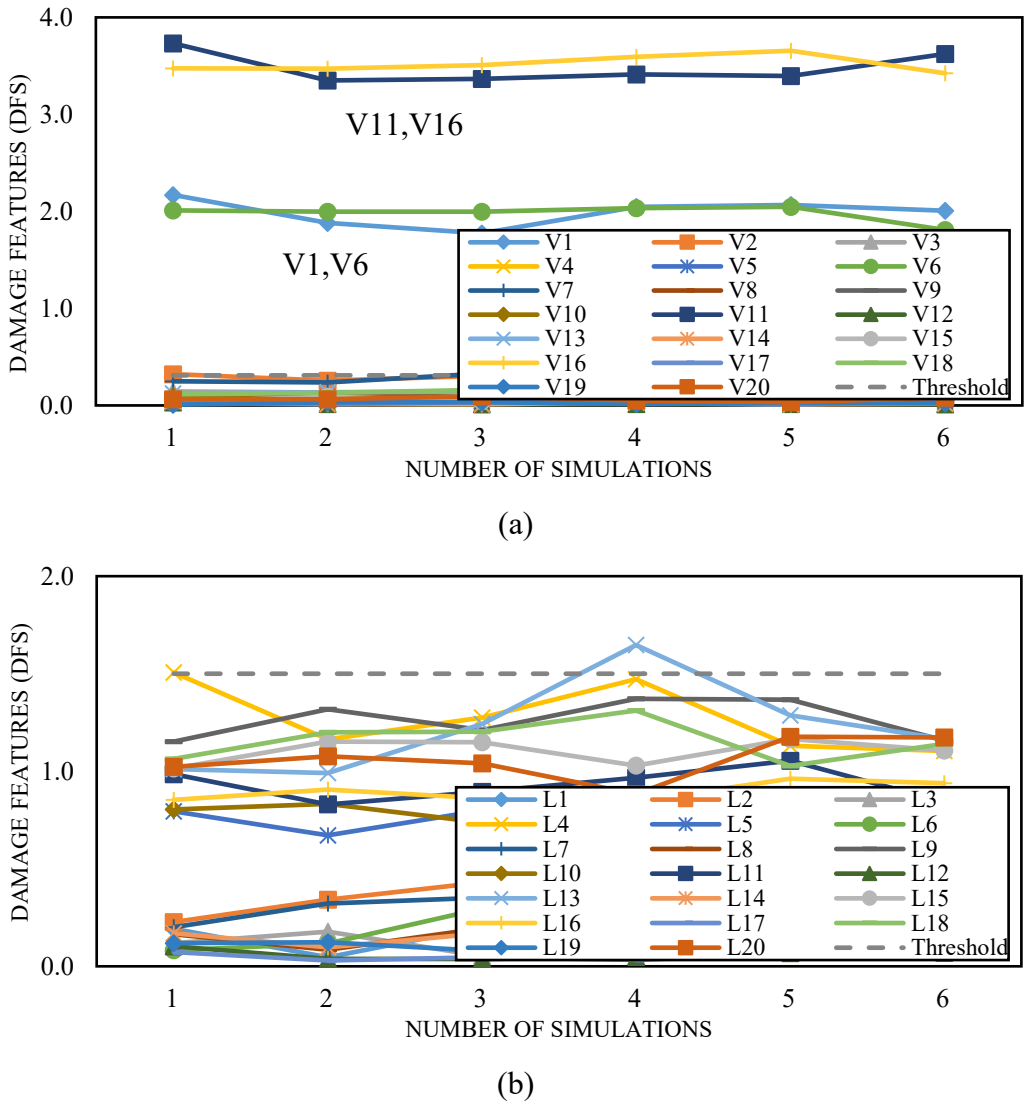

Figure 3.6 Damage Features (DFs) for DC-1(ii): (a) Vertical Cluster, (b) Longitudinal Cluster

3.4.3.2 *Damage case DC-2: longitudinal members between nodes 1-2 and 6-7: (i) 20% stiffness loss (ii) 30% stiffness loss*

In this damage case, the longitudinal members between nodes 1-2 and 6-7 are assumed to have lost stiffness by (i) 20% and (ii) 30%. The Damage Feature (DFs) for this case are shown in Figure 3.7 and Figure 3.8 for case 2(i) and case 2 (ii) where (a) and (b) represent results from the vertical and longitudinal cluster, respectively.

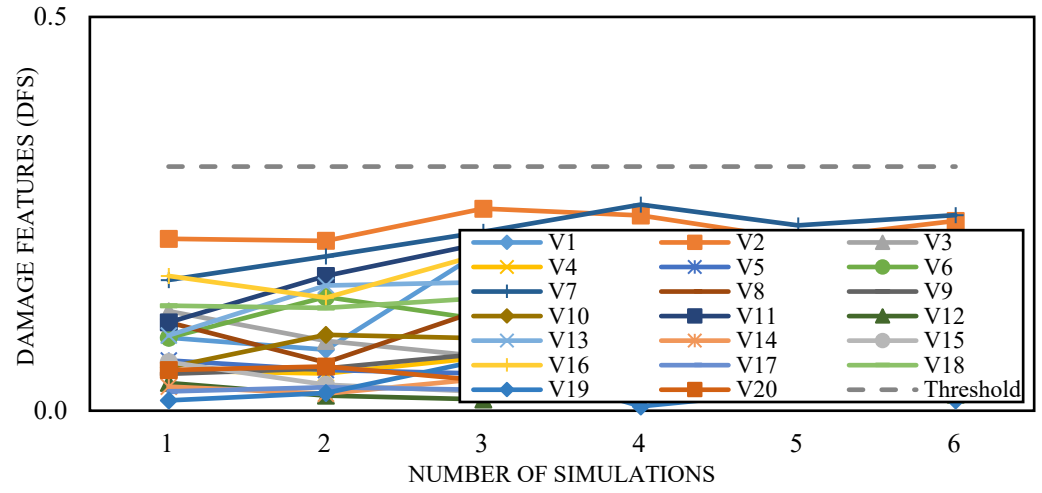

(a)

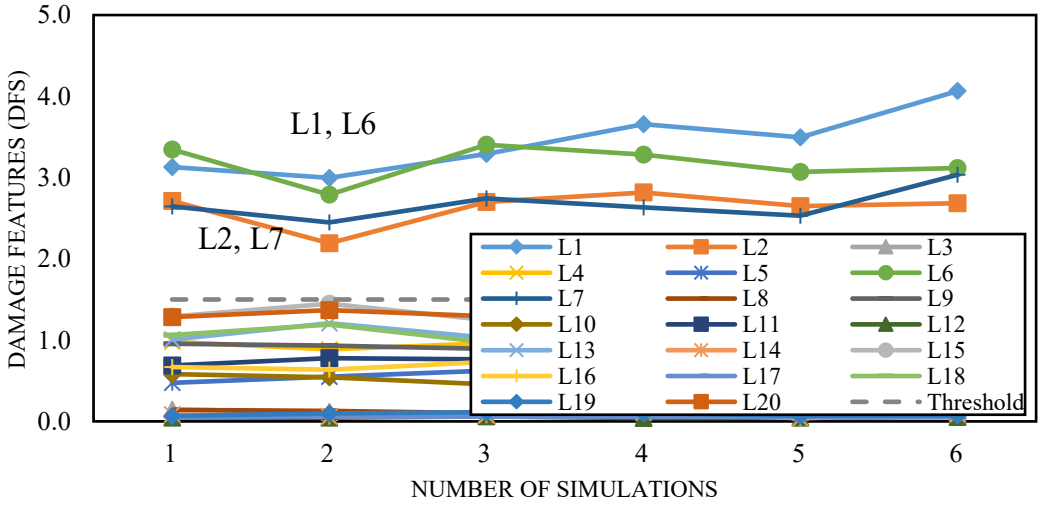

(b)

Figure 3.7 Damage Features (DFs) for DC-2(i): (a) Vertical Cluster, (b) Longitudinal Cluster

It can be observed that the average DFs for vertical clusters shown in Figure 3.7(a) and Figure 3.8(a) are all very close to or below the threshold value indicating that no damage is likely in the vertical system for both levels of damage. In the longitudinal system shown in Figure 3.7(b) and Figure 3.8(b), the highest DFs are obtained for L1 and L6 with an average value of 3.30 and 6.99 for 20% and 30% damage levels, respectively. Nodes L2 and L7 exhibit DFs around 2.65 and 4.96, respectively. The average DFs for the rest of the nodes are close to or below the threshold. This is indicative of the fact that damage is present and its likely location is in the longitudinal members between nodes 1-2 and 6-7 with no damage occurred elsewhere. Similar to Damage Case 1, the relative severity of damage is assessed by observing the increase in DF values of the affected members.

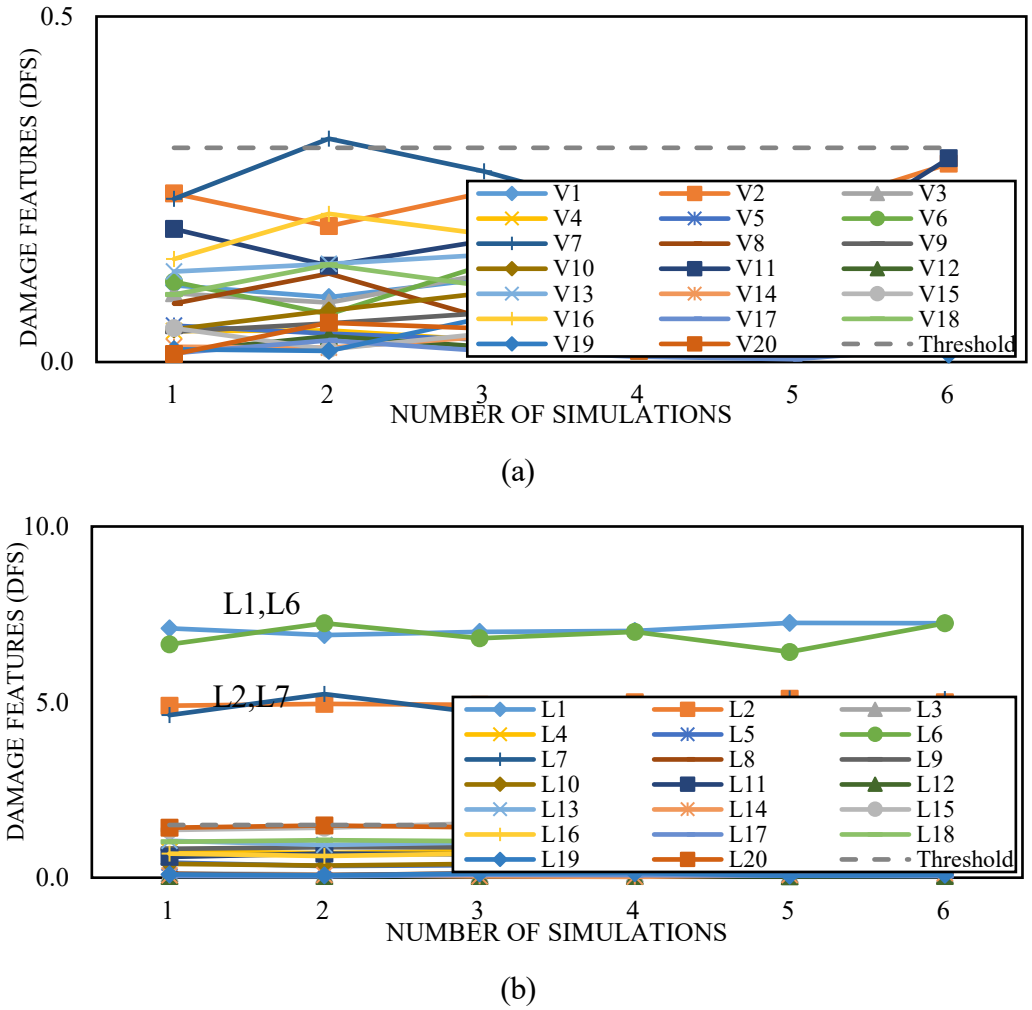

Figure 3.8 Damage Features (DFs) for DC-2(ii): (a) Vertical Cluster, (b) Longitudinal Cluster

3.4.3.3 *Damage case DC-3: diagonal members between nodes 2-13 and 7-18: 30% stiffness loss*

In this damage case, the longitudinal members between nodes 1-2 and 6-7 are assumed to have lost stiffness by 30%. The DFs for the case are shown in Figure 3.9(a) and Figure 4.7Figure 3.9(b) for vertical and longitudinal clusters respectively.

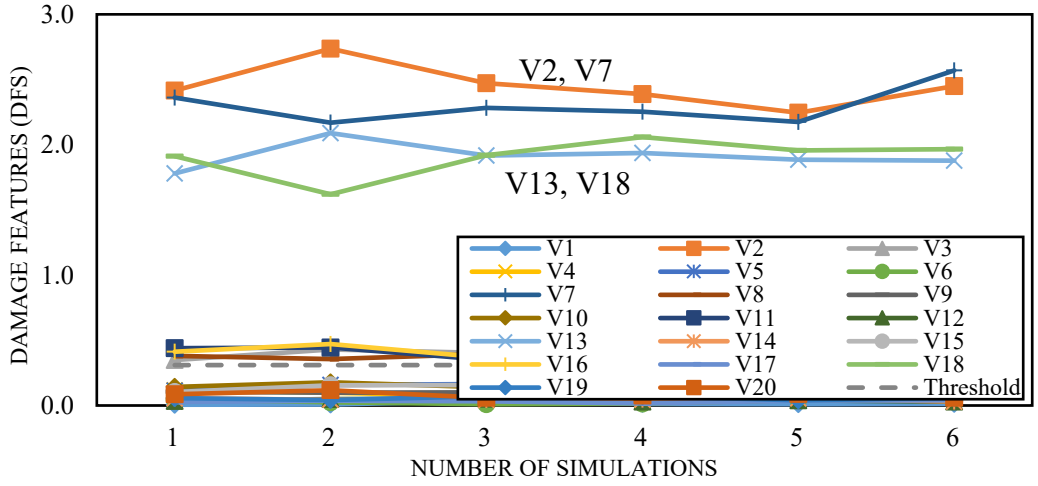

(a)

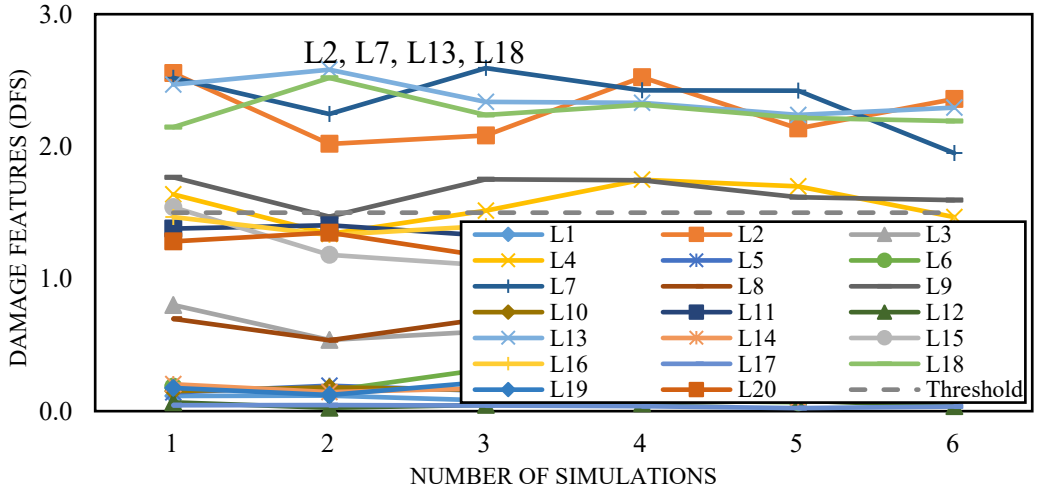

(b)

Figure 3.9 Damage Features (DFs) for DC-3: (a) Vertical Cluster, (b) Longitudinal Cluster

In this case, both the vertical and longitudinal cluster systems exhibit DFs above the thresholds. The vertical cluster shows DFs for V2, V7, V13, V18 to be above the

threshold with an average value of 2.14. The longitudinal cluster shows DFs for the corresponding sensors L2, L7, L13, L18 above the threshold with an average value of 2.32. The diagonal members have both vertical and longitudinal directional components and therefore, are expected to show a likelihood of damage in both the cluster systems. The DFs for all the other nodes for both clusters are close to or below the respective thresholds. Therefore, it is likely that damage has occurred in the diagonal members between nodes 2-13 and 7-18.

3.4.3.4 Damage case DC-4: longitudinal member between nodes 6-7 and vertical member between nodes 2-12: 30% stiffness loss

In this damage case, the longitudinal member between nodes 6-7 and vertical members between nodes 2-12 are assumed to have lost stiffness by 30%. The DFs for the case are shown in Figure 3.10(a) and Figure 3.10(b) for vertical and longitudinal clusters respectively. For this damage case, the vertical cluster system exhibits high DFs for sensors V2 and V12 with average values of 5.64 and 3.83 respectively. The longitudinal system shows DFs above the threshold for sensors L6 and L7 with average values of 5.81 and 3.49 respectively. No other DFs for vertical and longitudinal clusters are high enough above the respective thresholds. Therefore, it can be inferred by combining the results of both clusters that, the damage is likely in the vertical member between nodes 2-12 and longitudinal members between nodes 6-7.

3.4.3.5 Damage case DC-5: vertical member between nodes 2-12 and diagonal member between nodes 7-18: 30% stiffness loss

In this damage case, the vertical and diagonal members between nodes 2-12 and 7-18 respectively are assumed to be damaged in the form of 30% stiffness loss. The DFs for the case are shown in Figure 3.11(a) and Figure 3.11(b) for vertical and longitudinal clusters respectively. The vertical cluster, in this case, shows DFs above the threshold for sensors V2 and V12 with an average value of 5.29 and 3.99 respectively. It also shows high DFs of average 1.51 for sensors V7 and V18. The longitudinal cluster shows DFs above the threshold for only sensors L7 and L18 with an average value of 2.39. Combining both the results, it can be inferred that the vertical system indicates damage

in vertical members between nodes 2-12 as well as a diagonal member between nodes 7-18, while the longitudinal system indicating damage in only the diagonal member between nodes 7-18. This result is consistent with the assumption that each cluster will indicate damage in members that have directional components along that cluster.

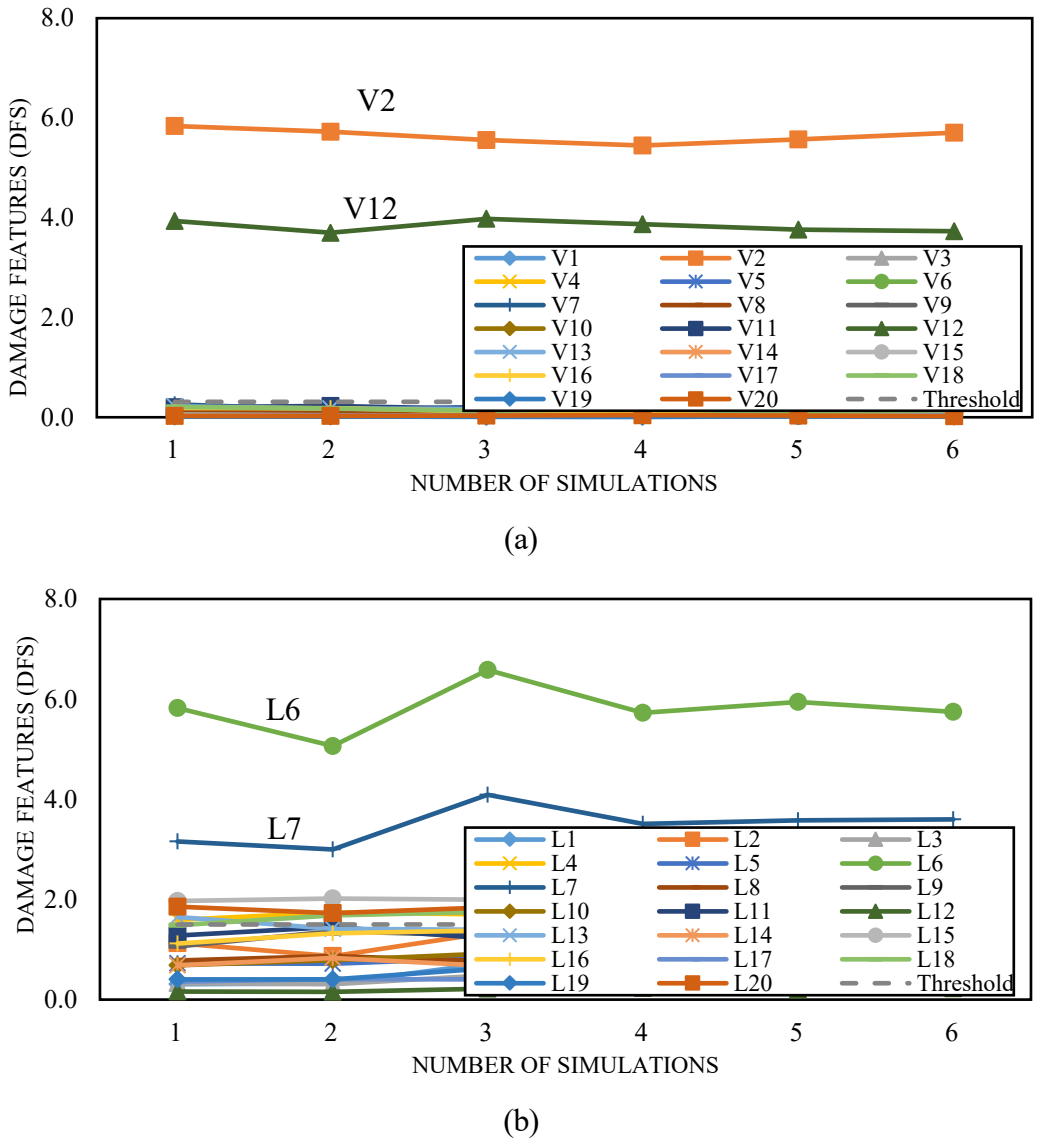

Figure 3.10 Damage Features (DFs) for DC-4: (a) Vertical Cluster, (b) Longitudinal Cluster

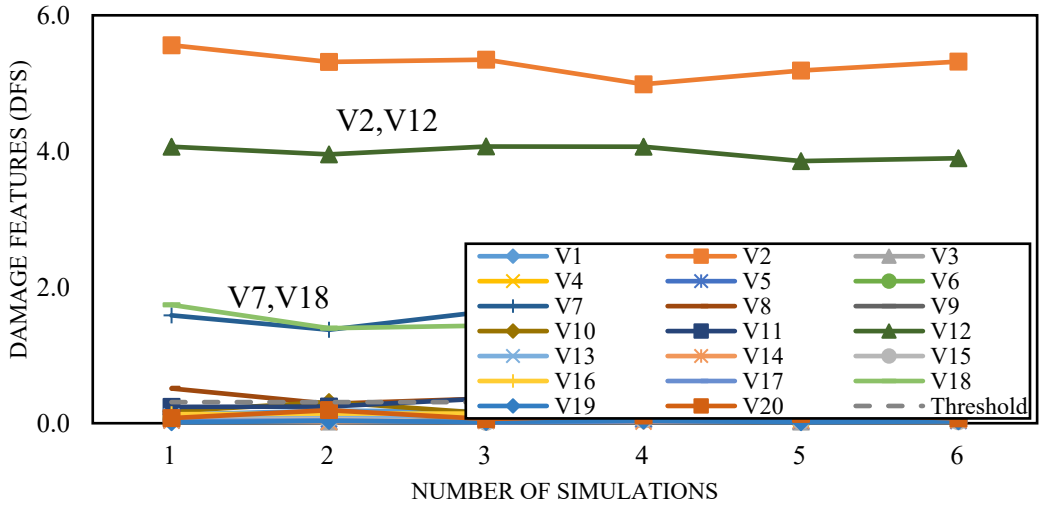

(a)

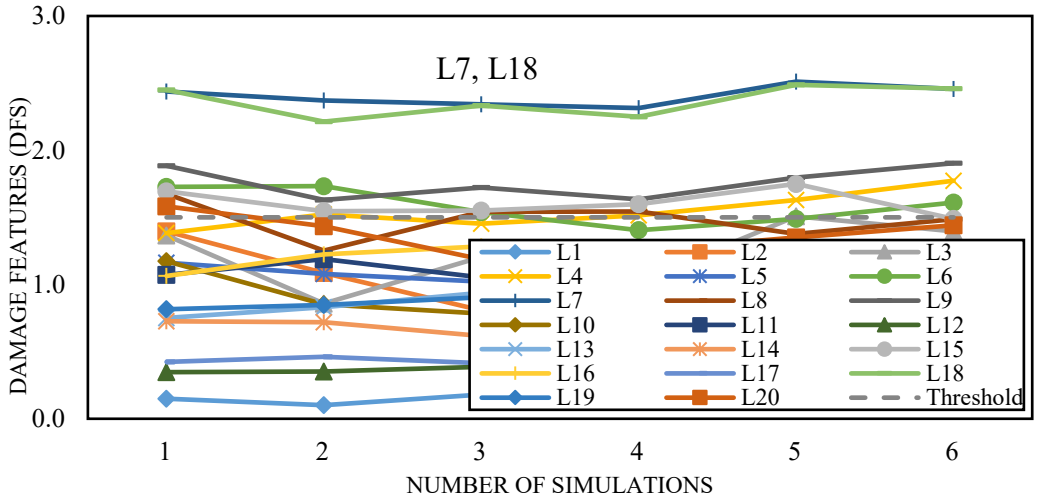

(b)

Figure 3.11 Damage Features (DFs) for DC-5: (a) Vertical Cluster, (b) Longitudinal Cluster

3.4.3.6 Damage case DC-6: longitudinal member between nodes 14-15 and bracing member between nodes 12-18: 30%stiffness loss

In this damage case, the longitudinal top chord member between nodes 14-15 and a bracing member between nodes 12-18 are both assumed to have lost stiffness by 30%. The results are shown in Figure 3.12(a) and Figure 3.12 (b). The vertical cluster system shows all the DFs close to or below the threshold. This is expected since the induced damage is in members with no vertical directional components. The longitudinal cluster shows very high DFs for sensors L14, followed by L15, L12, and L18, which connect

the affected members. At the same time, the surrounding nodes which are L13, L17, L19, and L20 show DFs above the threshold but close to or below the affected ones. The longitudinal bracing member is not as effective during the passage of a train and therefore, the connecting nodes (i.e. L12 and L18) do not demonstrate as high DFs as the main top chord would at similar damage level (i.e. L14 and L15). However, the method is still able to localize the damage in the longitudinal member between nodes 14-15 as well as a bracing member between nodes 12-18.

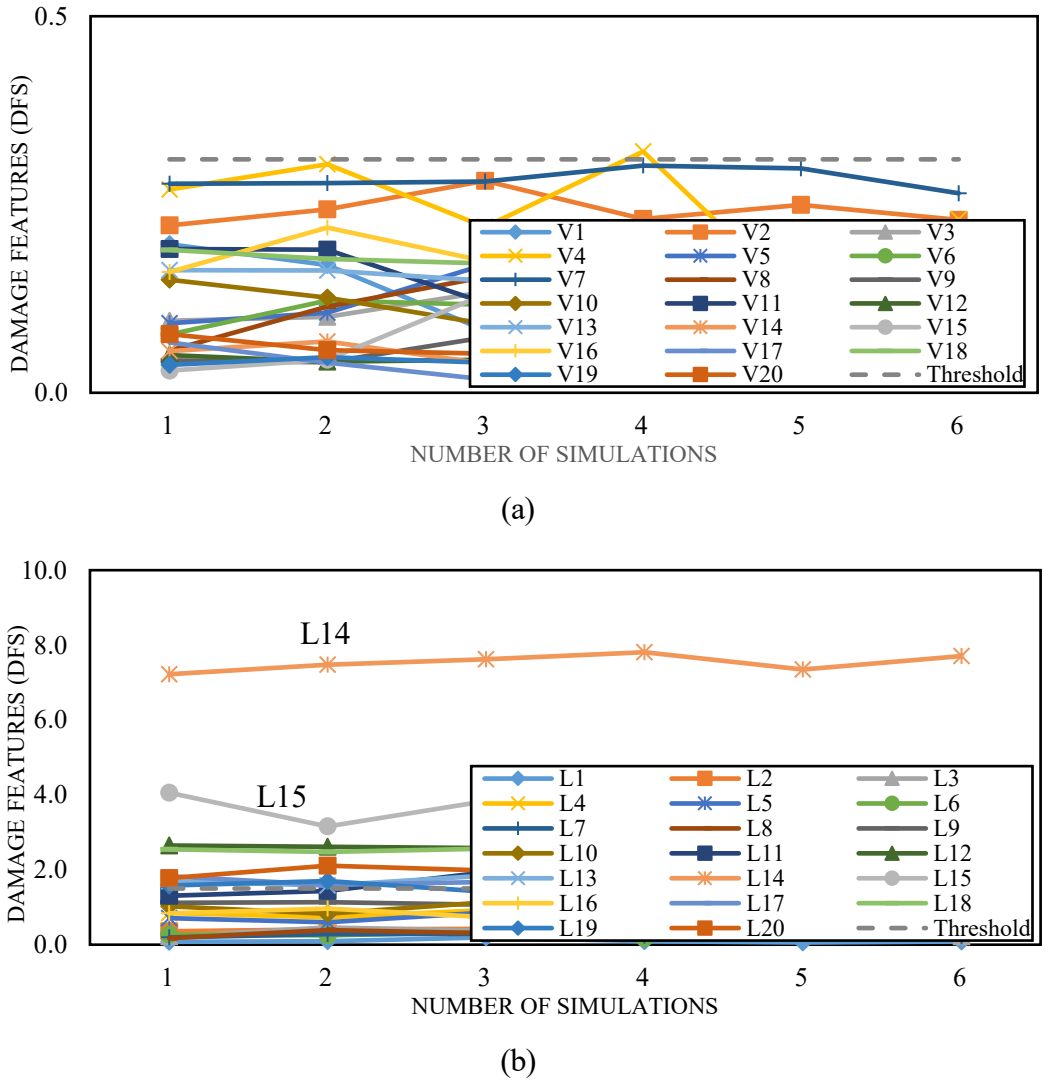

Figure 3.12 Damage Features (DFs) for DC-6: (a) Vertical Cluster, (b) Longitudinal Cluster

3.5 Conclusion

This chapter presents a novel damage identification method for railway truss bridges utilizing bridge acceleration response to operational train loading. The results presented in this study demonstrate the potential of the proposed method for truss bridges especially for detecting small to moderate damage associated with stiffness loss in the vertical, diagonal, and longitudinal members. The method under operational condition can detect and locate damage in vertical, longitudinal, and diagonal members since the train load is effective in vertical and longitudinal directions only. The method can be extended to include pure transverse bracing members if response under transverse loading is considered. While for some damage cases (example include DC-3) some additional adjacent nodes could be identified as damaged due to DFs above the threshold, these DFs are still very low and could be due to stress redistribution as the damage occurred. In such a situation, additional information could be obtained by combining the information from this presented method with other damage detection methods, such as the strain-based method developed in Chapter 4.

While the presented bridge is a short span one, it consists of a substantial number of truss members spread over six bays. The instrumentation plan is designed assuming one bi-axial sensor at each main connection as it facilitates damage detection at the truss member level. In practice, it is not feasible to measure the response from all the nodes of the truss bridge. It is also not a requirement to include all the nodes in the sensor cluster system. The sensor cluster system can be formulated based on the number of available sensors. In such a scenario, the damage detection method will demonstrate results based on the available sensors, and as expected damage localization cannot be achieved at the member level.

One of the limitations of the proposed method is that small localized damage, while identifiable, is difficult to locate accurately. Even though train-track-bridge interaction is not explicitly modeled in this study, random noise is added to the data in recognition of such effects. The proposed method is based on the linear behavior of the structure dealing with low levels of vibration. Therefore, this method and

most other damage detection methods presented in the literature do not apply to structures where data is affected by nonlinear behavior. Finally, the effect of environmental condition changes on the measurement errors is also not considered in this study which could affect the performance of the method as it affects all damage detection methods in the literature. Currently, researchers (for example, Gu et al., Kostic and Gül, Huang et al., Zhang et al.) are working on this topic extensively and developing methods using artificial neural networks to compensate for environmental effects [103-106]. Further studies are needed to integrate such methods with the damage detection method presented in this research. Despite such limitations, the method has great promise for practical implementation and further research to address these limitations would improve the efficiency and robustness of the method.

The proposed method can overcome some of the current limitations regarding the monitoring of truss railway bridges. Moreover, once the system is installed, continuous real-time monitoring is possible. It offers the opportunity to detect mild to relatively moderate damage to develop economical maintenance strategies and address the problem before it becomes too costly to repair. The verification of this method using experimental results has been conducted and discussed in Chapter 5. Validation of this method through a real-life bridge investigation is beyond the scope of this research.

4 DAMAGE DETECTION OF STEEL-TRUSS RAILWAY BRIDGES USING OPERATIONAL STRAIN RESPONSE[3]

4.1 Overview

In this chapter, a strain-response based damage detection framework is developed which accomplished *Task 2* of the research objective. As mentioned in Chapter 1, strain monitoring is usually a common and inexpensive means to assess the condition of bridges and. The proposed method developed in this chapter utilizes operational strain data obtained from instrumented truss elements in response to the passage of a train. The baseline bridge response and damaged bridge responses are analyzed using two data analysis methods: coefficient of variation and principal component analysis (PCA).

In the first method, strain time-history responses obtained under baseline and damaged bridge conditions are used to compute the coefficient of variation matrices. The results are presented in terms of the difference of the covariance matrix (DM) of the truss bridge between the baseline and damaged condition. The damage in the bridge is detected and located by observing the coefficients of the difference matrix as structural changes occur in the bridge.

In the second method, strain time-history responses under baseline and damaged bridge conditions are used to compute the principal components (PC) which are then ranked based on their corresponding eigenvalues. PCA is a statistical tool that has the potential to be useful for developing effective damage detection frameworks, as demonstrated by researchers [89, 107-111]. The results are demonstrated in terms of Damage Indicators (DI) which are obtained by comparing the geometric distance of coordinates of the principal component space between the baseline and damaged bridge condition.

[3] A modified version of this chapter has been published in the following journals as follows:
Azim, M.R., and Gül, M. (2020). Damage detection framework for truss railway bridges utilizing statistical analysis of operational strain response. *Structural Control and Health Monitoring*, 27(8), e2573.
It can be accessed using DOI: **https://doi.org/10.1002/stc.2573**
Azim, M.R., and Gül, M. (2020). Data-driven damage identification technique for truss railroad bridges utilizing principal component analysis of strain response. *Structure and Infrastructure Engineering.*
It can be accessed using DOI: **https://doi.org/10.1080/15732479.2020.1785512**

The strain-based methods presented are numerically verified through a finite element model of a truss railroad bridge. It is shown that the strain-based methods could identify, locate, and assess the severity of damage in the railway bridge. Moreover, the method provides damage sensitive features at the element level which is different from the nodal damage features extracted from the acceleration-based method presented in the previous chapter. Therefore, if utilized together, both methods can complement each other.

4.2 Theoretical derivation

4.2.1 Coefficient of variation analysis

This method utilizes the strain-time history of the elements of the truss bridge. Therefore, the first step is to obtain the strain response of the truss members and construct the strain matrix **S(t)** which is shown in Eq. (4.1). Thus, each column of the matrix **S(t)** is the strain time history response of each instrumented truss element due to the passage of a train.

$$\mathbf{S(t)} = \begin{pmatrix} s_1(t_1) & \cdots & s_{Ns}(t_1) \\ \vdots & \ddots & \vdots \\ s_1(t_n) & \cdots & s_{Ns}(t_n) \end{pmatrix} \tag{4.1}$$

Here,

N_s is the number of strain gauges,
n is the number of observations in the analyzed data window ($n > N_s$);

These responses are then normalized with respect to maximum absolute strain response to obtain the normalized strain matrix shown in Eq. (4.2).

$$\mathbf{S'(t)} = \frac{\mathbf{S(t)}}{\max(abs(s(t)))} \tag{4.2}$$

At time t_k, the vector of the normalized measurement will be like Eq. (4.3), where k=1,2..n.

$$s'(t_k) = \left(\frac{s_1(t_k)}{\max(abs(s(t)))} \quad \frac{s_2(t_k)}{\max(abs(s(t)))} \cdots \quad \cdots \quad \frac{s_{Ns}(t_k)}{\max(abs(s(t)))} \right) \tag{4.3}$$

The coefficient of variation between each measurement is computed and Covariance Matrix, **M** is formulated based on each analyzed data window, the size of which is N_s * N_s. The components of this matrix, m_{ij} are computed using Eq. (4.4) where $\bar{s}_i'$and $\bar{s}_j'$ are averages of normalized strain responses from sensors *i* and *j*.

$$m_{ij} = \sum_{k=1}^{n} \{s_i'(t_k) - \bar{s}_i'\} * \{s_j'(t_k) - \bar{s}_j'\} \tag{4.4}$$

These covariance matrices are computed for the truss bridge for the baseline and damaged condition. Then damage can be identified as a Difference Matrix **(DM)** shown in Eq. (4.5). Here, $\mathbf{M^U}$ and $\mathbf{M^D}$ are covariance matrices for baseline and damaged conditions respectively.

$$\mathbf{DM} = \left| \mathbf{M}^{\mathrm{U}} - \mathbf{M}^{\mathrm{D}} \right| \tag{4.5}$$

If no structural changes occur, the changes in the coefficients of the **DM** are expected to be very small and could be attributed to the operational variability and measurement noise. When damage occurs, the mean values and components of the covariance matrix are expected to change significantly, and therefore, high *DM* values will be observed for the elements damaged or affected by the damage. Therefore, by observing the changes in the values of the difference matrix, the damage could be detected and located.

4.2.2 Principal component analysis

In this method, similar to the previous method, the first step is to obtain the strain response of the truss members and construct the strain matrix **S(t)** after the passage of a train which is shown in Eq. (4.1). Then, principal component analysis is performed on the strain dataset which provides N_s number of eigenvalues λ_i, with N_s orthogonal eigenvectors $\boldsymbol{\psi_i}$. These are obtained utilizing Eq. (4.6) and (4.7). The

coefficient of variation between each measurement is computed and covariance Matrix, **C** is formulated, the size of which is N_s * N_s. Here, $\bar{S}$ is the mean of **S**.

$$\mathbf{C} = \frac{1}{n-1}(\mathbf{S} - \bar{S})(\mathbf{S} - \bar{S})^T \tag{4.6}$$

Then, eigenvalues and vectors are obtained by satisfying the equation shown in Eq. (4.7) where $\boldsymbol{\psi}$ and $\boldsymbol{\lambda}$ are eigenvector matrix and eigenvalue matrix respectively.

$$\mathbf{C} \times \boldsymbol{\Psi} = \boldsymbol{\Psi} \times \boldsymbol{\lambda} \tag{4.7}$$

These eigenvectors are called principal components where each coefficient within a vector represents each sensor. These eigenvalues are sorted in decreasing order, i.e., $\lambda_1 > \lambda_2 > \ldots$. The corresponding eigenvectors $\boldsymbol{\psi_i}$ (i=1,2,…, N_s) represent the principal components from each time-history response with decreasing order of variance with $\boldsymbol{\psi_1}$ having the greatest variance. Most of the variance is contained within the first few principal components. For the example presented in this chapter, it is observed that the first two components contain 90% or more variance and deemed adequate for damage detection purposes. Considering more than 2 principal components does not necessarily result in improvement of the performance. Since these components are orthogonal vectors, these values from truss elements can be plotted in a 2-D principal component space as co-ordinates considering $\boldsymbol{\psi_1}$ and $\boldsymbol{\psi_2}$ as orthogonal axes. Figure 4.1 shows such a plot. Then the geometric distance, D is obtained for each sensor using Eq. (4.8).

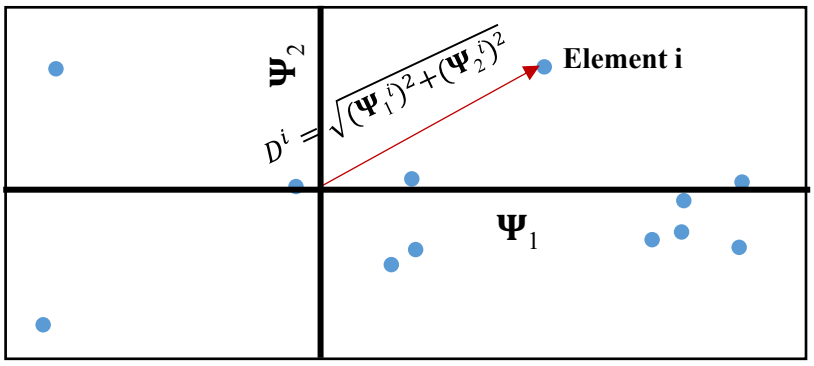

Figure 4.1 Plots of the first two PCs on the 2-D principal component space

$$D^i = \sqrt{(\Psi_1^i)^2 + (\Psi_2^i)^2}, i = 1, 2, \cdots, N_s \tag{4.8}$$

After obtaining D values for both baseline and damaged bridge, a damage indicator, (DI), is proposed, which compares these distances as shown in Eq. (4.9) where D_b and D_d represent distances for baseline and damaged bridge principal components respectively.

$$DI^i = \left| \frac{D_b^i - D_d^i}{D_b^i} \right| * 100, i = 1, 2, \cdots, N_s \tag{4.9}$$

If no structural changes occur, the values of baseline DI are expected to be very small. Since operational strain data is used, these baseline DI values could be attributed to the operational variability and measurement noise. When damage occurs, high DI values will be observed for the elements damaged or affected by the damage. Therefore, by observing the changes in the DI values, the damage could be detected and located.

4.3 Finite element modeling and instrumentation of the truss bridge

The finite element model of the bridge is used to validate the strain-based method is the same as the one described in Chapter 3, Section 2.3. This section describes the procedure for collecting strain data from this model.

To demonstrate the efficiency of the method, one side of the truss bridge shown in Figure 3.1 is considered for monitoring. The modeled truss bridge has 21 individual elements on each side. In an ideal situation, all the elements would be instrumented with strain gauges to monitor the entire bridge. However, in real life, due to financial and computational constraints, it is not always practical to install sensors in all the members of the truss bridge. Therefore, in this study, 12 elements have been chosen for instrumentation. These include 4 elements each from the bottom chord, verticals, and diagonals. Strain-gauges are installed at the midpoint of each element. The elements with strain-gauges are shown in Figure 4.2(top). In this figure, the elements annotated with double vertical lines are instrumented with strain gauges. Longitudinal strain responses are obtained from the top flange of

each truss element at the mid-span location by aligning the strain gauge along the longitudinal axes of the element as shown in Figure 4.2(bottom). In a real-life bridge, the number and type of strain gauges to be used will depend on economic considerations, the number of truss elements to be monitored, and desired levels of accuracy. Li and Wu suggested that distributed long-gauge strain sensors are sensitive to localized damage and therefore, could be utilized to obtain strain response from the truss bridge [112].

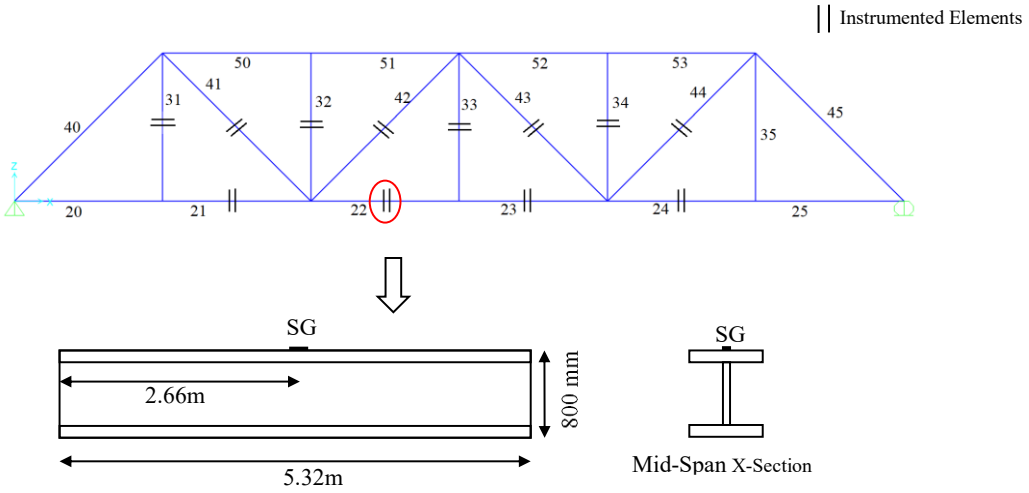

Figure 4.2 (top)The truss bridge elements instrumented with strain-gauges, (bottom) the longitudinal and cross-sectional profile of element 22 showing the location of strain measurement (not to scale)

Longitudinal strain time-history responses are obtained from each instrumented element of the bridge during each passage of a train as it crosses the bridge. In this study, three operational standard trains are considered. For the baseline condition, COOPER E80 (Tr-1) train loading is simulated at 40 km/h speed. To account for the speed and axle loading variability, for the damaged bridge, in addition to Tr-1, the COOPER E90 (Tr-2) train is simulated at 50 km/h speed, which already induces variations of axle loads and speed by 11% and 25% respectively. Further, to assess the performance of the method under the operational train at moving at high speed, COOPER E100(Tr-3) train is simulated at 100 km/h speed on the damaged bridge. Tr-3 represents operational variation in terms of change in axle loads from Tr-1 by +25%, and change is speeds by 150%. These are the American Railway

Engineering and Maintenance-of-Way Association (AREMA) standard train loads. The train loads are modeled as a series of axle loads to represent the above-mentioned design train loadings. Typical strain responses for some of the elements are shown in Figure 4.3.

(a)

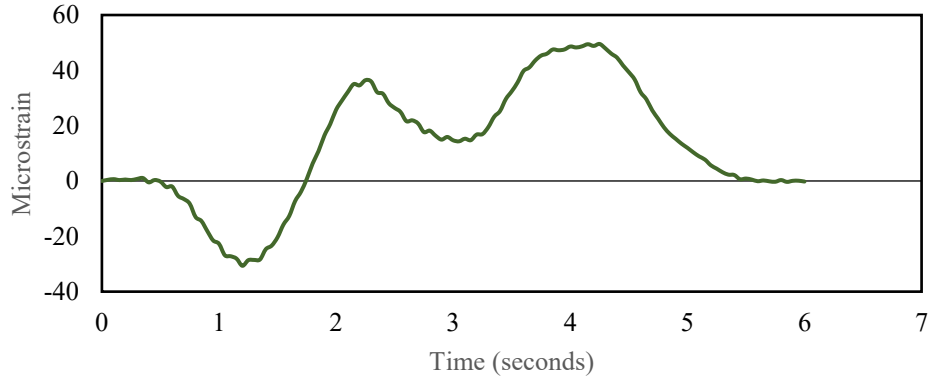

(b)

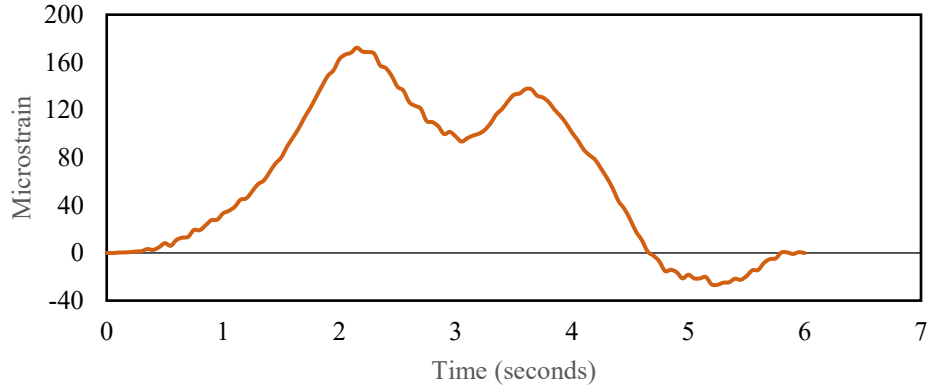

(c)

Figure 4.3 Strain response from various elements for baseline bridge condition in response to Tr-1: (a) element 21, (b) element 32, (c) element 44.

4.4 Analysis and results

Otter et al. identified various causes of damage in railway bridges which include accidents, fire damage, scouring, environmental degradation, failed and defective structural members, and support problems [22]. All these types of issues reported can cause damage to the structural members which results in strength and/or stiffness loss. In this study, the damage associated with stiffness reduction of truss members will be presented. The damaged truss members are simulated with a reduced modulus of elasticity and also loss of thickness in the cross-sections (different levels of damage severity are considered) along the entire length of the individual members. Damage simulated in this manner represents a gradual decrease of stiffness in a member likely caused by corrosion, and decay of member. Also, the effect of the change in boundary condition is demonstrated as another damage case. Change in support behavior could occur due to corrosion or blocked bridge support. This could result in change is the structural configuration of the entire bridge and may lead to unexpected force and stress redistribution among the structural elements. In this study, this damage is simulated by adding fixity against the longitudinal translation of the roller support on the right. All these damage cases are described in Table 4.1. These damage cases are visually shown in Figure 4.4.

Table 4.1 Damage cases simulated in this study

Damage Case	Damage location and severity
DC-1	Element 22: stiffness loss by (a) 5% (b) 10%, (c) 20%
DC-2	Element 33: stiffness loss by (a) 5% (b) 10%, (c) 20%
DC-3	Element 44: stiffness loss by (a) 5% (b) 10%, (c) 20%
DC-4	Element 22: reduction in the flange and web thickness so that cross-sectional area is reduced by (a) 9%, (b) 17% and (c) 25%
DC-5	Multiple damages combining damage cases of (a) DC-2(b) and DC-4(a) and (b) DC-2(c) and DC-4(c)
DC-6	Element 20: stiffness loss by (a) 20% (b) 30%
DC-7	Roller support develops fixity against longitudinal translation

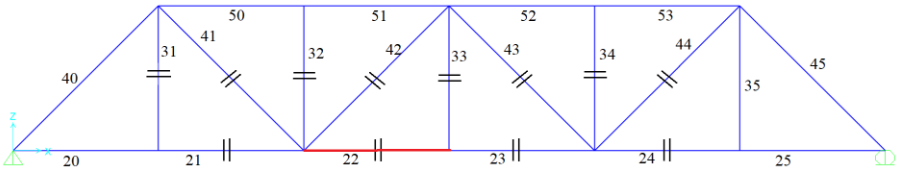

(a)

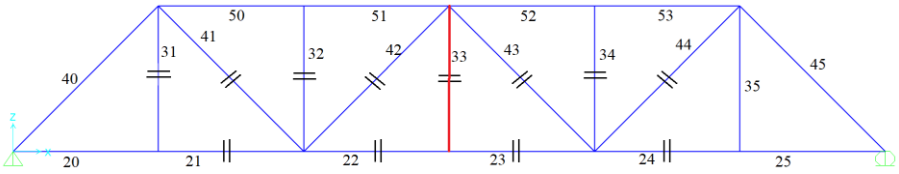

(b)

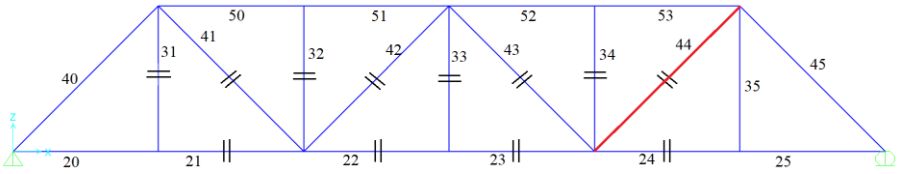

(c)

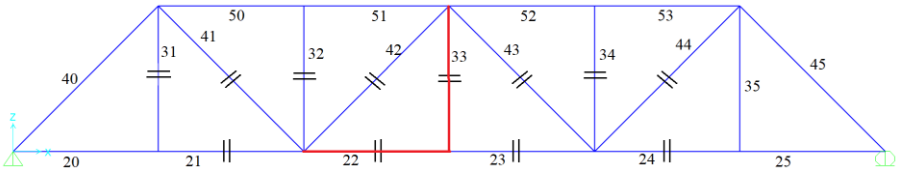

(d)

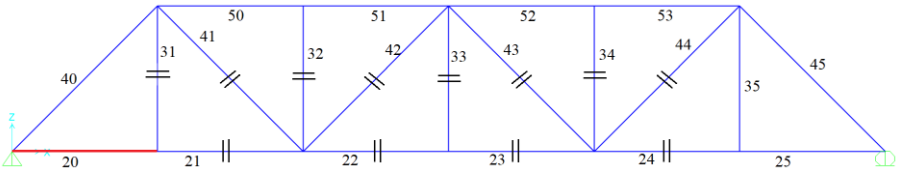

(e)

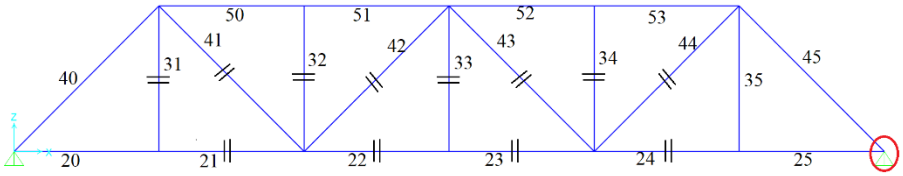

(f)

Figure 4.4 Damage cases analyzed: (a) DC-1, DC- 4, (b) DC-2, (c) DC-3, (d) DC-5 (e) DC-6, and (f) DC-7

4.4.1 Results from the coefficient of variation analysis

4.4.1.1 Estimation of the threshold coefficient of the difference matrix

Initially, covariance analysis is conducted for the baseline bridge to assess the range of difference caused by the variations in axle loads and speeds and measurement error due to noisy data. So, three sets of strain data are considered which are the responses of the baseline bridge to Tr-1, Tr-2, and Tr-3 moving at their respective speeds as mentioned before. Then, by using Tr-1 as the fixed train, DMs are obtained by comparing Tr-1 data with Tr-1, Tr-2, and Tr-3 data using the procedure outlined in the "Theoretical Derivation" section for the baseline bridge. To obtain a meaningful threshold, these comparative data sets are simulated 200 times each with an added 5% random noise, and average DMs are obtained. Finally, the maximum value among all the coefficients from the three average DMs is set as the threshold coefficient for the difference matrix. In this study, for the presented instrumentation plan, the value of the threshold coefficient is found to be 0.0021. Therefore, if a component of the difference matrix is higher than this threshold coefficient, it could be attributed to structural change due to damage.

In the subsequent sections, the results of different damage cases are presented. The results for each damage case are presented as average difference matrix (DM) after comparing baseline Tr-1 with damaged Tr-1, Tr2, and Tr-3 which were simulated multiple times with 5% random noise. These results are shown in Figure 4.5 through Figure 4.11. In these figures, the matrix is color-coded according to the scale shown beside the matrix. Also, the coefficients which are higher than the threshold coefficient are highlighted in black fonts.

4.4.1.2 Stiffness loss in element 22: DC-1

In this damage case, the truss element number 22 is simulated to be damaged due to stiffness reduction of (a) 5%, (b) 10%, and (c) 20%. This is shown in Figure 4.4(a). The difference matrices (DMs) for these levels of damages are shown in Figure 4.5(a) and (b) and (c) respectively.

Elmt	21	22	23	24	31	32	33	34	41	42	43	44	Scale
21													0.10
22		0.017	0.007	0.003	0.005	0.002	0.007		0.010	0.006	0.004	0.009	0.08
23		0.007											0.06
24		0.003											0.04
31		0.005											0.02
32		0.002											0.00
33		0.007											
34													
41		0.010											
42		0.006											
43		0.004											
44		0.009											

(a)

Elmt	21	22	23	24	31	32	33	34	41	42	43	44	Scale
21		0.003											0.10
22	0.003	0.034	0.014	0.005	0.009	0.005	0.013		0.019	0.012	0.008	0.017	0.08
23		0.014	0.004				0.003					0.003	0.06
24		0.005											0.04
31		0.009											0.02
32		0.005											0.00
33		0.013	0.003										
34													
41		0.019											
42		0.012											
43		0.008											
44		0.017	0.003										

(b)

Elmt	21	22	23	24	31	32	33	34	41	42	43	44	Scale
21		0.005	0.004				0.004		0.004	0.003		0.004	0.10
22	0.005	0.078	0.029	0.011	0.020	0.010	0.029		0.040	0.024	0.018	0.036	0.08
23	0.004	0.029	0.010	0.002	0.003		0.006		0.005	0.004	0.004	0.007	0.06
24		0.011	0.002										0.04
31		0.020	0.003										0.02
32		0.010											0.00
33	0.004	0.029	0.006				0.004		0.003		0.003	0.004	
34													
41	0.004	0.040	0.005				0.003					0.002	
42	0.003	0.024	0.004									0.002	
43		0.018	0.004				0.003					0.003	
44	0.004	0.036	0.007				0.004		0.002	0.002	0.003	0.005	

(c)

Figure 4.5 DM for Damage case (DC-1): stiffness loss in element 22 by (a) 5%, (b)10%, and (c) 20%

It can be observed from Figure 4.5(a), (b) and (c) that, the major difference in covariance occurs between element 22 and the rest. The coefficients for other

elements are very small. The maximum absolute difference is 0.017, 0.034, and 0.078 for 5%, 10%, and 20% stiffness loss, respectively, i.e. around 8.1 times, 16.2 times, and 37.1 times the identified threshold, respectively. It is observed that, as the damage severity increases, so does the coefficients of DMs of the damaged element. At higher damage level, other elements of the bridge also show coefficients above the threshold due to redistribution of stress and strains. Overall, observing the results, the presence of damage in element 22 is identified, localized and its severity is relatively assessed effectively.

4.4.1.3 Stiffness loss in element 33: DC-2

In this damage case, the truss element number 33 (which is a vertical member) is simulated to be damaged due to the stiffness reduction of 5%, 10%, and 20%. This is shown in Figure 4.4(b). The results in terms of the DMs are shown in Figure 4.6(a), (b), and (c). In this case, the results show that the major difference of coefficients occurs between element 33 and the rest with maximum absolute differences of 0.016, 0.034, and 0.085 respectively for element 33 which are around 7.6, 16.2, and 40.5 times the threshold respectively. All the remaining coefficients are very close to zero. Therefore, the likely location of the damage is in element 33. At higher damage severity (20%), some additional elements exhibit coefficients beyond the threshold value due to stress redistribution which is expected. Overall, the damage is successfully identified and located and relatively quantified.

4.4.1.4 Stiffness loss in element 44: DC-3

In this damage case, the truss element number 44 (which is a diagonal member) is simulated to be damaged due to the stiffness reduction of 5%, 10%, and 20%. This damage is shown in Figure 4.4(c). The results in terms of the difference matrices are shown in Figure 4.7(a), (b), and (c) respectively. In this case, similar to the previous damage cases, the results show that the major difference of coefficients occurs between the damaged element 44 and the rest with a maximum absolute difference of 0.023, 0.048, and 0.099 respectively. These values are around 11, 22.9, and 47.1 times the threshold values. While other elements exhibit coefficients

above the threshold but those are smaller compared to the element 44. Similar to DC-1 and DC-2, at 20% damage level, more elements exhibit coefficients above the threshold which is expected due to redistribution of stresses and strains.

Elmt	21	22	23	24	31	32	33	34	41	42	43	44	Scale
21							0.002						0.10
22							0.008						0.08
23							0.008						0.06
24							0.003						0.04
31							0.003						0.02
32							0.003						0.00
33	0.002	0.008	0.008	0.003	0.003	0.003	0.016		0.010	0.006	0.006	0.010	
34													
41							0.010		0.002				
42							0.006						
43							0.006						
44							0.010					0.002	

(a)

Elmt	21	22	23	24	31	32	33	34	41	42	43	44	Scale
21							0.005						0.10
22							0.015						0.08
23							0.015						0.06
24							0.005						0.04
31							0.007						0.02
32							0.005						0.00
33	0.005	0.015	0.015	0.005	0.007	0.005	0.034		0.020	0.013	0.012	0.020	
34													
41							0.020						
42							0.013						
43							0.012						
44							0.020						

(b)

Elmt	21	22	23	24	31	32	33	34	41	42	43	44	Scale
21							0.012		0.003			0.003	0.10
22						0.002	0.036					0.002	0.08
23							0.036						0.06
24							0.013					0.002	0.04
31							0.016						0.02
32		0.002					0.013		0.003			0.003	0.00
33	0.012	0.036	0.036	0.013	0.016	0.013	0.085	0.003	0.048	0.031	0.028	0.047	
34							0.003						
41	0.003					0.003	0.048		0.005	0.003	0.003	0.005	
42							0.031		0.003			0.003	
43							0.028		0.003			0.003	
44	0.003	0.002		0.002		0.003	0.047		0.005	0.003	0.003	0.006	

(c)

Figure 4.6 DM for Damage case (DC-2): stiffness loss in element 33 by (a) 5%, (b)10%, and (c) 20%

Elmt	21	22	23	24	31	32	33	34	41	42	43	44	Scale
21												0.003	0.10
22												0.010	0.08
23												0.008	0.06
24												0.003	0.04
31												0.006	0.02
32												0.002	0.00
33												0.009	
34													
41												0.011	
42												0.007	
43												0.007	
44	0.003	0.010	0.008	0.003	0.006	0.002	0.009		0.011	0.007	0.007	0.023	

(a)

Elmt	21	22	23	24	31	32	33	34	41	42	43	44	Scale
21												0.005	0.10
22			0.003									0.018	0.08
23		0.003	0.005				0.002		0.003	0.002		0.015	0.06
24												0.005	0.04
31												0.011	0.02
32												0.004	0.00
33			0.002									0.018	
34												0.002	
41			0.003									0.021	
42			0.002									0.013	
43												0.014	
44	0.005	0.018	0.015	0.005	0.011	0.004	0.018	0.002	0.021	0.013	0.014	0.048	

(b)

Elmt	21	22	23	24	31	32	33	34	41	42	43	44	Scale
21			0.003									0.009	0.10
22		0.009	0.012	0.003	0.005	0.003	0.006		0.009	0.007		0.032	0.08
23	0.003	0.012	0.016	0.003	0.007	0.004	0.010		0.014	0.009	0.005	0.025	0.06
24		0.003	0.003						0.003	0.003		0.009	0.04
31		0.005	0.007		0.007		0.002		0.004		0.002	0.019	0.02
32		0.003	0.004				0.003		0.004	0.004		0.007	0.00
33		0.006	0.010		0.002	0.003	0.005		0.007	0.006		0.031	
34											0.002	0.005	
41		0.009	0.014	0.003	0.004	0.004	0.007		0.011	0.008	0.003	0.036	
42		0.007	0.009	0.003		0.004	0.006		0.008	0.009		0.022	
43			0.005		0.002			0.002	0.003		0.003	0.025	
44	0.009	0.032	0.025	0.009	0.019	0.007	0.031	0.005	0.036	0.022	0.025	0.099	

(c)

Figure 4.7 DM for Damage case (DC-3): stiffness loss in element 44 by (a) 5%, (b)10%, and (c) 20%

4.4.1.5 Thickness loss in element 22: DC-4

In this damage case, the truss element number 22 is simulated to be damaged due to the reduction in thickness of the top and bottom flanges as well as the web. To simulate damage, flange and web thicknesses are reduced which results in a reduction in total cross-sectional area by around 9%, 17%, and 25% for case DC-4(a), 4(b), and 4(c) respectively. The difference matrices (DMs) for these levels of damages are shown in Figure 4.8(a), (b), and (c) respectively. From Figures 4.10, it can be inferred that the changes in coefficients of DMs are higher for element 22 compared to the rest of the elements. The maximum absolute differences of 0.033, and 0.071 and 0117 respectively have been obtained for DC-4(a) and DC-4(b) and DC-4(c), respectively, i.e. around 16 times, and 34 times and 56 times the identified threshold, respectively. Since the damaged element is the same, the pattern of the results is similar to those of DC-1. Overall, observing the results, the presence of damage in element 22 is identified, localized and its severity is relatively assessed effectively.

4.4.1.6 Multiple damaged elements: DC-5

This damage case is a combination of (a) DC-2(b) and DC-4(a) and (b) DC-2(c) and DC-4(c), where elements 33 and 22 have been damaged at the same time. The damage is shown in Figure 4.4(d). The result in terms of the difference matrix is shown in Figure 4.9(a) and (b). Similar to damage cases DC-2(b) and DC-4(a), the maximum difference of covariance is observed for elements 33 and 22 while the others are small. Comparing the difference of covariance between element 33 with 22 from the damage cases DC-2(b) and DC-4(a) with this damage case, it is seen that the result for this case is a sum of those damage cases with slight variation due to noise. Overall, the location of the damaged elements and also the relative severity of damage are assessed.

Elmt	21	22	23	24	31	32	33	34	41	42	43	44	Scale
21		0.002											0.10
22	0.002	0.033	0.014	0.004	0.008	0.004	0.013		0.018	0.012	0.009	0.017	0.08
23		0.014											0.06
24		0.004											0.04
31		0.008											0.02
32		0.004											0.00
33		0.013											
34													
41		0.018											
42		0.012											
43		0.009											
44		0.017											

(a)

Elmt	21	22	23	24	31	32	33	34	41	42	43	44	Scale
21		0.004	0.004				0.004		0.004	0.003		0.004	0.10
22	0.004	0.071	0.029	0.008	0.018	0.009	0.027		0.038	0.023	0.019	0.034	0.08
23	0.004	0.029	0.005	0.003	0.002		0.003					0.003	0.06
24		0.008	0.003				0.002					0.002	0.04
31		0.018	0.002										0.02
32		0.009											0.00
33	0.004	0.027	0.003	0.002			0.003					0.002	
34													
41	0.004	0.038							0.002				
42	0.003	0.023											
43		0.019											
44	0.004	0.034	0.003	0.002			0.002						

(b)

Elmt	21	22	23	24	31	32	33	34	41	42	43	44	Scale
21	0.003	0.005	0.007	0.003	0.003		0.006		0.006	0.005	0.003	0.007	0.10
22	0.005	0.117	0.045	0.013	0.028	0.014	0.042		0.059	0.037	0.029	0.054	0.08
23	0.007	0.045	0.007	0.004	0.003		0.005		0.003			0.005	0.06
24	0.003	0.013	0.004				0.003		0.003	0.002		0.004	0.04
31	0.003	0.028	0.003										0.02
32		0.014											0.00
33	0.006	0.042	0.005	0.003			0.005					0.004	
34													
41	0.006	0.059	0.003	0.003					0.003				
42	0.005	0.037		0.002									
43	0.003	0.029											
44	0.007	0.054	0.005	0.004			0.004						

(c)

Figure 4.8 DM for Damage case (DC-4): reduction of the cross-sectional area in element 22 by (a) 9%, (b)17%, and (c) 25%

Elmt	21	22	23	24	31	32	33	34	41	42	43	44	Scale
21		0.003					0.003						0.10
22	0.003	0.033	0.014	0.005	0.008	0.006	0.031		0.019	0.012	0.009	0.018	0.08
23		0.014					0.015						0.06
24		0.005					0.004						0.04
31		0.008					0.007						0.02
32		0.006					0.006						0.00
33	0.003	0.031	0.015	0.004	0.007	0.006	0.034		0.021	0.014	0.012	0.020	
34													
41		0.019					0.021		0.005	0.002	0.003	0.003	
42		0.012					0.014		0.002				
43		0.009					0.012		0.003				
44		0.018					0.020		0.003			0.003	

(a)

Elmt	21	22	23	24	31	32	33	34	41	42	43	44	Scale
21		0.007	0.005				0.004		0.004	0.004		0.004	0.10
22	0.007	0.117	0.045	0.015	0.027	0.017	0.090		0.063	0.039	0.030	0.057	0.08
23	0.005	0.045	0.007	0.003	0.003	0.002	0.031						0.06
24		0.015	0.003				0.009						0.04
31		0.027	0.003				0.015						0.02
32		0.017	0.002				0.013		0.005	0.003	0.003	0.004	0.00
33	0.004	0.090	0.031	0.009	0.015	0.013	0.079	0.002	0.047	0.030	0.026	0.043	
34							0.002						
41	0.004	0.063				0.005	0.047		0.010	0.005	0.005	0.007	
42	0.004	0.039				0.003	0.030		0.005	0.003	0.002	0.004	
43		0.030				0.003	0.026		0.005	0.002	0.003	0.003	
44	0.004	0.057				0.004	0.043		0.007	0.004	0.003	0.005	

(b)

Figure 4.9 DM for Damage case (DC-5): multiple damages combining (a)DC-2(b) and DC-4(a), and (b) DC-2(c) and DC-4(c)

4.4.1.7 Stiffness loss in element 20: DC-6

So far it is demonstrated that the method is effective in detecting and localizing damage in elements that are monitored directly by strain gauges. However, as discussed before, it is not practical to monitor all the elements of a truss bridge. It is important that the method still provides useful diagnostic info for damaged members for which strain response is not available. To show how the proposed method performs in such a situation, damage cases DC-6 is investigated. In this damage case, element 20 is damaged which is not instrumented. In this case, element 20 shown in Figure 4.4(e) is damaged due to stiffness loss of 20% and 30% respectively. The results for this damage case are presented in Figure 4.10(a) and (b) respectively.

Elmt	21	22	23	24	31	32	33	34	41	42	43	44	Scale
21		0.004	0.003						0.003		0.002	0.003	0.10
22	0.004	0.006	0.005		0.003				0.003		0.003	0.003	0.08
23	0.003	0.005	0.004										0.06
24													0.04
31		0.003											0.02
32													0.00
33													
34													
41	0.003	0.003											
42													
43	0.002	0.003											
44	0.003	0.003											

(a)

Elmt	21	22	23	24	31	32	33	34	41	42	43	44	Scale
21	0.003	0.007	0.006		0.003		0.004		0.006		0.004	0.005	0.10
22	0.007	0.012	0.011	0.002	0.006		0.005		0.007	0.003	0.006	0.007	0.08
23	0.006	0.011	0.009		0.003		0.003		0.005		0.004	0.005	0.06
24		0.002											0.04
31	0.003	0.006	0.003										0.02
32													0.00
33	0.004	0.005	0.003										
34													
41	0.006	0.007	0.005										
42		0.003											
43	0.004	0.006	0.004										
44	0.005	0.007	0.005										

(b)

Figure 4.10 DM for damage case (DC-6): stiffness loss in element 20 by (a) 20% damage, (b) 30% damage (damaged element not instrumented)

It is observed from the results that the differences in coefficients are relatively high for elements 21, 22, and 23, especially at 30% damage level. As the damage severity increases, the changes in these coefficients also increase for these elements, and differences from the rest of the elements are more discernable. However, these values while above the threshold, are still very small compared to results of DC-1 and DC-4 in which damaged element is monitored. So, while damage is not exactly located, the results still provide information that the location is somewhere close to elements 21, 22, and 23 at 30% damage level.

4.4.1.8 Detection of change in boundary conditions: DC-7

In this damage case, the effect of the change in support condition on the truss bridge is simulated. Here, the damage is simulated as a change of the roller support with pinned support on the right as shown in Figure 4.4(f). In this case, the results already do not include information from the connected elements 25, 35, and 45 which are not instrumented. The difference matrix is shown in Figure 4.11. Looking at the difference matrix, it can be seen that, this is global damage with significant changes in absolute values of coefficients in the DM for all instrumented elements, which is expected. Change of support from roller to pinned causes longitudinal reaction force which is aligned with the bottom chord elements. As a result, redistribution of the axial forces and consequently the change in strains are mainly concentrated on the bottom chord elements, which is observed in the difference matrix. Besides, the changes in the coefficients are very high compared to all the previous damage cases. Overall, it can be concluded that this is an instance of a global damage case that is severely affecting the bottom chord elements. It is to be noted though that since the strain gauges are installed in the truss elements, the damage is identified and located in terms of those elements most affected due to the boundary condition change (i.e., the bottom chord elements), which is very useful for a stand-alone method. To obtain further information to exactly locate the change in support condition, displacement or acceleration data should be obtained directly from the support.

Elmt	21	22	23	24	31	32	33	34	41	42	43	44		Scale
21		0.058	0.049	0.023	0.062	0.020	0.079	0.004	0.100	0.058	0.055	0.098		0.20
22	0.058	0.153	0.160	0.091	0.078	0.027	0.098	0.006	0.136	0.077	0.064	0.126		0.16
23	0.049	0.160	0.164	0.065	0.098	0.034	0.125	0.008	0.169	0.097	0.084	0.160		0.12
24	0.023	0.091	0.065	0.074	0.113	0.044	0.155	0.014	0.194	0.125	0.093	0.185		0.08
31	0.062	0.078	0.098	0.113			0.005		0.003	0.002		0.005		0.04
32	0.020	0.027	0.034	0.044					0.004	0.003	0.003			0.00
33	0.079	0.098	0.125	0.155	0.005		0.006		0.005		0.005			
34	0.004	0.006	0.008	0.014										
41	0.100	0.136	0.169	0.194	0.003	0.004	0.005		0.024	0.010		0.014		
42	0.058	0.077	0.097	0.125	0.002	0.003			0.010	0.006	0.009	0.002		
43	0.055	0.064	0.084	0.093		0.003	0.005			0.009	0.008	0.007		
44	0.098	0.126	0.160	0.185	0.005				0.014	0.002	0.007	0.011		

Figure 4.11 DM for due to change in boundary condition (DC-7)

4.4.2 Results from principal component analysis

4.4.2.1 Estimation of threshold damage indicator

Initially, PCA is performed on the baseline bridge to estimate a threshold damage indicator that can be attributed to operational variation and measurement error due to noisy data. So, three sets of strain data are considered with one set each from Tr-1, Tr-2, and Tr-3. Then using Tr-1 strain data as the common baseline bridge response, it is compared with baseline bridge response to Tr-1, Tr-2, and Tr-3 train loads. Thus, three threshold DIs for three operational conditions (Cond-1, Cond-2, and Cond-3) are obtained. Each of these data sets is simulated 200 times with an added 5% artificial noise and DIs are obtained. Then DI with 99% confidence is chosen as threshold DI for each condition; in other words, the likelihood of Dis exceeding the threshold without structural change is only 1%. Therefore, DIs above this threshold is attributed to structural change due to damage. The threshold values obtained are 3.2, 3.4, and 3.5 respectively for the three operational conditions.

After establishing the thresholds, different damage cases are analyzed. For this purpose, baseline data is obtained from Tr-1 and damaged data is obtained from Tr-1, Tr-2, and Tr-3 to obtain DI for the three operational conditions. The results are presented in Figure 4.12 through to Figure 4.18, where each state of the bridge (baseline and different levels of damage) is simulated 5 times and presented in a single graph for each operational condition when the data is affected with 5% noise.

4.4.2.2 Stiffness loss in element 22: DC-1

In this damage case, the truss element number 22, which is part of the bottom chord members, is simulated to be damaged due to stiffness reduction of 5%, then 10% and finally 20%. The damage indicators (DIs) for this damage case for the three operational conditions are shown in Figure 4.12(a), (b), and (c) respectively.

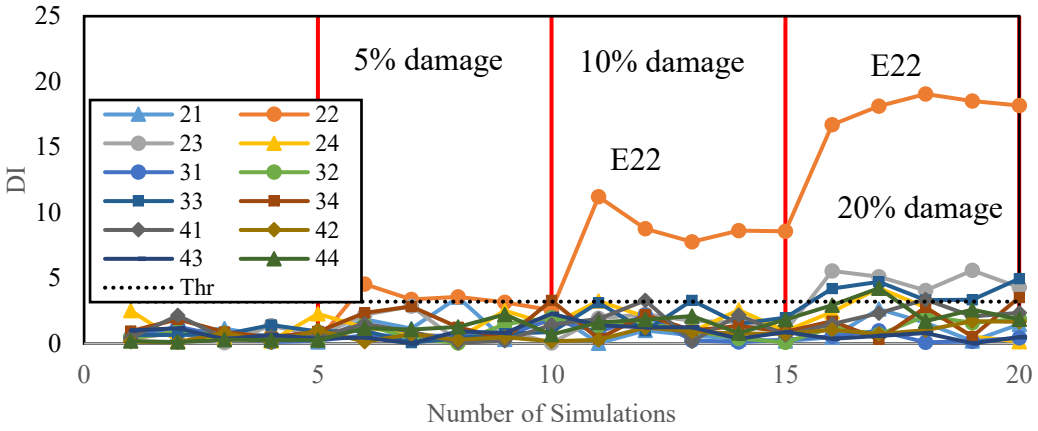

(a)

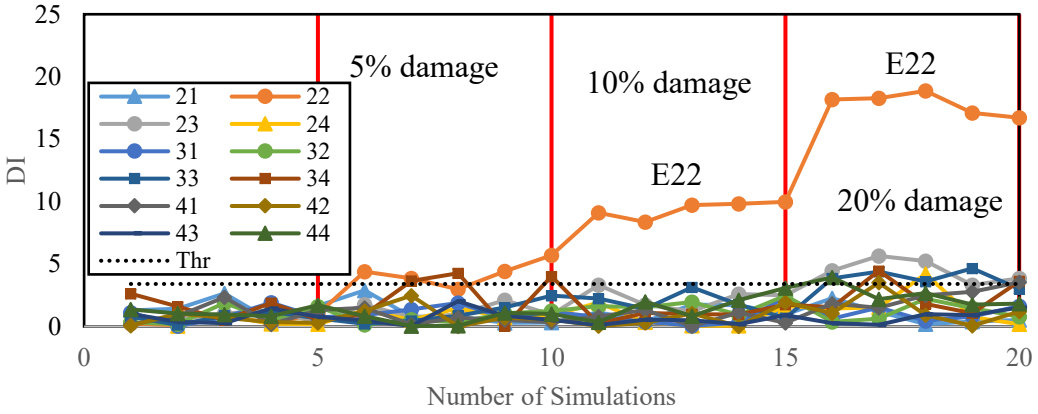

(b)

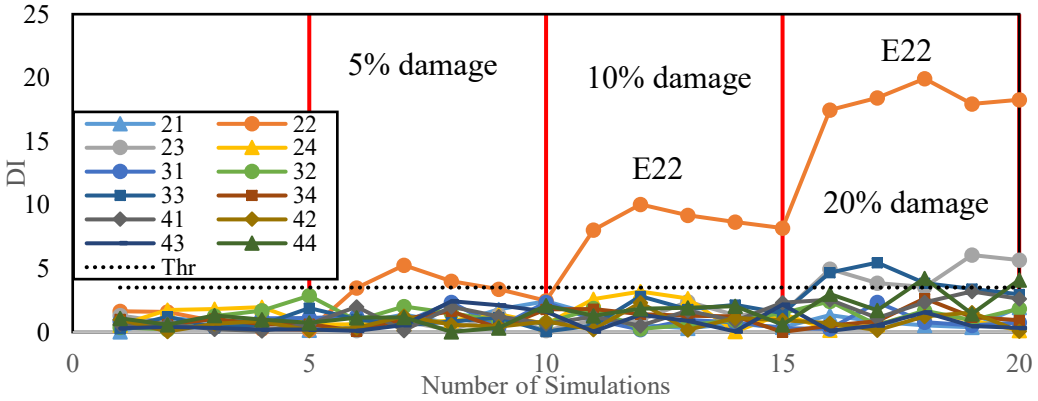

(c)

Figure 4.12 Damage indicators (DIs) for DC-1: (a) Cond-1, (b) Cond-2, (c) Cond-3

It can be observed that the presence of damage is detected from as early as 10% stiffness loss in the element for all three operational conditions since the DIs for element 22 are higher than threshold while DIs for all other elements are below or

close to the threshold. The DIs for element 22 also increase as the severity of stiffness loss increases. For example, for Cond-1 shown in Figure 4.12(a), the average DIs for element 22 are 3.4, 9.0, and 18.1 respectively for the three levels of damage. while threshold DI is 3.2. Similar results obtained for Cond-2 and Cond-3. Therefore, the severity of damage is relatively assessed.

4.4.2.3 Stiffness loss in element 33: DC-2

In this damage case, the truss element number 33 which is a vertical member is simulated to be damaged due to stiffness reduction of 5%, then 10%, and finally 20%. The DIs for this damage case for the three operational conditions are shown in Figure 4.13(a), (b), and (c) respectively. Similar to DC-1, it can be observed that the presence of damage is detected from the early stages. In this damage scenario, stiffness loss of 10% and upwards could be identified in all three operational conditions. For example, for Cond-3 shown in Figure 4.13(c), the average DIs for the element 33 are 5.6, 9.3, and 19.2 respectively for the three levels of damage while the threshold DI for such operational condition is 3.5. So, for 5% stiffness loss, observed DIs are below the threshold and therefore not detected, while 10% and 20% damage is identified. Overall, damage level of 10% and upwards could be detected, located, and relatively quantified for all operational conditions.

4.4.2.4 Stiffness loss in element 44: DC-3

In this damage case, the truss element number 44 which is a diagonal member is simulated to be damaged due to stiffness reduction of 5%, then 10%, and finally 20%. The DIs for this damage case for the three operational conditions are shown in Figure 4.14(a), (b), and (c) respectively. Similar to previous damage cases, it can be observed that the presence of damage is detected from the early stages. In this damage case, at the 5% damage level, the damage is not detected. Stiffness loss of 10% and upwards could be identified and located in all three operational conditions. For example, for Cond-3 shown in Figure 4.14(c), the average DIs for element 44 are 4.0, 8.9, and 17.8 respectively for the three levels of damage while the threshold DI is 3.5.

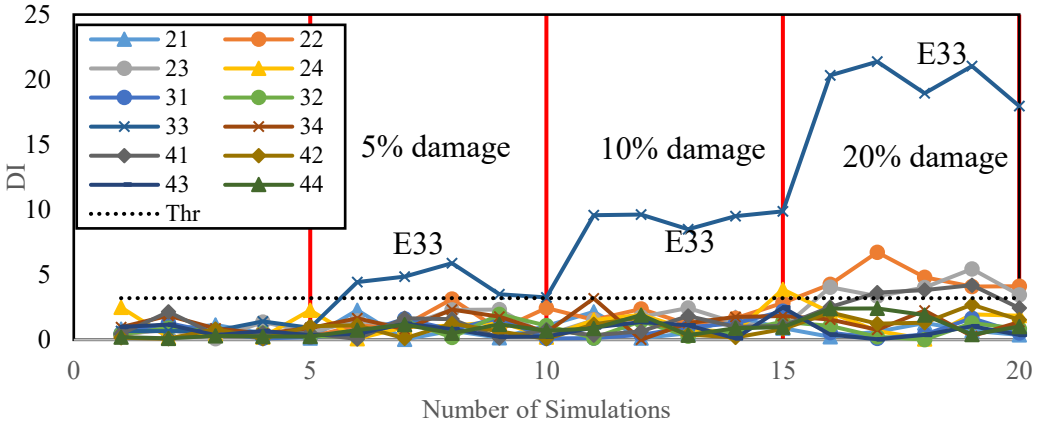

(a)

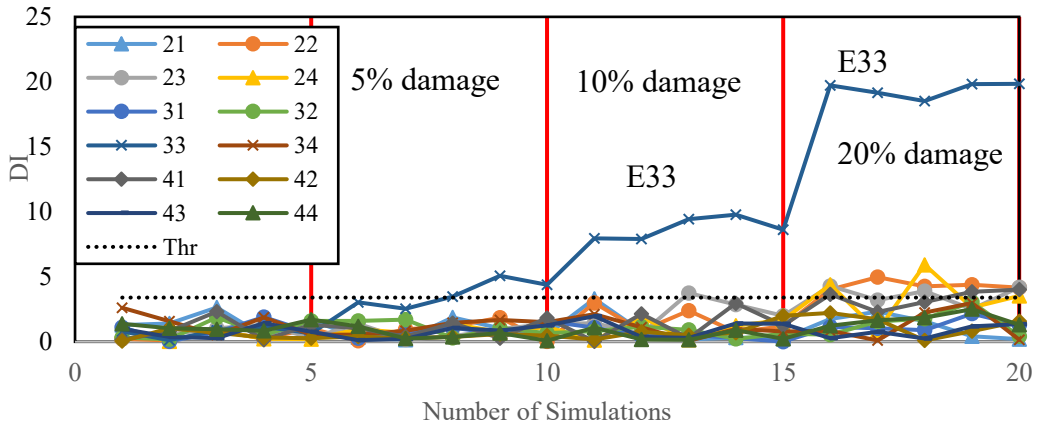

(b)

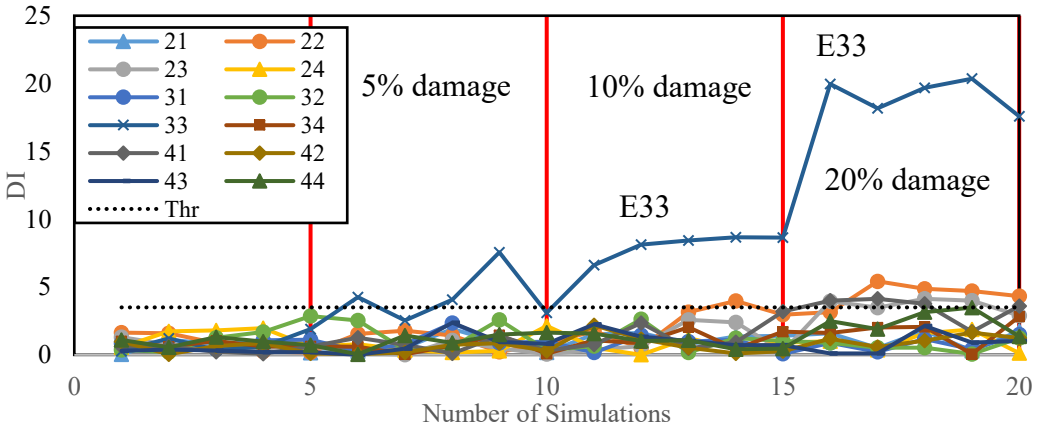

(c)

Figure 4.13 Damage indicators (DIs) for DC-2: (a) Cond-1, (b) Cond-2, (c) Cond-3

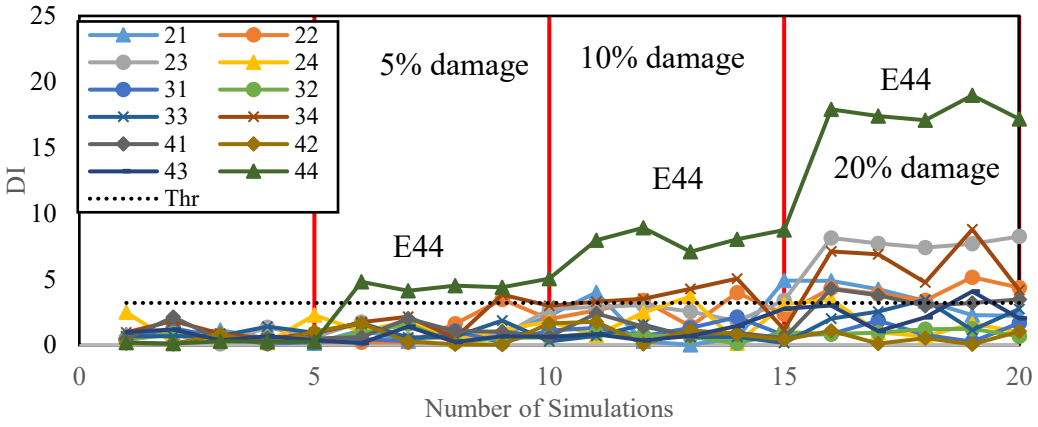

(a)

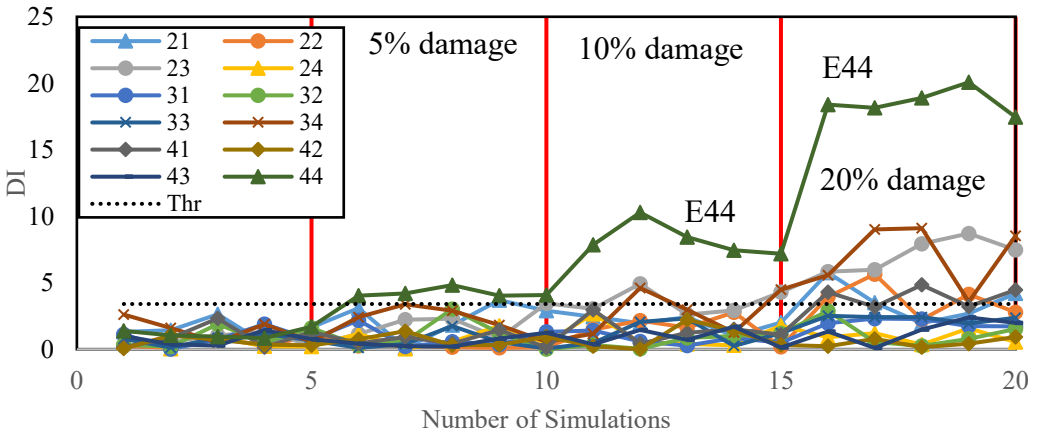

(b)

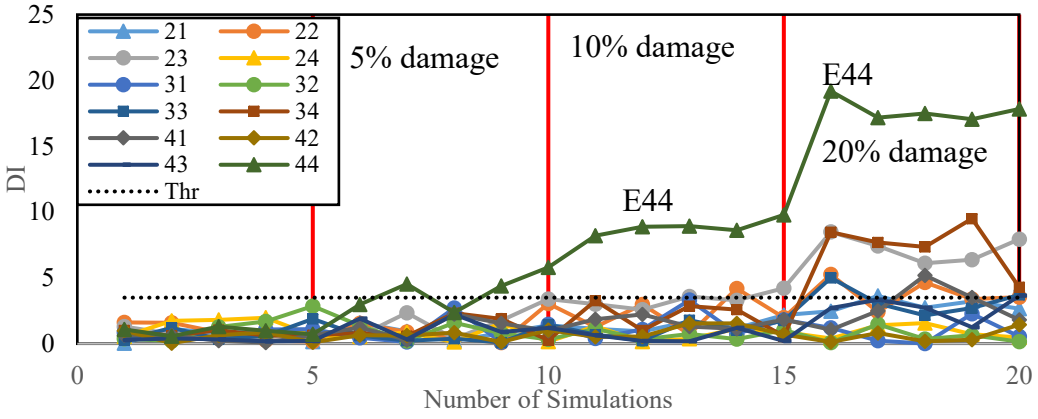

(c)

Figure 4.14 Damage indicators (DIs) for DC-3: (a) Cond-1, (b) Cond-2, (c) Cond-3

It is observed that when stiffness loss is relatively high (i.e. 20% or more) in an element, some of the neighboring elements could exhibit DIs which are higher than

the threshold due to stress redistribution. This is expected at a high damage level and only seems to occur in a limited number of neighboring elements. As an example, for the DC-3, at 20% damage level, elements 34 and 23 exhibit higher DIs than the threshold in addition to the damaged element 44. These members are connected to element 44 and therefore could be affected by force redistribution. In such a scenario, global damage detection methods that rely on acceleration response of steel truss bridges such as the one developed in the previous chapter or other global methods could be relied upon to garner further information [113, 114].

4.4.2.5 Thickness loss in element 22: DC-4

In this damage case, the truss element number 22 is simulated to be damaged due to the reduction in thickness of the top and bottom flanges as well as the web. To simulate damage, flange and web thicknesses are reduced which results in a reduction in total cross-sectional area by around 9%, 17%, and 25% for case DC-4(a), 4(b), and 4(c) respectively. The damage indicators (DIs) for these levels of damages are shown in Figure 4.15(a), (b), and (c) respectively. It can be observed that the presence of damage is detected from as early as 10% stiffness loss in the element for all three operational conditions since the DIs for element 22 are higher than threshold while DIs for all other elements are below or close to the threshold. The DIs for element 22 also increase as the severity of stiffness loss increases. For example, for Cond-1 shown in Figure 4.15(a)**,** the average DIs for element 22 are 7.7, 17.9, and 24.3 respectively for the three levels of damage. while threshold DI is 3.2. Considering the levels of damage these DIs are consistent with the results obtained from DC-1. Similar results obtained for Cond-2 and Cond-3. Therefore, the severity of damage is relatively assessed. Overall, observing the results, the presence of damage in element 22 is identified, localized and its severity is relatively assessed effectively.

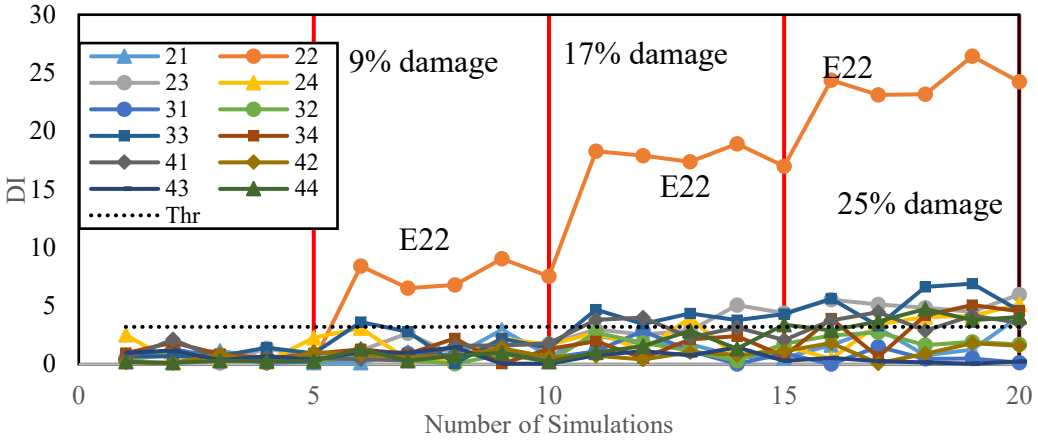

(a)

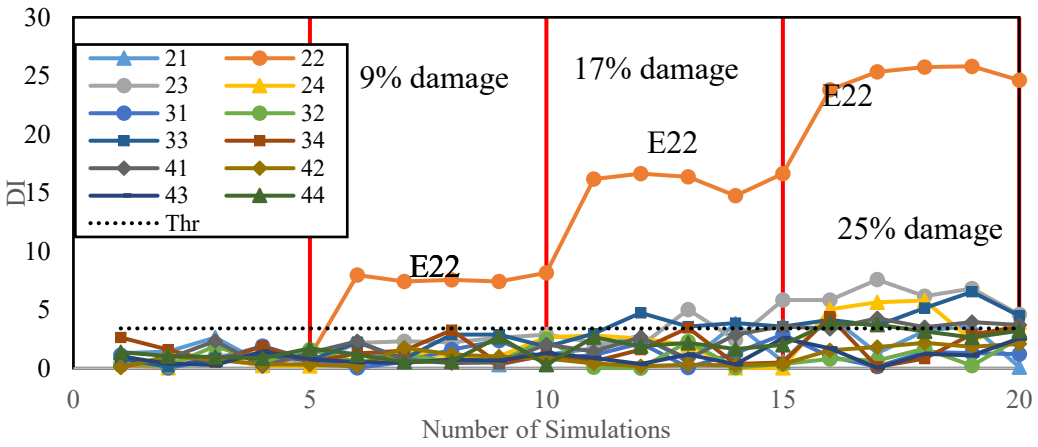

(b)

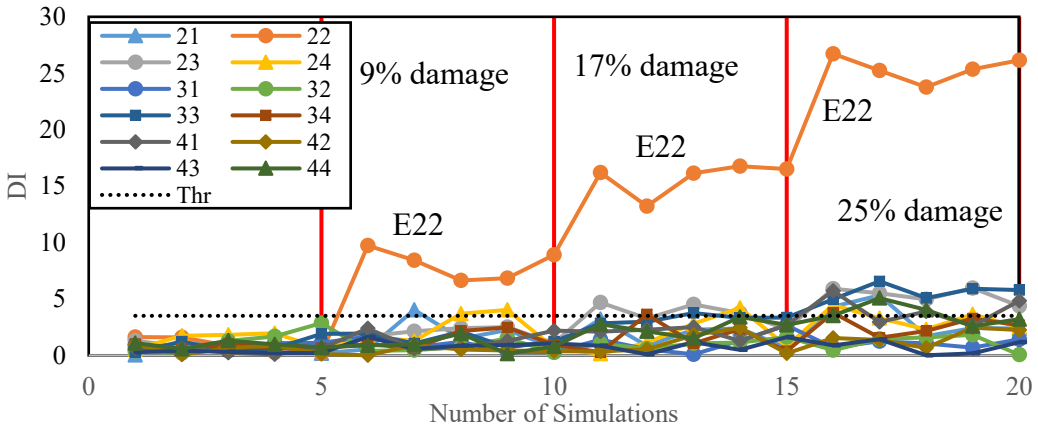

(c)

Figure 4.15 Damage indicators (DIs) for DC-4: (a) Cond-1, (b) Cond-2, (c) Cond-3

4.4.2.6 Multiple damaged elements: DC-5

This is a combination of damage cases DC-2 and DC-4. In this damage case, the truss element 22 and 33 are simulated to be damaged due to reduction in cross-sectional area in element 22 and stiffness in element 33 of initially 9% and 10% and to 25% and 20% respectively. The DIs for this damage case for the three operational conditions are shown in Figure 4.16(a), (b), and (c) respectively.
The results indicate that DIs for element 22 and 33 are significantly higher than the threshold for all three operational conditions. While some adjacent elements like element 23, 41 also show DIs above the threshold at the severe damage level, these DIs are still below the DIs of the damaged elements. Overall, the presence of multiple damages is identified, located, and relatively quantified.

4.4.2.7 Stiffness loss in element 20: DC-6

In this damage case, the truss element 20 is simulated to be damaged from baseline by 20%, and 30%. In this case, there is no strain data available for this element as shown in Figure 4.4(e). The results of analyzing such a damage case based on available data are presented in Figure 4.17(a), (b), and (c). It is seen that for all three operational conditions, information on the likelihood of damage is provided by the DIs of adjacent element 21 at damage level 20% and 30%. The 5% and 10% damage are not detectable as these are very small damage to significantly affect strain data of adjacent elements. For 20% and 30% damage, while element 21 shows DIs above the threshold, the values are still very small. For example, for Cond-1, the average DIs of element 21 at 20% and 30% damage levels are 4.5 and 5.7 respectively. Comparing with DC-1, which showed significantly high DIs for element 21 even for 10% damage, it can be inferred that, the damaged member, in this case, is likely not element 21 but its adjacent member which is not monitored. These results are expected since based on the previous damage cases it is demonstrated that strain data provides localized information of damage and therefore is very effective in isolating damage location even for very small damage when an affected member is monitored. For the same reason, not much information can be obtained for small damage when affected member is not monitored and at the same time data contains

high operational variability. Overall, still useful diagnostic info on damage in a non-monitored element could be gleaned from adjacent connected elements for damage levels of 20% and upwards.

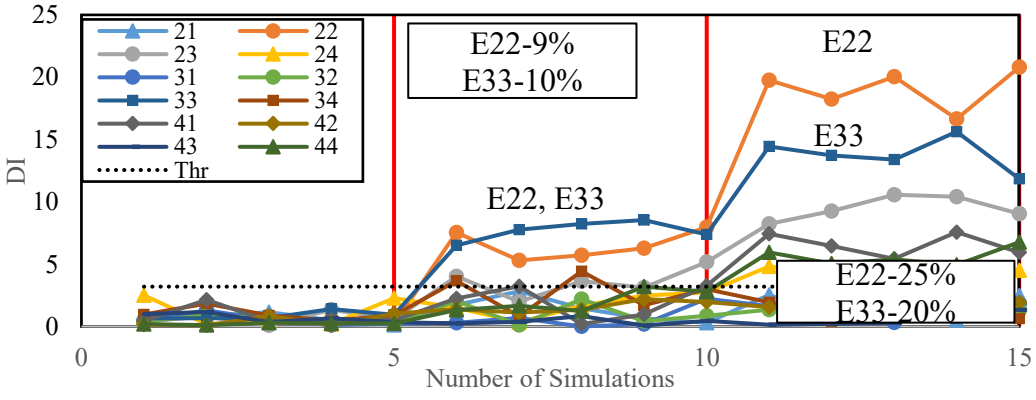

(a)

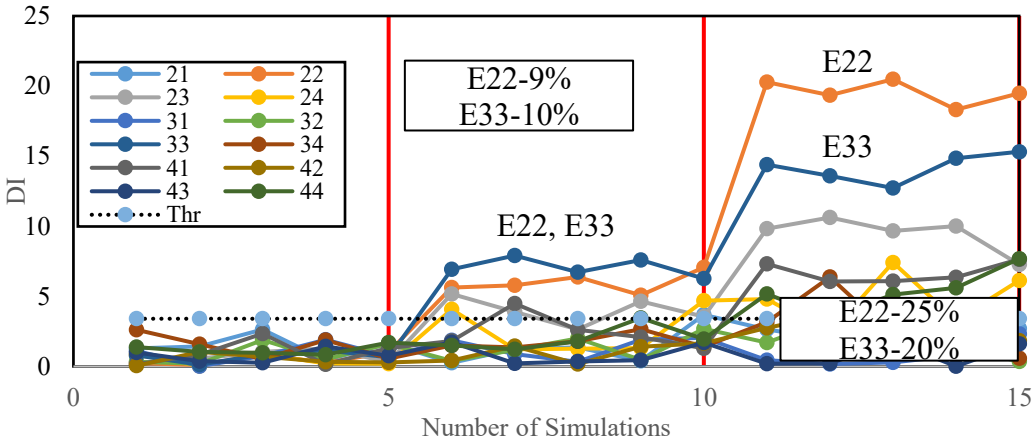

(b)

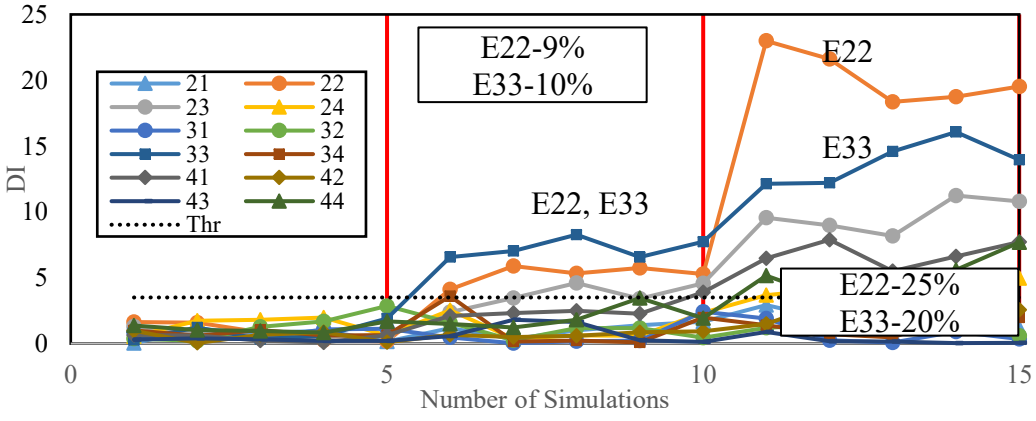

(c)

Figure 4.16 Damage indicators (DIs) for DC-5: (a) Cond-1, (b) Cond-2, (c) Cond-3

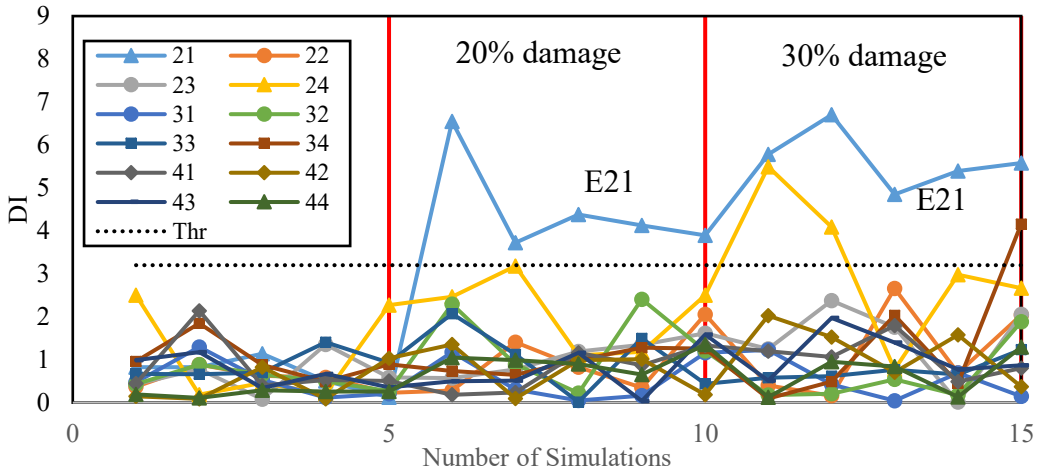

(a)

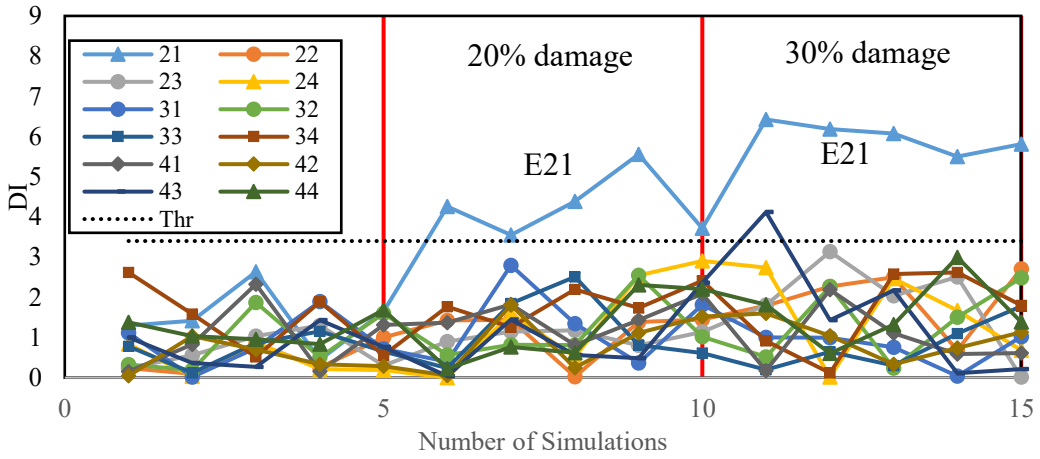

(b)

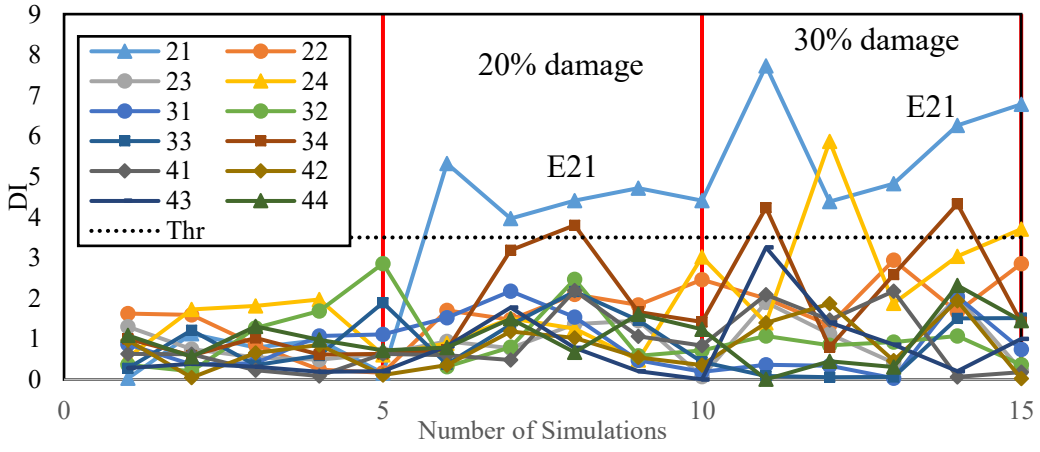

(c)

Figure 4.17 Damage indicators (DIs) for DC-6: (a) Cond-1, (b) Cond-2, (c) Cond-3

4.4.2.8 Detection of change in boundary conditions: DC-7

In this damage case, the effect of the change in support condition on the truss bridge is simulated. Here, the damage is simulated by introducing restraint against longitudinal translation on the right pier roller support (i.e., the roller support becomes a pinned support). This damage is shown visually in Figure 4.4(f). The results are shown in Figure 4.18(a), (b), and (c).

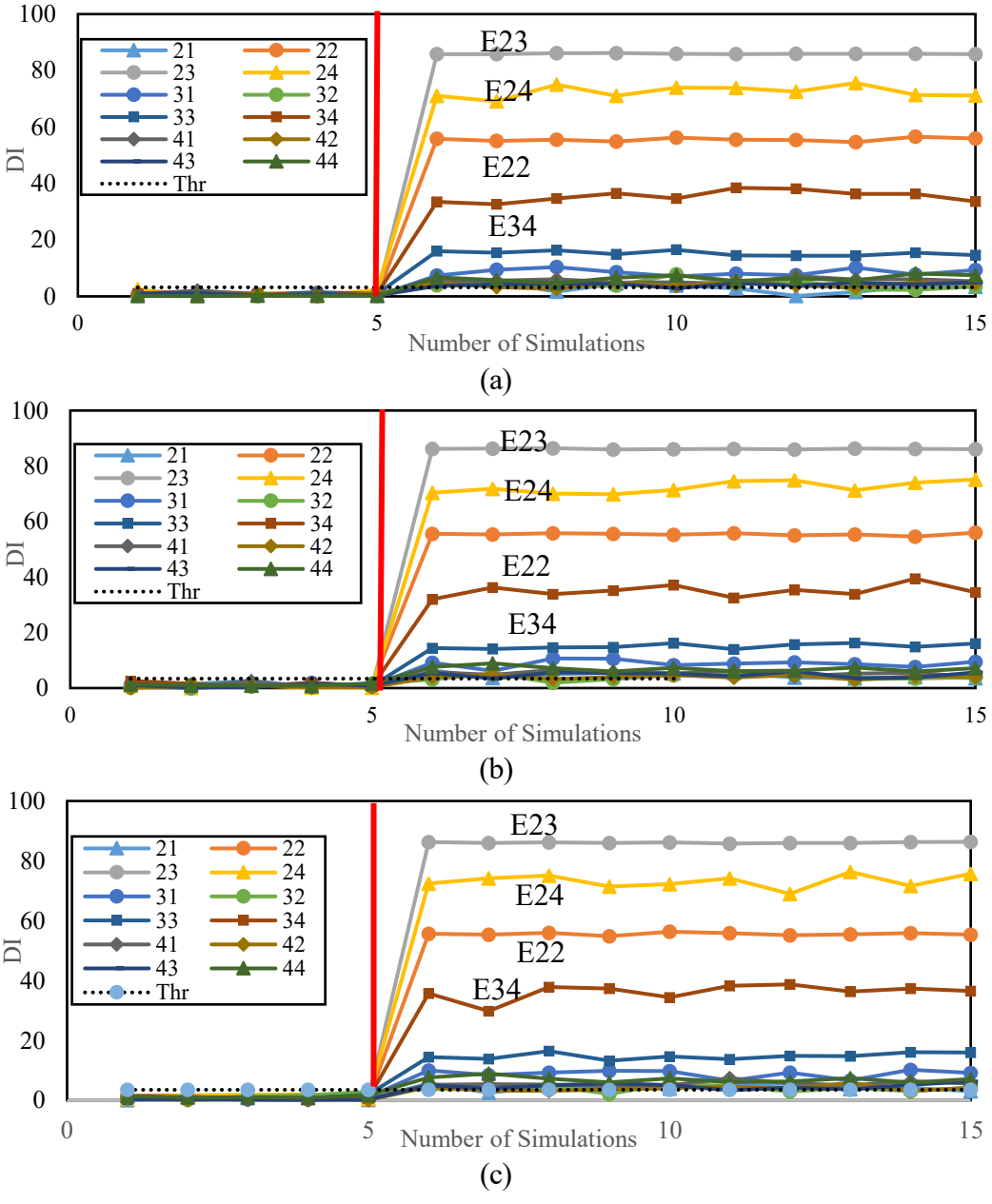

Figure 4.18 Damage indicators (DIs) for DC-7: (a) Cond-1, (b) Cond-2, (c) Cond-3

It can be seen that; such boundary condition change has a global effect on the truss bridge response. All the elements show DIs above the threshold. Significantly high DIs are observed for multiple elements, specifically for the bottom chord elements E22, E23, and E24. Also, two vertical elements E34 and E33 which are closest vertical elements to the right support are shown to be affected by the boundary condition change. Change of support from roller to hinge causes longitudinal reaction force which mainly changes the response of the bottom chord elements and the vertical elements to some extent. Redistribution of the axial forces and consequently the strains are mainly concentrated on these elements as observed in the result. It can be observed that the effect of noise on the DIs for this damage case is less compared to the previous damage cases (i.e., the changes in DIs of the elements between simulations are smaller compared to the other damage cases at the same level of noise). Therefore, it can be concluded that this is severe global damage and the method could be useful in detecting such damage.

4.5 Conclusion

In this chapter, two data-driven damage detection methods for railway truss bridges are presented that utilize operational strain time-history response. In this chapter, two data analysis techniques and two corresponding damage sensitive features are described. The 1st method comprises the coefficient of variation analysis which provides information on damage in terms of the difference of covariance matrix (DM). In the second method, principal component analysis is performed and the damage is identified in terms of damage indicators (DI). The results of both the data analysis methods are have been presented for different damage scenarios which include stiffness and cross-sectional area loss in truss elements and boundary condition changes. The results show that both these methods have the potential to identify, locate, and relatively assess the severity of the simulated damage using operational data. Most of the damage detection methods for truss bridges have limited ability to detect and locate damage due to small stiffness changes in individual truss elements using operational data. The main contribution of the proposed damage detection framework is its potential to identify small damage in

individual elements under variable operational conditions if the damaged elements are monitored with a strain gauge.

For the truss elements not monitored, the methods still provide useful information about damage identification based on the response of adjacent monitored elements at higher damage levels. If the number of instrumented elements is further reduced, the proposed method could still provide information on damage and its location based on the available sensors, especially when the damage is severe, but the efficiency of the method will be reduced. Besides, as shown before, at higher damage levels, adjacent elements in addition to the affected elements could indicate the presence of damage in those elements. In such situations, to obtain more information on the location of damage, the proposed method could be incorporated as a part of the damage detection framework comprising the acceleration-based method presented in the previous chapter [113].

In this study, the efficiency of the proposed method is demonstrated for the distributed loss of cross-sectional area and stiffness by instrumenting elements with one strain gauge only. The method also shows good performance in detecting global damage due to boundary condition changes. However, detection of damage within highly localized damages such as those caused by cracking and buckling of elements are not within the scope of the current research since identification and localization of cracks with strain gauges is usually not feasible.

Like the previous chapter, the train-track-bridge interaction could influence the response of the bridge and consequently could affect the performance of the presented damage detection method. However, detailed modeling of such interaction and other train track related issues such as track irregularity, wheel flats are not within the scope of the present research. Similarly, it is recognized that the effects of environmental condition changes are not considered in this study, which could influence the strain data, and consequently, the damage detection results similar to most damage detection methods in the literature if not all. Temperature changes can alter the physical properties and vibration responses of the bridges [111]. For real-life application, the proposed method needs to be combined with

techniques to separate the effect on the presented method due to temperature changes from the actual damage. Currently, research is ongoing (such as those by Gu et al., Kostic and Gül, Huang et al., Zhang et al.) towards developing damage detection methods by incorporating the use of artificial neural networks to compensate for environmental effects [103-106]. Further research is needed to integrate such methods with the damage detection methods presented in this research.

The presented methods could complement existing SHM techniques by providing the opportunity to detect mild to moderate damage and thereby assisting in developing economical maintenance strategies. Verification of this method using experimental results and/or a real-life bridge investigation is beyond the scope of this research.

5 EXPERIMENTAL INVESTIGATION ON VIBRATION-BASED DAMAGE DETECTION OF RAILWAY BRIDGES[4]

5.1 Overview

This chapter could be considered as a subsequent study to the previous works of the author described in Chapters 2 and 3 [113, 116]. The goal of this study is to demonstrate the performance of the method on experimental bridge prototypes, which is the final task (*Task 3*) of this research. In this chapter, the results of the experimental investigations on a vibration-based damage identification framework for a steel girder type and a truss bridge based on acceleration responses to operational loading are presented. Two experimental bridges are fabricated. The first bridge is a simple steel deck bridge and the next one is a timber truss bridge with a steel deck. The results are presented in terms of Damage Features (DFs) from each sensor, which are obtained by comparing the actual acceleration response from the sensors to the predicted response from the time-series model. The damage in the bridge is detected by observing the change in damage features of the bridge as structural changes occur in the bridge. The relative severity of the damage can also be quantitatively assessed by observing the magnitude of the changes in the damage features. The experimental results show the potential usefulness of the proposed method for future applications on condition assessment of real-life bridge infrastructures.

5.2 Theoretical derivation

The detailed derivation of the method is provided in Chapter 2, Section 2.2.

5.3 Experimental validation on a simple slab bridge

As part of the experimental investigation plan to validate the proposed method, a simply supported slab bridge is considered as shown in Figure 5.1. The bridge deck

[4] A modified version of this chapter has been published in the following journal as follows:
Azim, M.R., Zhang, H., and Gül, M. (2020). Damage detection of railway bridges using operational vibration data: theory and experimental verifications. *Structural Monitoring and Maintenance*, 7(2), 149-166.
It can be accessed using DOI: **https://doi.org/10.12989/smm.2020.7.2.149**

is made of hot rolled steel W44, which has a yield strength of 250 MPa and ultimate strength of 310 MPa. The modulus of elasticity of the steel is 200 GPa. The dimensions of the bridge are as follows: length of 2000mm, width of 330 mm, and thickness of 6.35 mm. The bridge is instrumented with three tri-axial wireless accelerometers (Brand: Lord Microstrain Sensing, Model: G-Link-200 [117]) denoted as N1, N2, and N3 in Figure 1.1. These are placed at 1/4th, mid-span, and 3/4th span along the direction of travel. A moving vehicle is used to generate vertical accelerations data from the sensors. The vertical acceleration response is collected at a frequency of 512 Hz. The vehicle is shown in Figure 5.2. The vehicle is controlled by a motor. By adjusting the power transmitted to the motor, the speed of the vehicle can be changed.

The sensor cluster system is presented in Table 5.1. Each sensor cluster consists of a reference channel (whose output is predicted) and its adjacent channels (which are used as inputs to predict the output of the reference channel). As discussed in the theoretical derivation of the method, the adjacent channels to each reference channel, include the reference channel itself. For example, the output of N2 is predicted from inputs from adjacent channels N1, and N3 as well as the N2 channel itself which together forms one cluster. For this bridge, there are 3 cluster systems.

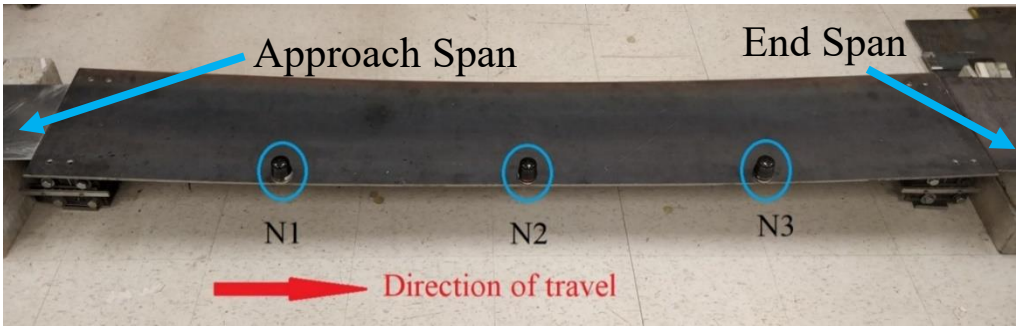

Figure 5.1 Experimental setup for the simple bridge under baseline condition

Figure 5.2 Vehicle to induce vibration in the bridge

Table 5.1 Sensor clusters for the simple deck bridge

Sensor Cluster	Output of the ARMAX model (Reference channel)	Inputs to the ARMAX model (Reference channel+ Adjacent channels)
1	N1	N1, N2
2	N2	N1, N2, N3
3	N3	N2, N3

5.3.1 Estimation of threshold damage feature

Initially, the two different configurations of the vehicle are passed over the baseline bridge several times. The 1st configuration (Vehicle-1) weighs around 2.5 kg and passed over the bridge at an average speed of 0.25 m/s. The 2nd configuration (Vehicle-2) weighs around 3.0 kg and passed over the bridge at an average speed of 0.35 m/s. After obtaining the total response, the initial free vibration portion of the data when the vehicle is off the bridge are extracted from each experiment. Some sample data for the baseline bridge due to the passage of Vehicle-1 is shown in Figure 5.3.

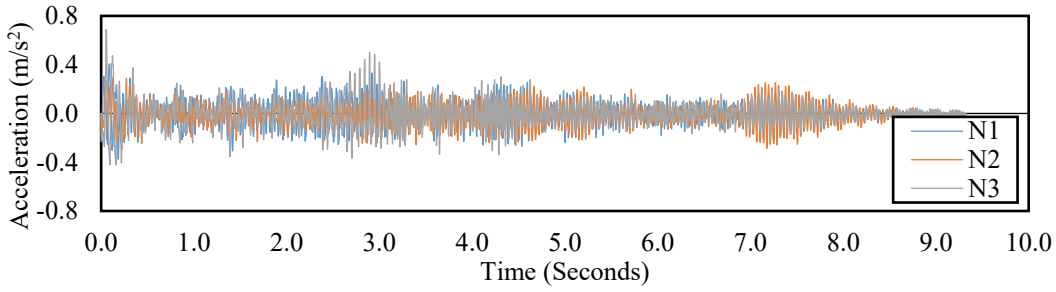

(a)

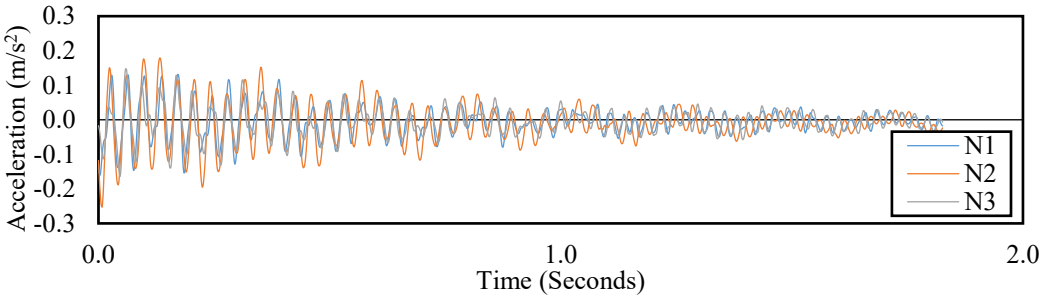

(b)

Figure 5.3 Acceleration response of the bridge: (a) total response (b) extracted free response

To estimate the threshold DF, considering the operational variation, one set of baseline data from Vehicle-1 is compared with 5 sets of baseline data from Vehicle-2. These data sets are then analyzed by the proposed sensor cluster-based method. Then fit ratios are obtained by comparing the measured data to the predicted data from the method. This results in five different FRs and therefore, five different DFs from each of three accelerometers for the baseline bridge. Finally, the maximum DF among these 15 DFs is considered as the threshold damage feature which in this experimental investigation is found to be 5.40. So, any DF value above 5.40 is expected to imply structural change.

5.3.2 Damage investigation

Two damage cases are considered for experimental validation of the proposed method for the simple deck bridge. These are, DC-1: 15% reduction in the cross-sectional area centered at the mid-span, and DC-2: 30% reduction in the cross-sectional area centered at the 1⁄4 span along the direction of travel. The results for these two damage cases are discussed in the subsequent paragraphs.

5.3.2.1 Damage features for DC-1: 15% reduction in the cross-sectional area centered at the mid-span

In this damage case, the bridge has a 24.8 mm by 250 mm cut centered at the mid-span at each side as shown in Figure 5.4(a) so that there is 15% in the cross-sectional area. Vehicle-2 is passed over this damaged bridge six times and free acceleration responses are extracted. The analysis results for this damage case are shown in Figure 5.4(b) in which damaged bridge responses from Vehicle-2 are compared with the Vehicle-1 data used during threshold estimation. As seen in Figure 5.4(b), maximum DFs are obtained for N2 (located at the mid-span) with average values of 6.70. The other nodes N1 and N3 show average DFs of 2.5 and 3.5 respectively which are below the threshold value of 5.4. Based on the values of DFs, it is indicative that damage is present with a likely location around the mid-span.

It is noted that there are some variations in DFs between experiments. For example, for N2, the maximum DF is 9.1 for experiment 2 and the minimum is 5.3 for experiment 4. The speed of the vehicle varied while passing over the bridge due to the curvature of the deck. Besides, the travel paths of the vehicle between experiments were not the same. These two issues could have affected the free response of the bridge apart from the actual presence of damage.

5.3.2.2 Damage features for DC-2: 30% reduction in the cross-sectional area centered at the 1/4th span along the direction of travel

In this damage case, the bridge has a 49.5 mm by 250 mm cut near the 1/4th span as shown in Figure 5.5(a) so that there is a 30% loss in the cross-sectional area centered at the 1/4th span. Similar to the previous damage case, Vh-2 is passed over this damaged bridge six times and the acceleration response is obtained. The results analyzing this damage case are shown in Figure 5.5(b).

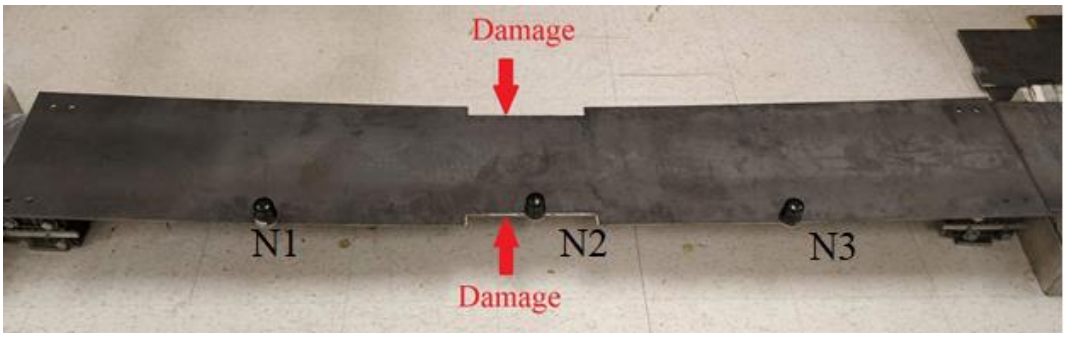

(a)

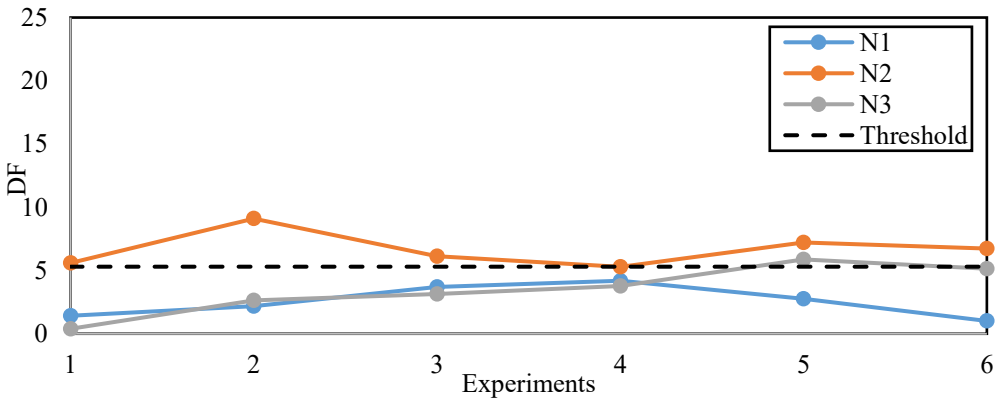

(b)

Figure 5.4 (a) Visual of damage case DC-1, (b) DFs for DC-1

As seen in Figure 5.5(b), maximum DFs are obtained for N1 (located near approach span) with average values of 18.1. The other nodes N1 and N3 show average DFs of 11.6 and 10.6 respectively. Based on the values of DFs, it is indicative that damage is present with a likely location near the sensor installed closer to the approach span, which is consistent with the applied damage. Also, by comparing the DFs of this damage case with the previous one, it is seen that the DFs are more than two times higher in this case. The average DFs of all the nodes are above the threshold. This is likely because this severe damage caused some load re-distribution over the entire bridge. The variations between DFs could be attributed to the same reasons discussed in the previous damage case.

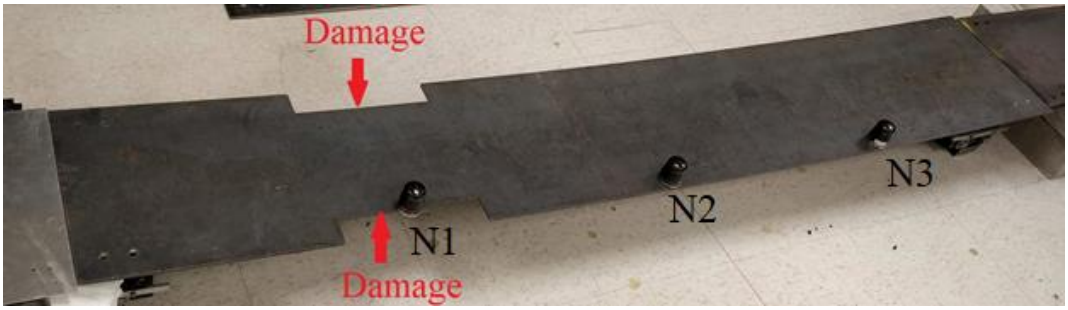

(a)

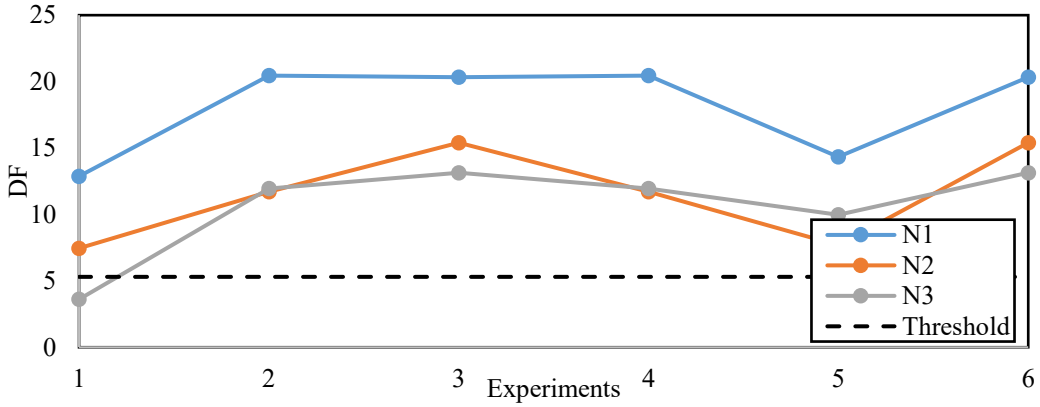

(b)

Figure 5.5 (a) Visual of damage case DC-2, (b) DFs for DC-2

5.4 Experimental validation on a truss bridge

The second experimental setup includes a simply supported truss bridge as shown in Figure 5.6. The total span of the truss is 2m. The truss elements are cut into rectangular cross-sections from S-P-F (Spruce, pine, and fir) dimension lumber pieces. These are timber pieces made up of Spruce, Pine, and Fir woods. The pieces used in this research are graded as "No.2" which are suitable for engineering applications such as trusses according to the Canadian Wood Council (CWC) [118]. According to CWC, the modulus of elasticity of the material varies from 6.5 to 8.5 GPa depending on the grade of the lumber [119]. The material properties are provided here for information purposes and are not required for applying the proposed methods in laboratory and/or real-life validation studies. The information needed for developing a data collection plan are: the type of bridge (i.e., girder or truss) and the geometric information of the nodes (i.e. member connectivity) to develop sensor cluster networks. The dimensions and cross-sectional properties are

presented in Table 5.2. The truss elements are bolted to the gusset plates made of same dimension lumber pieces using 6.35 mm diameter steel bolts. The bridge deck is made of hot rolled steel W44, which has the modulus of elasticity of is 200 GPa. The dimensions of the bridge are as follows: 2m length, 330 mm width, and 6.35 mm thickness.

Figure 5.6 Experimental setup for the truss bridge under baseline condition

Table 5.2 Truss element section properties

Truss element	Length (mm)	Width (mm)	Thickness (mm)
Top and Bottom Chord	500	25	12
Verticals	300	25	12
Diagonals	580	25	12
Cross bracings	350	25	25

To validate the proposed method, one side of the truss bridge is instrumented with uniaxial accelerometers. At each connection, two accelerometers are placed to collect acceleration response in both vertical and longitudinal directions as shown in Figure 5.7 (a) and (b). Therefore, in total 12 uniaxial accelerometers (Brand: PCB Piezotronics, Model: 393A03 [120]) are placed on one side of the truss bridge. Instrumenting with 12 accelerometers on one side of the truss does add some mass to the bridge on that side. However, it does not cause any stability issues for the truss bridge. Since the same instrumentation setup is used for both baseline and damaged bridge, there is no change in mass due to instrumentation between

experiments. The change in mass between experiments is only due to the replacement of original truss elements with damaged elements.

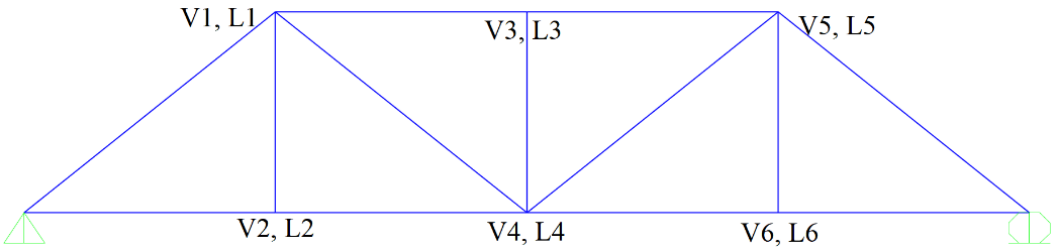

(a)

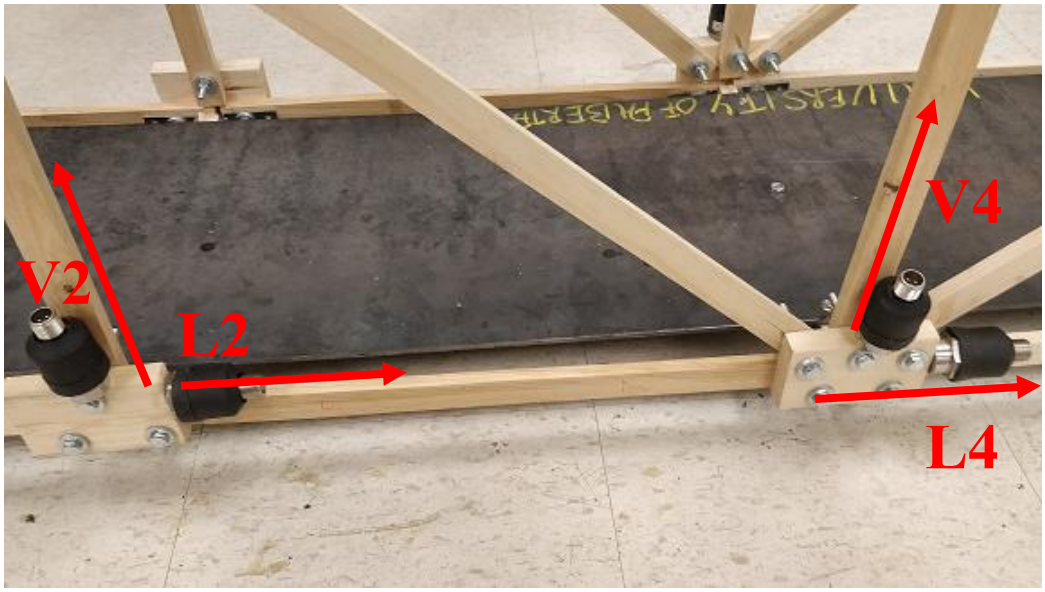

(b)

Figure 5.7 (a) Schematic diagram showing the instrumentation of the truss bridge (b) Enlarged view of the sensors V2-L2 on the actual bridge

These accelerometers are designated according to the vertical and longitudinal direction ('V' and 'L' respectively). The vertical and longitudinal cluster system is formulated based on the assumption that the vertical cluster would identify damage in vertical truss elements while the longitudinal cluster would identify damage in the elements aligned in the longitudinal direction. The vertical and longitudinal sensor cluster systems are presented in Table 5.3. Similar to the example presented for the steel deck bridge, each sensor cluster consists of a reference channel (whose output is predicted) and its adjacent channels (which are used as inputs to predict the output of the reference channel). Since the output of the reference channels also

depends on the input from the reference channel, the reference channel is included as part of the adjacent channels that form the sensor cluster system. In this truss bridge, for example, the output of vertical sensor V1 is predicted from the inputs of V1, V2, and V4. V1 is the output channel itself which is also included as input. V2 and V4 are adjacent channels to V1 which are vertically and diagonally connected to V1. Similarly, the output of longitudinal sensor L1 is predicted from the inputs of L1, L3, and L4. L1 is the output channel itself which is also included as input. L3 and L4 are adjacent channels to L1 which are longitudinally and diagonally connected to L1.

Table 5.3 Sensor clusters for the truss bridge

Vertical Sensor Cluster		**Longitudinal Sensor Cluster**	
The output of the ARMAX model (Reference channel)	Inputs to the ARMAX model (Reference channel+ Adjacent channels)	The output of the ARMAX model (Reference channel)	Inputs to the ARMAX model (Reference channel+ Adjacent channels)
V1	V1, V2, V4	L1	L1, L3, L4
V2	V1, V2	L2	L2, L4
V3	V3. V4	L3	L1, L3, L5
V4	V1, V3, V4, V5	L4	L1, L2, L4, L5, L6
V5	V4, V5, V6	L5	L3, L4, L5
V6	V5, V6	L6	L4, L6

5.4.1 Estimation of threshold damage feature

Initially, the vehicle is passed over the baseline truss bridge several times as shown in Figure 5.8 to obtain a few sets of baseline data which include the vibration response during the passage of the vehicle and a few seconds of free vibration response. To incorporate variation in vehicle load and speed, two-vehicle weight and speed combinations are considered. The 1st configuration is Vh-1 weighing 3.5 kg moving at an average speed of 0.35 m/s. The 2nd configuration is Vh-2 weighing 5.0 kg moving at an average speed of 0.25 m/s.

To estimate threshold DFs, one set of baseline data in response to Vh-1 is compared with five sets of baseline data in response to Vh-2. For both types of vehicle passage, data sets are collected at a frequency of 2048 Hz. These data sets are then analyzed by the sensor cluster-based proposed method. Then fit ratios are obtained by comparing the actual data to the predicted response from the method for both vertical and longitudinal cluster. Finally, the maximum difference of fit ratios among the five different experiments is calculated as the threshold damage feature which in this experimental investigation is found to be 5.89 and 2.07 for vertical cluster and longitudinal cluster respectively. So, any DF values above these thresholds are expected to imply structural changes that affect the corresponding cluster.

Figure 5.8 Vehicle passing over the truss bridge deck

5.4.2 Damage investigation

To validate the proposed damage detection method for the truss bridge, two damage cases are investigated. These are, DC-A: 33% thickness loss in vertical element between nodes 1 and 2, and DC-B: 33% thickness loss in longitudinal element between nodes 2 and 4.

The results for these two damage cases are discussed in the subsequent paragraphs. The results for the damage cases are presented when baseline data in response to the passage of Vehicle-1 is compared with damaged bridge data in response to Vehicle-2.

5.4.2.1 Damage features for DC-A: 33% thickness loss in element between nodes 1 and 2

In this damage case, the vertical truss element between nodes 1 and 2 is damaged by reducing its thickness from 12 mm to 8 mm resulting in a 33% reduction in cross-sectional area and consequently axial stiffness. The Damage Features (DFs) for the case are shown in Figure 5.9 where (a) and (b) represent results from the vertical and longitudinal clusters, respectively. From vertical cluster analysis, the average DF for V1 is around 31.4 which is almost 3 times higher than the threshold. The average DF for V2 is around 12.2 which is also higher than the threshold. The longitudinal clusters show that all the DFs are very close to or below the threshold indicating that no damage likely in the longitudinal direction. Overall, by observing the DFs of both vertical and longitudinal clusters, it can be inferred that damage is present and its likely location is in the vertical members between nodes V1 and V2. The results also show that the method can detect and locate damage in the vertical element.

5.4.2.2 Damage features for DC-B: 33% thickness loss in element between nodes 2 and 4

In this damage case, the longitudinal truss element between nodes 2 and 4 is damaged by reducing the cross-sectional thickness by 33%. The location of the damage is shown in Figure 5.10 (a). The Damage Features (DFs) for this case are shown in Figure 5.10 where (b) and (c) represent results from the vertical and longitudinal clusters, respectively.

(a)

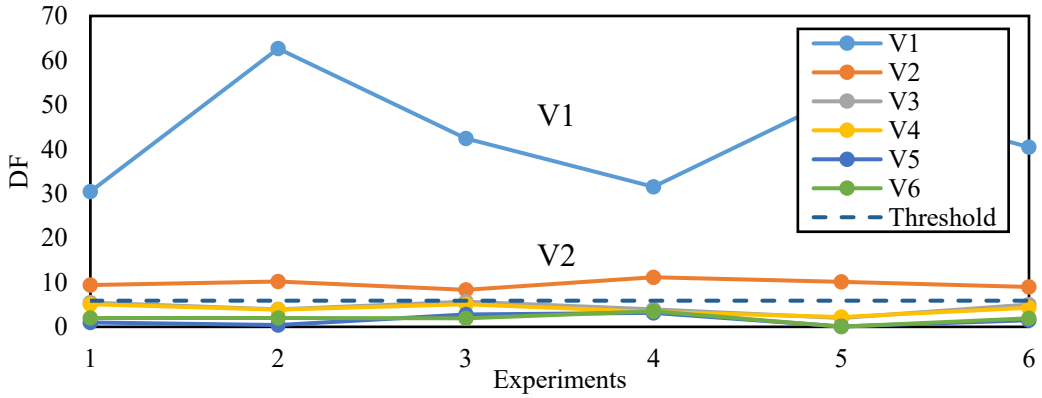

(b)

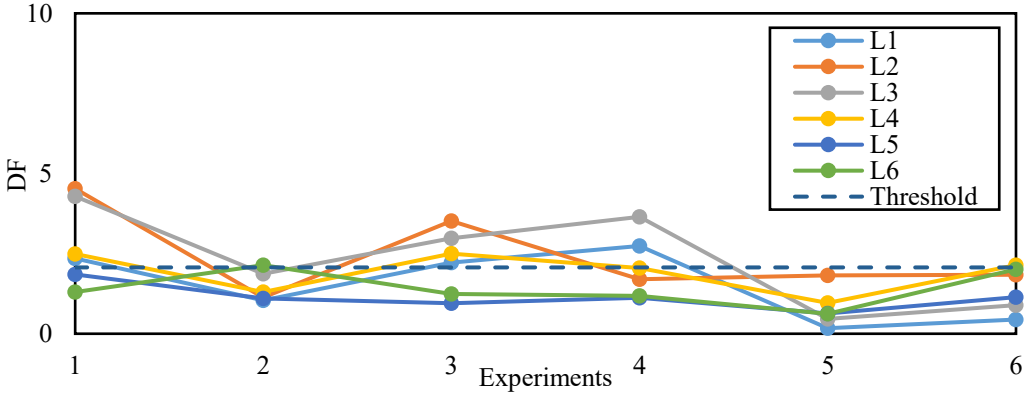

(c)

Figure 5.9 Results of DC-A: (a) actual location of damage, (b) DFs from vertical cluster analysis, (c) DFs from longitudinal cluster analysis

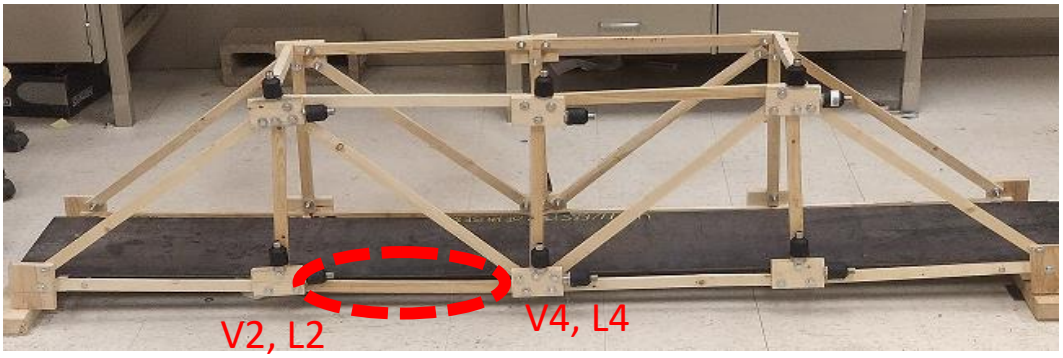

(a)

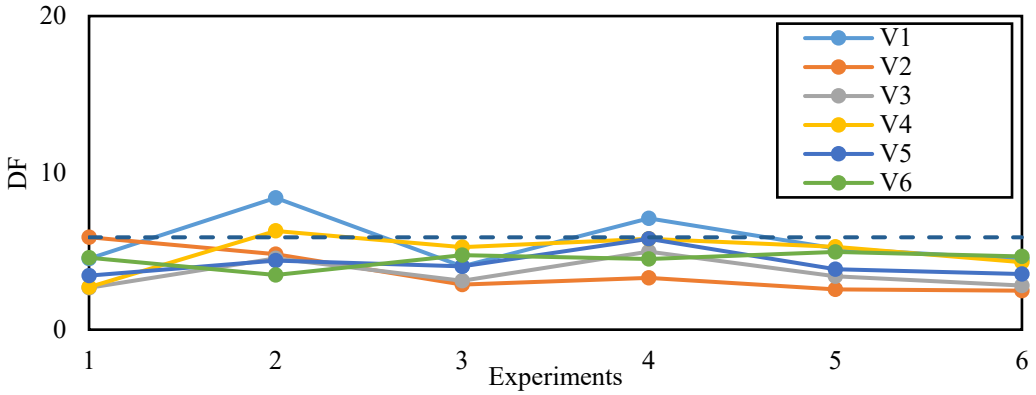

(b)

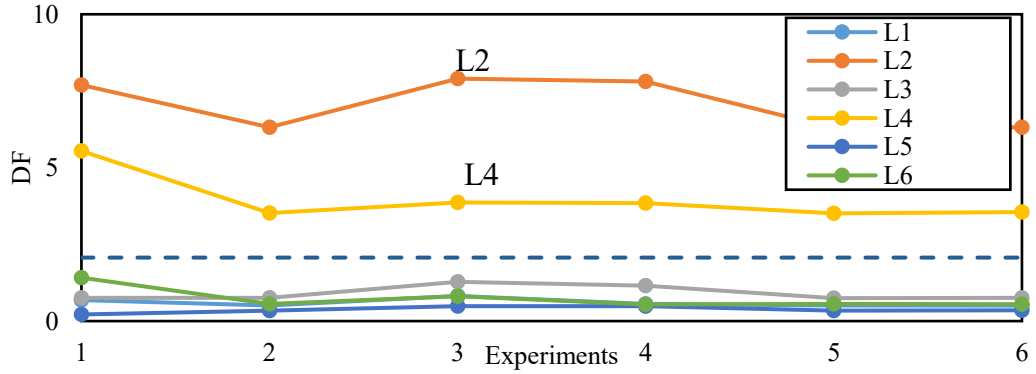

(c)

Figure 5.10 Results of DC-B: (a) actual location of damage, (b) DFs from vertical cluster analysis, (c) DFs from longitudinal cluster analysis

It can be observed that the average DFs for vertical clusters are all very close to or below the threshold value indicating that no damage is likely in the vertical system. In the longitudinal system, the highest DFs are obtained for L2 and L4 with average values of 3.6 and 3.2 respectively. The average DFs for the rest of the nodes are

below the threshold. This is indicative of the fact that damage is present and its likely location is in the longitudinal truss element between nodes 2 and 4 with no damage likely have occurred elsewhere.

Fabrication error resulted in differences in elevations between nodes that otherwise are supposed to be aligned longitudinally. Similar to the slab bridge, the speed of the vehicles varied while passing over the truss bridge and between experiments due to the curvature of the deck. Besides, the travel paths of the vehicle between experiments were not always similar. These issues might have influenced the free vibration response apart from the damage itself, which resulted in the variation of DFs between experiments.

5.5 Conclusion

This chapter presents the results of experimental investigations performed based on a novel damage identification method for railway girder and truss bridges utilizing bridge acceleration response to operational train loading. For experimental validation on a girder bridge, a simple steel deck is used. For truss bridge, a timber truss has been built which also included a steel deck. Conducting tests on a timber truss bridge also provides additional validation, that the method is not limited to steel bridges only, rather it can be applied to different materials such as wood here as long as a sensor cluster system can be implemented. A controllable 2 axle vehicle is used to simulate vehicle loading. Since the method relies on the comparison of free vibration response from the baseline and the damaged bridge due to the passage of a single vehicle, it is suited to railway bridges. Trains usually pass over railway bridges following a schedule and usually, there is a time gap between each passage of a train. This makes the process of acquisition of useful free vibration data for railway bridges convenient, unlike other types of bridges (such as highway bridges) where vehicle movements are random and often multiple vehicles pass over the bridge at the same time.

The experimental results presented in this study show that the proposed method could detect, locate, and assess the investigated damage cases. It is shown that the

time-series analysis-based method under operational condition can detect and locate damage in the deck type bridge using only vertical acceleration response. For the truss bridge, a bi-axial sensor cluster system could provide information on damage on vertical and longitudinal elements using vertical and longitudinal acceleration responses respectively. This method is presented for the instrumentation plan consisting of bi-axial accelerometers in each joint to facilitate element level damage localization. However, it is not practical to instrument all the joints especially if the bridge span is long. In such a situation, element level damage localization may not be possible.

It is acknowledged that fabrication errors might have occurred while building the test setup, especially in the truss bridge, since each element is manually sized and bolted. Even though the method is presented for railway bridges, during experiments, the railway track has not been included.

Finally, since the experimental tests are performed inside the laboratory, the effect of environmental condition changes on the measurement errors is also not considered in this study which could affect the performance of the method as it affects all damage detection methods in the literature. Currently, researchers (i.e., Gu et al., Kostic and Gül, Huang et al., Zhang et al.) are working on this topic extensively and developing methods using artificial neural networks to compensate for environmental effects [103-106].

Despite such limitations, the experimental results demonstrate that the proposed method has great promise for practical implementation and further research to address these limitations would improve the efficiency and robustness of the method for real-life application.

6 CONCLUSIONS AND RECOMMENDATIONS FOR FUTURE RESEARCH

6.1 Summary and conclusions

In this research, two damage detection methods have been developed which are expected to be useful for monitoring railway bridges. The damage detection framework utilizes operational acceleration and strain data of the railway bridge in response to the passage of trains which are two most commonly utilized parameters for monitoring of bridges.

The acceleration-based method relies on the sensor-cluster analysis technique. The principal of sensor cluster analysis is developed from the equation of motion which shows that the response of a particular degree of freedom (DOF) can be predicted from the response of its adjacent channels. To predict the response of a DOF, a time-series analysis technique has been applied. The method has been numerically applied to a steel girder and a truss bridge [113,116]. In both these bridges, acceleration responses from instrumented nodes have been obtained from the finite element models of these bridges to the passage of trains and free vibration responses have been extracted when the train is off the bridge. Then responses of each node are predicted from the adjacent channels. The predicted responses are compared with the actual measured responses and Fit Ratios (FR) are obtained for baseline and damaged bridge. When, there is no damage, the actual and predicted responses are close but not the same and therefore the FR values are very high. When damage occurs, the time series model could not predict the baseline response using the damaged data which results in lower FR values. So, a Damage Feature (DF) is calculated as the difference of FR values. By comparing the change in DFs from the baseline bridge to the damaged bridge, the damage could be identified and located. For the girder bridge, it was found that vertical acceleration is adequate to obtain information on the simulated damage cases. However, for the truss bridge, analysis of vertical acceleration was found to be not adequate. So, a bi-axial instrumentation plan has been proposed to collect vertical and longitudinal acceleration responses. These responses were analyzed through vertical and

longitudinal cluster systems, to identify damage in the corresponding directions. The method is also validated for a simple steel deck type bridge and a timber truss bridge through laboratory experiments [121]. The acceleration-based method showed useful potential for identifying, locating, and assessing the relative severity of the damage, in terms of nodal DFs.

A strain-based damage detection framework is developed and demonstrated for the truss railway bridge. Two data analysis method is presented as part of this method. These include the coefficient of variation analysis and principal component analysis. These techniques have been applied to the operational strain responses obtained from the instrumented truss elements. In the first method, the covariance matrix is calculated from the strain data for baseline and damaged bridge and the difference in the coefficients between these two matrices is used for identification of damage [122]. In the second method, principal components (PC) are calculated from the strain responses from the baseline and the damaged bridge. The first two PCs for each truss element are plotted in a 2-D principal component space and the geometric distances are calculated. The differences of these geometric distances from the baseline to the damaged bridge are proposed as damage indicators [123].

Both acceleration and strain-based methods could be utilized independently to assess the condition of railway bridges, which is the main contribution of this research. These methods provide bridge owners with two independent damage assessment tools for railway bridges. Since these methods are independent, combining both methods into a framework could be useful in improving the efficiency of the damage detection performance.

These two methods provide two different damage sensitive features (from nodes and elements). If both methods are utilized together, then these can complement and validate the results of each other. Also, it will be useful to have both methods in place to obtain further information, when individual methods do not provide enough information (for example when a particular type of response is not available). One way to combine the methods is by converting the nodal DFs from the acceleration-based method to DFs in terms of elements. Then, the DFs could be

normalized with respect to the threshold values and summed together. However, this is beyond the scope of this research.

It is to be noted that the damage sensitive features presented in this thesis do not provide any information on the type of change in the physical properties of the system since no physical parameters are directly compared in the non-parametric methods. Rather, the damage sensitive features provide information, that there may be a change in the structure (i.e., damage) that corresponds to the change in responses collected from the sensors. This damage feature relatively quantifies the change in the response since, the higher the change in the response, the higher will be the value of the damage feature.

6.2 Recommendations for future research

While the present research shows the potential use of operational data analysis for damage detection of railway bridges; the application of the developed methods needs to be addressed by further studies. To overcome the limitations of existing research, the following research should be conducted:

- One of the major challenges towards the application of these methods to real-life railway bridges is how to separate the effects of environmental condition changes such as temperature, humidity from the actual damage. Temperature changes can alter the physical properties and vibration responses of the bridges [115]. Since the changes in environmental conditions could falsely indicate damage or mask the presence of actual damage, for real-life application, the proposed method needs to be combined with techniques to separate the effect on the presented method due to temperature changes from the actual damage. Over the years, researchers have utilized seasonal time series models such as Autoregressive Integrated Moving Averages (ARIMA), and Seasonal Autoregressive Integrated Moving Averages (SARIMA) to identify, assess and model the seasonal trends from time-series data [124-127]. These are mainly utilized for forecasting future trends in data rather than predicting

anomaly in response due to structural changes or environmental condition changes. For example, the threshold damage feature of the baseline bridge may vary depending on whether the data is obtained during summer or winter even if there is no structural change and other factors such as operational train loads, speeds remain the same. Therefore, how to distinguish between the damage features obtained from the bridge due to actual damage from those due to variation in environmental conditions (such as changes in temperature) remains a challenge. As mentioned in the previous chapters, currently, research is ongoing (such as those by Gu et al., Kostic and Gül, Huang et al., Zhang et al.) towards developing damage detection methods by incorporating the use of artificial neural networks to compensate for environmental effects [103-106]. These researches propose procedures for separating the effect of temperature changes from the actual damage. Through further research, such procedures for separating environmental effects could be integrated into the procedures for damage detection presented in this thesis. Conducting this research is beyond the scope of this thesis.

- In this research, train-track-bridge interaction is not considered. So, detailed train-track-bridge interaction studies should be conducted to identify if train and track related issues such as track irregularities could compromise the damage detection framework.
- The presented methods are validated only for the distributed loss of stiffness in bridge elements and change in support behaviors. Future studies could be conducted to investigate other types of damage cases, for example, the formation of localized cracks in bridge elements, the effect of support settlement on the bridge superstructure, etc.
- The proposed methods are developed and validated considering the linear behavior of the bridges dealing with low levels of operational vibration and strain response. Future studies could be conducted to develop methods considering the non-linear behavior of bridges as the proposed methods like

most damage detection methods presented in literature do not apply when the structural response is affected by non-linear behavior.

- Finally, one of the major limitations of the current research is the lack of real-life validation studies. It is acknowledged that real-life application of the presented methods will involve significant challenges which are not simulated and/or replicated in the numerical and laboratory experimental studies conducted in this research. Therefore, the methods must be validated by testing on real-life railway bridges to assess the applicability of the presented damage detection framework.

REFERENCES

[1] Little, R.G. (2002). Controlling cascading failure: understanding the vulnerabilities of interconnected infrastructures. *Journal of Urban Technology,* 9(1), 109-123.

[2] Moore J., Glencross-Grant, R., Mahini, S. and Patterson, R.A. (2011). Towards predictability of bridge health. Proceedings of 2011 Regional Convention, 103-110.

[3] Jayasekera, D. (2001). Another rail disaster in India claims 59 lives. *The International Committee of the Fourth International (ICFI).* Can be accessed from https://www.wsws.org/en/articles/2001/06/ind2-j27.html

[4] Department for Transport. (2010). Rail accident report: failure of bridge RDG1 48 (river Crane) between Whitton and Feltham-14 November 2009. https://assets.publishing.service.gov.uk/media/547c8ff7e5274a4290000195/R172010_100923_Feltham.pdf

[5] VanZwol, T. R., Cheng, J. R., & Tadros, G. (2008). Long-term structural health monitoring of the Crowchild Trail Bridge. *Canadian Journal of Civil Engineering,* 35(2), 179-189.

[6] Kurata, M., Kim, J., Zhang, Y., Lynch, J. P., Van der Linden, G., Jacob, V., Sheng, L.H. (2011). Long-term assessment of an autonomous wireless structural health monitoring system at the new Carquinez Suspension Bridge. *Proceeding of the SPIE Smart Structures and Materials+ Nondestructive Evaluation and Health Monitoring*, USA, Volume 798312.

[7] Chae, M., Yoo, H., Kim, J., & Cho, M. (2012). Development of a wireless sensor network system for suspension bridge health monitoring. *Automation in Construction,* 21, 237-252.

[8] Koo, K., Brownjohn, J., List, D., & Cole, R. (2013). Structural health monitoring of the Tamar suspension bridge. *Structural Control and Health Monitoring,* 20(4), 609-625.

[9] Ding, Y., An, Y., and C. Wang, C. (2016). Field monitoring of the train-induced hanger vibration in a high-speed railway steel arch bridge. *Smart Structures and Systems*. 17(6), 1107-1127.

[10] Comanducci, G., Magalhães, F., Ubertini, F., and Cunha, Á. (2016). On vibration-based damage detection by multivariate statistical techniques: Application to a long-span arch bridge.*Structural Health Monitoring,* 15(5), 505-524.

[11] Bernal, D., & Beck, J. (2004). Preface to the special issue on phase I of the IASC-ASCE structural health monitoring benchmark. *Journal of Engineering Mechanics ASCE,* 130, 1-2.

[12] Lynch, J. P., & Loh, K. J. (2006). A summary review of wireless sensors and sensor networks for structural health monitoring. *Shock and Vibration Digest,* 38(2), 91-130.

[13] Fan, W., & Qiao, P. Z. (2011). Vibration-based damage identification methods: a review and comparative study. *Structural Health Monitoring-an International Journal,* 10, 83-111.

[14] ASCE. (2017). Infrastructure Report Card: Rail. Can be accessed from https://www.infrastructurereportcard.org/cat-item/rail/

[15] Rakoczy, A.M., Nowak, A.S., and Dick, S. (2016). Fatigue reliability model for steel railway bridges. *Structure and Infrastructure Engineer*ing, 12(12), 1602-1613.

[16] Vegnoli, M., Prescott, R.R., and Andrews, J. (2017). Railway bridge structural health monitoring and fault detection: State-of-the-art methods and future challenges. *Structural Health Monitoring*, 17(4).

[17] Office of Comptroller and Auditor General of India. (2015). Compliance audit on union government, Railways, Report No. 24 Part 2, India.

[18] London Office of rail and road. (2015). Passenger rail usage 2015-16 Q1 statistical release, UK.

[19] Banerji, P., and Chikermane, S. (2011). Structural health monitoring of a steel railway bridge for increased axle loads. *Structural Engineering International*, 21(2), 1-7.

[20] Banerji, P., and S. Chikermane. (2012). Condition assessment of a heritage arch bridge using a novel model updation technique. *Civil Structural Health Monitoring*, 2(1), 1-16.

[21] Lee, G.C., Mohan, S.B., Huang, C., and Fard, B.N. (2013). A study of U.S. bridge failures (1980-2012). *Technical Report MCEER*-13-0008, Federal Highway Administration, USA.

[22] Otter, D., Joy, R., Jones, M.C., and Maal, L. (2012). Need for bridge monitoring systems to counter railroad bridge service interruptions. *Transportation Research Record: Journal of Transportation Research Board*, 2313, 134-143.

[23] Rytter, A. (1993), Vibration based inspection of civil engineering structures. *Ph. D. dissertation*, Aalborg University, Denmark.

[24] Brownjohn, J.M.W., Tjin, S.C., Tan, G.H., and Tan, B. L. (2004), A structural health monitoring paradigm for civil infrastructure. Proceedings of the 1st International Symposium on Engineering Surveys for Construction Works and Structural Engineering, Nottingham, UK.

[25] Fan, W., and Qiao, P. (2011). Vibration-based damage identification methods: a review and comparative study. *Structural Health Monitoring*, 10(1), 83-111.

[26] Das, S., Saha, P., and Patro, S.K. (2016). Vibration-based damage detection techniques used for health monitoring of structures: a review. *Civil Structural Health Monitoring*, 6(3), 477-507.

[27] Gomes, G.F., Mendez, Y.A.D., Alexandrino, P.S.L., da Cunha Jr., S.S., and Ancelotti Jr., A.C. (2019). A review of vibration based inverse methods for damage detection and identification in mechanical structures using optimization algorithms and ANN. *Archives of Computational Methods in Engineering*, 26, 883-897.

[28] Barai, S.V., and Pandey, P.C. (1997). Time-delay neural networks in damage detection of railway bridges. *Advances in Engineering Software*, 28(1997), 1-10.

[29] Salawu, O.S. (1997). Detection of structural damage through changes in frequency: a review. *Engineering Structures*, 19(9), 718-723.

[30] Tributsch, A., and Adam, C. (2018). An enhanced energy vibration based approach for damage detection and localization. *Journal of Structural Control and Health Monitoring*, 25(1), e2047.

[31] Shokrani, Y., Dertimanis, V.K., Chatzi, E.N., and Savoia, M.N. (2018). On the use of mode shape curvatures for damage localization under varying environmental conditions. *Journal of Structural Control and Health Monitoring*, 25(4), e2132.

[32] Moaveni, B., Hurlebus, S., and Moon, F. (2012). Special issue on real-world applications of structural identification and health monitoring methodologies. *Journal of Structural Engineering, ASCE*, 139(10). 10.1061/(ASCE)ST.1943-541X.0000779

[33] Hearn, G., and Testa, R. B. (1991). Modal analysis for damage detection in structures. *Journal of Structural Engineering, ASCE,* 117(10), 3042-3063.

[34] Sadhu, A., Narasimhan, S., and Goldack, A. (2013). Decentralized modal identification of a pony truss bridge using wireless sensors. *Journal of Bridge Engineering*, ASCE, 19(6), 04014013.

[35] Sadhu, A., Goldack, A., and Narasimhan, S. (2015). Ambient modal identification using multirank parallel factor decomposition. *Structural Control and Health Monitoring*, 22(4), 595-614.

[36] Doebling, S.W., Farrar, C.R., Prime, M.B., and Shevitz, D.W.(1996). Damage identification and health monitoring of structural and mechanical systems from changes in their vibration characteristics: a literature review. Report: *A-13070-MS*, Los Alamos National Laboratory, New Mexico, United States.

[37] Lu, Z.R., and Liu, J.K. (2011). Identification of both structural damages in bridge deck and vehicular parameters using measured dynamic responses. *Computers and Structures,* 89, 1397-1405.

[38] Scianna, A.M., and Christenson, R. (2009). Probabilistic structural health monitoring method applied to the bridge health monitoring benchmark problem. *Transportation Research Record: Journal of Transportation Research Board,* 2131, 92-97.

[39] Ko, J.M., Sun, Z.G., and Ni, Y.Q. (2002). Multi-stage identification scheme for detecting damage in cable-stayed Kap Shui Mun Bridge. Engineering Structures, 24(2002), 857-868.

[40] Yoshioka, T., Takahashi, M., Yamaguchi, H., and Matsumoto, Y. (2011). Damage assessment of truss diagonal members based on frequency changes in local higher modes. *Procedia Engineering*, 14, 3119–3126.

[41] Mehrjou, M., Khaji, N., Moharrami, H., and A. Bahreininejad. (2008). Damage detection of truss bridge joints using Artificial Neural Networks. *Expert Systems with Applications.* 35(3), 1122-1131.

[42] Catbas, F.N., Ciloglu, S., Hasancebi, O., Grimmelsman, K., and Aktan, A. (2007). Limitations in Structural Identification of Large Constructed Structures. *Journal of Structural Engineering*, *ASCE,* 133(8), 1051–1066.

[43] Balsamo, L., Betti, R., Beigi, H. (1994). A structural health monitoring strategy using cepstral features. *Journal of Sound and Vibration*, 169(1), 3-17.

[44] Gül, M., and Catbas, F.N. (2009). Statistical pattern recognition for structural health monitoring using time series modeling: Theory and experimental verifications. *Mechanical Systems and Signal Processing,* 23(7), 2192-2204.

[45] Zhang, Q.W. (2007). Statistical damage identification for bridges using ambient vibration data. *Computers & Structures*, 85(7-8), 476-485.

[46] Sohn, H., Czarnecki, J.A., and Farrar, C.R. (2000). Structural health monitoring using statistical process control. *Journal of Structural Engineering*, ASCE*,* 126 (11), 1356–1363.

[47] Sohn, H., Farrar, C.R., Hunter, N.F., and Worden, K. (2001). Structural health monitoring using statistical pattern recognition techniques. *Dynamic Systems and Measurement Control*, 123 (4), 706-711.

[48] Nair, K.K., Kiremidjian, A.S., and Law, K.H. (2006). Time series-based damage detection and localization algorithm with application to the ASCE benchmark structure. *Journal of Sound and Vibration*, 291(1), 349–368.

[49] Roy, K., Bhattacharya, B., and Ray-Chaudhuri, S. (2015). ARX model based damage sensitive features for structural damage localization using output-only measurements. *Journal of Sound Vibration*, 349, 99–122.

[50] Gül, M., and Catbas, F.N. (2011). Damage assessment with ambient vibration data using a novel time series analysis methodology. *Journal of Structural Engineering, ASCE*, 10.1061/(ASCE)ST.1943-541X.0000366.

[51] Gül, M., and Catbas, F.N. (2011). Structural health monitoring and damage assessment using a novel time series analysis methodology with sensor clustering. *Journal of Sound and Vibration*, 330, 1196-1210.

[52] Mei, Q., and Gül, M. (2014). Novel sensor clustering-based approach for simultaneous detection of stiffness and mass changes using output-only data. *Journal of Structural Engineering,* ASCE, 141 (10), 04014237.

[53] Mei, Q., and Gül, M. (2016). A fixed-order time series model for damage detection and localization. *Civil Structural Health Monitoring*, 6, 763-777.

[54] Celik, O., Terrell, T., Necati, C.F. and Gül, M. (2018), Sensor clustering technique for practical structural monitoring and maintenance, *Structural Monitoring and Maintenance*, 5(2), 273-295.

[55] Do, N. T., Mei, Q., and Gül, M. (2019). Damage assessment of shear-type structures under varying mass effects. *Structural Monitoring and Maintenance*, 6(3), 237–254.

[56] Andersen, P. (1997). "Identification of civil engineering structures using ARMA models." Ph.D. Thesis, Aalborg University, Aalborg, Denmark.

[57] Monroig, E., and Fujino, Y. (2006). "Damage Identification Based on a Local Physical Model for Small Cluster of Wireless Sensors." In the 1st Asia-Pacific Workshop on Structural Health Monitoring, Yokohama, Japan.

[58] Sweeney, R.A.P., and Unsworth, J. F. (2010). Bridge inspection practice: two different North American railways. *Journal of Bridge Engineering*, 15(4), 439-444.

[59] Kim, C.W., Kitauchi, S., Chang, K.C., McGetrick, P. J., Sugiura, K., and Kawatani, M. (2014). Structural damage diagnosis of steel truss bridges by outlier detection. *Proceedings of the 11th International Conference on Structural Safety and Reliability,* ICOSSAR, 4631-4638.

[60] Moreu, F., and LaFave, J. (2012). Current research topics: railroad bridges and structural engineering, *Newmark Structural Engineering Laboratory Report Series*, 032, University of Illinois at Urbana-Champaign, USA.

[61] Moreu, F., LaFave, J., and Spencer, B. (2012). Structural health monitoring of railroad bridges – Research needs and preliminary results, *ASCE Structural Congress*, 2141-2152.

[62] Choi, J.Y., Park, Y.G., Choi, E.S., and Choi, J.H. (2010). Applying precast slab panel track to replace timber track in an existing steel plate girder railway bridge, *Journal of Rail and Rapid Transit*, 224 (3), 1-9.

[63] Wiberg, J. (2006). Bridge monitoring to allow for reliable dynamic FE modelling, a case study of the new Årsta railway bridge*, KTH Royal Institute of Technology*, Stockholm, Sweden.

[64] Arangio, S., and Beck, J.L. (2012). Bayesian neural networks for bridge integrity assessment. *Journal of Structural Control and Health Monitoring*, 19, 3-21.

[65] An, Y., and Ou, J. (2013). Experimental and numerical studies on model updating method of damage severity identification utilizing four cost functions. *Structural Control and Health Monitoring*, 20, 107-120.

[66] Scott, R.H., Banerji, P., Chikermane, S., Srinivasan, S., Basheer, P.A.M., Surre, F., Sun, T., and Grattan, K.T.V. (2013). Commissioning and evaluation of a fiber-optic sensor system for bridge monitoring. *IEEE Sensors Journal*, 13(7), pp 2555-2562.

[67] You, T., Gardoni, P., and Hurlebaus, S. (2014). Iterative damage index method for structural health monitoring. *Structural Monitoring and Maintenance*, 1(1), 89–110.

[68] Baitsthakur, S., and Chakraborty, A. (2020). Modified Hamiltonian Monte-Carlo-based Bayesian finite element model updating of steel truss bridge. *Structural Control and Health Monitoring*, e2556.

[69] Beskhyroun. S., Oshima, T., and Mikami, S. (2010). Wavelet-based technique for structural damage detection. *Structural Control and Health Monitoring*, 17, 473-494.

[70] Farahani, R.V., and Penumadu, D. (2016). Damage identification of a full-scale five-girder bridge using time-series analysis of vibration data. *Engineering Structures,* 115, 129-139.

[71] Kopsaftopoulos, F.P., and Fassois, S.D. (2010). Vibration based health monitoring for a lightweight truss structure: Experimental assessment of several statistical time series methods. *Mechanical Systems and Signal Processing*, 24(7), 1977–1997.

[72] Xu, Z.D., Liu, M., Wu, Z., and Zeng, X. (2011). Energy damage detection strategy based on strain responses for long-span bridge structures. *Journal of Bridge Engineering*, *ASCE,* 6(5), 644-652.

[73] Wang, L., Chan, T.H.T., Thambiratnam, D.P., Tan, A.C.C., and Cowled, C.J.L. (2012). Correlation-based damage detection for complicated truss bridges using multi-layer genetic algorithms. *Advances in Structural Engineering*, 15(5), 693-706.

[74] Nuno, K. (2013). Damage detection of a steel truss bridge using frequency response function curvature method, Stockholm. *ISRN KTH/BKN/R-148-SE, ISSN 1103-4289.*

[75] Siriwardane, S.C. (2015). Vibration measurement-based simple technique for damage detection of truss bridges: a case study. *Journal of Case studies in Engineering Failure Analysis*, 4, 50-58.

[76] Prajapat, K., and Chaudhury, S.R. (2017). Damage detection in railway truss bridges employing data sensitivity under Bayesian framework: a numerical investigation. *Journal of Shock and Vibration*, 4, 1-9.

[77] Zhan, J. W., Xia, H., Chen, S. Y., and Roeck, G.D. (2011). Structural damage identification for railway bridges based on train-induced bridge responses and sensitivity analysis. *Journal of Sound and Vibration.* 330, 757-770.

[78] Bowe, C., Quirke, P., Cantero, D., and O'Brien, E.J. (2015). Drive-by structural health monitoring of railway bridges using Train Mounted Accelerometers. *5th ECCOMAS Thematic Conference on Computational Methods in Structural Dynamics and Earthquake Engineering*, Greece.

[79] George, R.C., Posey, J., Gupta, A., Mukhopadhyay, S., and Mishra, S.K. (2017). Damage detection in railway bridges under moving train load. *Proceedings of the Society for Experimental Mechanics Series. Model Validation and Uncertainty Quantification,* 3, 349-354.

[80] Kaloop, M.R., J.W. Hu, and M.A. Sayed. (2016). Yonjung high-speed railway bridge assessment using output-only structural health monitoring measurements under train speed changing. *Journal of Sensors*, Hindawi Publishing Corporation, 2016, 4869638.

[81] Gonzalez, I., and Karoumi, R. (2015). BWIM aided damage detection in bridges using machine learning. *Civil Structural Health Monitoring*, 5, 715-725.

[82] Neves, A.C., Gonzalez, I., Leander, J., and Karoumi, R. (2017). Structural health monitoring of bridges: a model-free ANN-based approach to damage detection. *Civil Structural Health Monitoring*, 7, 689-702.

[83] Quirke, P., Bowe, C., Obrien, E.J., D. Cantero, P., Antolin, J.M., and Goicolea. (2017). Railway bridge damage detection using vehicle-based inertial measurements and apparent profile. *Engineering Structures*, 153, 421-442.

[84] Catbas F.N., H. B. Gokce, and M. Gül. (2012). Nonparametric analysis of structural health monitoring data for identification and localization of

changes: Concept, lab, and real-life studies. *Structural Health Monitoring*, 11 (5), 1-14.

[85] Hong, W., Cao, Y., and Wu, Z. (2016). Strain-based damage assessment method for bridges under moving vehicular load using long-gauge strain sensing. *Journal of Bridge Engineering, ASCE,* 21(10). 10.1061/(ASCE)BE.1943-5592.0000933.

[86] Yam, L.Y., Leung, T.P., Li, D. B., and Xue, K. Z. (1996). Theoretical and experimental study of modal strain analysis. *Journal of Sound and Vibration*, 191(2), 251–260.

[87] dos Santos, F.L.M., Peeters, B., Lau, J., Desmet, W., and Goes, L.C.S. (2015). The use of strain gauges in vibration-based damage detection. *11th International Conference on Damage Assessment of Structures, Journal of Physics: Conference Series,* 628, 012119.

[88] Wipf, T. J., B. M. Phares, and J.D. Doornink. (2007). *Monitoring the Structural Condition of Fracture-Critical Bridges Using Fiber Optic Technology*. Ames, IA: Center for Transportation Research and Education: Iowa State University, USA.

[89] Posenato, D., Kripakaran, P., Inaudi, D., and Smith, I.F.C. (2010). Methodologies for model-free data interpretation of civil engineering structures. *Computers and Structures*, 88(7/8), 467-482.

[90] Van Der Kooi, K. and Hoult, NA. (2018). Assessment of a steel model truss using distributed fibre optic strain sensing. *Engineering Structures*, 171, 557-568.

[91] Catbas F.N., Gül, M, Gokce, H.B., Zaurin, R., Frangopol, D.M., and Grimmelsman, K.A. (2014). Critical issues, condition assessment and monitoring of heavy movable structures: emphasis on movable bridges, *Structure and Infrastructure Engineering*, 10(2), 261-276.

[92] Moreu, F., Jo, H., Li, J., Kim, R.E., Cho. S., Kimmle, A., Scola, S., Le, H., Spencer Jr., B.F., and LaFave, J.M. (2015). Dynamic assessment of timber railroad bridges using displacements. *Journal of Bridge Engineering, ASCE,* 20(10), 04014114.

[93] Moreu, F., Jo, H., Li, J., Kim, R.E., Cho. S., Kimmle, A., Scola, S., Le, H., Spencer Jr., B.F., and LaFave, J.M. (2016). Reference-free displacements for condition assessment of timber railroad bridges. *Journal of Bridge Engineering, ASCE,* 21(2), 04015052.

[94] Li, Y. Y. (2010). Hypersensitivity of strain-based indicators for structural damage identification: A review. *Mech. Syst. Sig. Process.*, 24(3), 653–664.

[95] Moreu, F., Kim, R.E., and Spencer, B.F. (2017). Railroad bridge monitoring using wireless smart sensors. *Structural Control and Health Monitoring*, 24, e1863.

[96] Ljung, L. (1999). System identification: theory for the user. *Prentice-Hall*, Upper Saddle River, NJ, USA.

[97] Box, G. E., Jenkins, G. M., and Reinsel, G. C. (2013). Time series analysis: forecasting and control, 4th Edition. *John Wiley & Sons, Hoboken*, NJ, USA.

[98] CSI. (2014). Analysis reference manual for SAP2000, ETABS, SAFE, and CSiBridge. *Computers and Structures Inc*., Berkeley, California, USA.

[99] Box, G.E.P., Jenkins, G.M., and G.C. Reinsel, (1994). Time Series Analysis: Forecasting and Control, *Prentice-Hall*, Englewood Cliffs, NJ, USA,1994.

[100] Do, N., and Gül, M. (2020). A time series based damage detection method for obtaining separate mass and stiffness damage features of shear-type structures, *Engineering Structures*, 208,109914.

[101] Carden, E.P., Brownjohn, J.M.W. (2008). ARMA modelled time-series classification for structural health monitoring of civil infrastructure, *Mech Syst Sig Process*, 22(2), 295-314.

[102] Salcher, P., Pradlwarter, H., & Adam, C. (2014). Reliability of high-speed railway bridges with respect to uncertain characteristics. *Proceedings of the 9th International Conference on Structural Dynamics*, Porto, Portugal.

[103] Gu, J., Gül, M., and Wu, X. (2017). Damage detection under varying temperature using Artificial Neural Networks. *Structural Control and Health Monitoring,* Wiley, 24(11), e1998.

[104] Kostic, B., and Gül, M. (2017). Vibration based damage detection of bridges under varying temperature effects using time series analysis and artificial neural networks. *Journal of Bridge Engineering*, *ASCE*, 22(10), 04017065.

[105] Huang, M., Gül, M., and Zhu, H. (2018). Vibration-based structural damage identification under varying temperature effects. *Journal of Aerospace Engineering, ASCE*, 31(3), 04018014.

[106] Zhang, H., Gül, M., and Kostic, B. (2019). Eliminating temperature effects in damage detection for civil infrastructures using times series analysis and auto-associative neural networks. *Journal of Aerospace Engineering*, 32(2), 04019001.

[107] Goi, Y., and Kim, C.W. (2017). Damage detection of a truss bridge utilizing a damage indicator from multivariate autoregressive model. *Civil Structural Health Monitoring*. 7, 153-162.

[108] Mujica, L. E., Rodellar, J., Fernandez, A., and Guemes, A. (2010). Q-statistic and T2-statistic PCA-based measures for damage assessment in structures. *Structural Health Monitoring*, 10, 539-553.

[109] Cavadas, F., Smith, I. F., and Figueiras, J. (2013). Damage detection using data-driven methods applied to moving-load responses. *Mechanical Systems and Signal Processing*, 39(1), 409-425.

[110] Li, J., Dackermann, U., Xu, Y., and Samali, B. (2011). Damage identification in civil engineering structures utilizing PCA-compressed residual frequency response functions and neural network ensembles. *Structural Control and Health Monitoring*, 18(2), 207-226.

[111] Nie, Z., Guo, E., Li, J., Hao, H., Ma, H., and Jiang, H. (2020). Bridge condition monitoring using fixed moving principal component analysis. *Structural Control and Health Monitoring*, 27(6), e2535.

[112] Li, S.Z., and Wu, Z.S. (2007). Development of distributed long-gauge fiber optic sensing system for structural health monitoring. *Structural Health Monitoring,* 6(2), 133-143.

[113] Azim, M.R., and Gül, M. (2020). Damage detection of steel truss railway bridges using operational vibration data. *Journal of Structural Engineering, ASCE,* 146(3), 04020008. https://doi.org/10.1061/(ASCE)ST.1943-541X.0002547

[114] Jana, D., Mukhopadhyay, S., Chaudhuri, S. R. (2019). Fisher information-based optimal input locations for modal identification. *Journal of Sound and Vibrations*, 459, 114833.

[115] Peeters, B., and Roeck, G.D. (2000). One year monitoring of the Z24-Bridge: Environmental influences versus damage events. *Proceedings of IMAC 18, the International Modal Analysis Conference*, 1570–1576, San Antonio, Texas, USA.

[116] Azim, M.R., and Gül, M. (2019). Damage detection of steel girder railway bridges utilizing operational vibration response. *Structural Control & Health Monitoring*, 26(11), e2447. https://doi.org/10.1002/stc.2447

[117] Lord Sensing Microstrain. (2019). Information can be accessed from https://www.microstrain.com/wireless/g-link-200-oem

[118] CWC. (2020). Visual grading of dimension lumber. Canadian Wood Council, Ottawa, Canada. Accessed from: https://cwc.ca/how-to-build-with-wood/wood-products/lumber/grades/

[119] CWC. (2020). Timber. Canadian Wood Council, Ottawa, Canada. Accessed from: https://cwc.ca/wp-content/uploads/Timber.pdf.

[120] PCB Piezotronics. (2019). Information can be accessed from https://www.pcb.com/products?model=393a03

[121] Azim, M.R., Zhang, H., and Gül, M. (2020). Damage detection of railway bridges using operational vibration data: theory and experimental verifications. *Structural Monitoring and Maintenance*, 7(2), 149-166. https://doi.org/10.12989/smm.2020.7.2.149

[122] Azim, M.R., and Gül, M. (2020). Damage detection framework for truss railway bridges utilizing statistical analysis of operational strain response. *Structural Control and Health Monitoring*, 27(8), e2573. https://doi.org/10.1002/stc.2573

[123] Azim, M.R., and Gül, M. (2020). Data-driven damage identification technique for truss railroad bridges utilizing principal component analysis of strain response. *Structure and Infrastructure Engineering*. https://doi.org/10.1080/15732479.2020.1785512

[124] Kaiser, R., and Maravall A. (2001). Seasonal outliers in time series. *Estadistica,* 53, 97– 142.

[125] Zhang, G.P., and Qi, M. (2005). Neural network forecasting for seasonal and trend time series. *European Journal of Operational Research*, 160(2), 501-514.

[126] Ladiray, D., Mazzi, G.L., Palate, J., and Proietti, T. (2018). Seasonal adjustment of daily data. 16th Conference of the International Association of Official Statisticians (IAOS), Paris, France.

[127] Eymen, A., and Köylü, U. (2019). Seasonal trend analysis and ARIMA modeling of relative humidity and wind speed time series around Yamula dam. *Meteorology and Atmospheric Physics*, 131, 601-612.